Measurement Induced Synthesis of Energy and Quantum Coherence

Ph.D. thesis

by Mariia Gumberidze

Faculty of science

Palacký University

Olomouc 2022

Abstract

Quantum coherence, stemming from the possibility of state superpositions in a quantum realm, has been extensively studied in the last decade. Inspired by the breakthrough of quantum batteries, in this thesis we present our idea of coherent charging of a quantum system. In distinction to the unitary transformations mainly used in the relevant literature for this purpose, we contribute to the variety by the usage of different types of quantum operations, namely, measurements. In this thesis, we study complementary values of energy and coherence of the specific system manipulated by the means of quantum measurements. Our system consists of many copies of independent two-level systems (TLS) with initial non-zero but small energy and coherence values. The goal is to increase its coherent energy. We show two methods of enhancement and simultaneous concentration of both quantities with the help of the measurement procedure. The originality of such an approach lies in the admission of much a broader class of transformations of completely positive (CP) maps compared to unitary operators, corresponding to completely positive trace preserving maps (CPTP), used before. In addition, we explore the value of mutual coherence distinguishing the local and global contributions to the overall coherence of the system. Two approaches considered in the thesis are based on global (acting on all TLS) and pairwise (acting on pairs

of TLS) measurements. The first one has a large probability of success whereas the second is presumably advantageous in more feasible experimental realization. The procedure was optimized with the introduction of the projective operator valued measures and tested for decoherence-induced imperfections. An experiment based on the idea of the thesis was conveyed independently by exploiting a photon-based setup with quantum filters and the results show to agree with the corresponding theoretical findings.

Keywords: quantum thermodynamics, energy, relative entropy of coherence, mutual coherence, two-level systems

Title:	Measurement Induced Synthesis of Energy and Quantum Coherence
Author:	Mgr. Mariia Gumberidze
Supervisor:	Prof. Mgr. Radim Filip, Ph.D.
Co-supervisor:	Mgr. Michal Kolář, Ph.D.
Study progamme:	Optics and Optoelectronics
Institution:	Department of Optics, Faculty of Science, Palacký University Olomouc

Declaration: I hereby confirm that this is an original work of its author carried out under the guidance of a supervisor Prof. Mgr. Radim Filip, Ph.D. and a co-supervisor Mgr. Michal Kolář, Ph.D. It has not been submitted for a degree before. I agree with the further usage of the thesis according to the requirements of Palacký University and the Department of Optics.

Acknowledgements

I would like to thank my supervisor prof. Radim Filip and co-supervisor Michal Kolář for their unfailing guidance, brilliant ideas, support and endless useful scientific discussions throughout my PhD. My gratitude to the Department of Optics for a good working atmosphere. I appreciate the Fischer scholarship for the financing of my doctoral studies. Many thanks to the group of prof. Lutz for welcoming me in Stuttgart and introducing the quantum thermodynamics field to me. I am grateful to all my friends and parents who were supporting me through this period. Eventually, I would like to dedicate this work to the light memory of my father.

Contents

Chapter 1

Introduction

1.1 State of the art

Quantum coherence and entanglement, both stemming from interference phenomena in quantum mechanics, have undergone rapid development in the last decades. Although intrinsically different, they both appear to be consequences of the superposition principle, which is the fundamental non-classical characteristic of the quantum world.

As the entanglement has been a pivotal phenomenon in the field of quantum optics [1, 2], it has got a lot of research within the framework of the resource theory with multiple proposed measures of entanglement [3] with further wide application in the experiment, e.g. EPR states for testing Bell inequalities [4, 5]. First field-opening entanglement-based applications were quantum teleportation, dense coding, and entanglement swapping [6]. The latter also lies at the heart of the working principles of quantum repeaters [7]. Moreover, entanglement got an application in quantum cryptography, namely, in quantum key distribution protocols [8], quantum computation [9, 10, 11] and cluster states [12, 13].

Although coherence is not of any less importance than an entanglement in quantum theory, however, its systematic research started relatively later. The first trial to describe the resource theory of coherence was made in 2014 by Baumgratz, Cramer and Plenio [14]. The fundamental requirements towards the measures of coherence included the following: the demand of positivity and linearity, the non-increasing condition under the action of incoherent selective or non-selective operations represented with the help of Kraus operators [15] and convexity condition. By setting the notions of incoherent states and incoherent operations, first distance-based measures of coherence were introduced, e.g. relative entropy of coherence. Subsequently, the theory gained a lot of attention and developed into a much more comprehensive knowledge [16] with diverse measures having similar counterparts in entanglement. Moreover, tight connection of coherence and entanglement [17, 18] can also be seen from the possibility of measuring the quantum coherence of the system with the entanglement [19].

Manipulation of quantum resources is one of the fundamental problems in quantum physics. In an operational direction a considerable amount of research has been done in recent years on the manipulation of coherence [20, 21, 22], for example, coherence distillation [23, 24, 25, 26] and dilution [27]. Distillation describes extraction of a maximally coherent state from a general mixed state within the same fixed basis employing free or incoherent operations. Dilution denotes an opposite process of converting maximally coherent states into an arbitrary quantum state usually of a higher dimension using incoherent operations. Both distillation and dilution are studied in deterministic one-shot regime [23, 27] and probabilistic or asymptotic regime that admits the existence of infinite identical copies

of states [24, 25, 28].

Quantum coherence studies serve as prerequisites to a newly emerging research field of quantum thermodynamics originating from the combination of two scientific fields: quantum mechanics and thermodynamics. It is a relatively new area of study that emerged with the rise of quantum machines [29], namely, quantum engines, quantum batteries, and quantum computers [30]. One of the goals of quantum thermodynamics is to study the energy transformations of single individual quantum systems. From the side of quantum mechanics, it involves quantum superposition and, therefore, quantum coherence. On the other hand, from thermodynamics, it keeps the main interest in energy and methods on how to transform it. Therefore, a preferred representation in quantum thermodynamics is the energy basis. The latter makes it conceptually different from quantum information, which is basis independent. Already in the simplest two-level system (TLS), energy difference and quantum coherence are represented by non-commuting operators. Their values cannot be simultaneously arbitrarily high for a single system, and also their uncertainties are limited by fundamental commutation relations. Therefore, their simultaneous manipulations in the physical processes would bring trade-offs that are interesting to study.

Recently there has been a huge interest in the topic of quantum batteries [31, 32]. To recall, the working principle of classical batteries lies in converting a chemical energy into electrical energy, that is further utilized for performing a work. The effort is focused on creating quantum counterparts of classical batteries that would exploit purely quantum phenomena like coherence for efficient charging, storage, and work extraction processes in comparison with classical batteries [33]. On the other hand, it is

known that several quantum effects like correlations may lock part of the energy, therefore, limiting the amount of the extractable work [34]. However, the most basic aspect of quantum battery expanding small quantum coherences to a large ones remains largely unsolved.

One of the earliest papers [35] introduced a quantum battery complied of N two-level systems (or qubits) with a possibility of charging by unitary operations and, consequently, the notion of passive states. Latter are defined as states which don't allow work extraction with the means of unitary cyclic operations. The quality and precision of unitary operations were studied in practice [36], namely, Gaussian operations despite their performance turned out to be reliable. The role of the very quantum nature of charging effects in quantum batteries was explored [33, 37, 38]. The recent models of quantum batteries incorporate nowadays open quantum systems [38, 39, 40, 41], Heisenberg spin chain models [33, 37, 42] with entanglement resulting from spin interactions [43] or from an interaction with an additional external magnetic field [44], "Dicke" and "Rabi" batteries [45] representing collective and parallel coupling of two-level systems to cavities, etc. The role of the charger is played, e.g. by external electromagnetic fields or by quantum unitary or non-unitary operations acting locally or globally on two-level systems. For example, the battery was represented by two-level atoms charged by a harmonic driving field [46], consequently, the quantitative measure of charge saturation [47] was imposed for efficient charging power determination. The quantum battery field goes beyond the charging process of batteries with further investigation on aging [48], stability [49] and power enhancement [50]. In a recent paper [40], authors proposed an efficient way of storing excitonic energy in a quantum battery realized by a model of an open quantum network

with high structural symmetry by keeping it in a dark state. Such a state eliminates interactions with an environment, therefore, making the battery robust towards losses. Other work [51] concerns a stabilization process of an open quantum battery with a strategy based on a sequence of repeated projective measurements with minimized control power.

We would like to stress that our approach is different from original papers on quantum batteries in two major aspects. First, the energy increase is not the only figure of merit of our approach. We focus on simultaneous increase of energy and coherence to achieve enhanced quantum properties of the system. Second, the majority of related literature uses completely positive trace preserving (CPTP) maps [52] for increasing (charging) the energy of the system (battery). In our case, we enlarge the set of allowed quantum operations from CPTP to completely positive (CP) maps, by including quantum measurements. Though a cost for such generalization is the probabilistic nature of the operations. Nevertheless, when optimized for a specific goal, e.g. coherence increase, such operations can produce separable states, having only the local form of coherence (on subsystems only). To distinguish different (local vs. global) forms of coherence we employ mutual coherence [53] in the second part of thesis.

1.2 Outline of thesis

In this thesis, we want to study the simultaneous enhancement and synthesis of quantities and figures of merit, namely, energy and quantum coherence of the set of independent copies of two-level systems. We begin by introducing the concepts of projective and generalised measurements and the notions of coherence and its measures in Chapter 2. After a brief

discussion of the above-mentioned tools, we then move to the basic notions of the thesis, Chapter 3. We introduce the system of interest and universal measurement and how it changes a state of the system. Afterwards, we define quantities of interest, namely, energy and coherence. In addition, we present some preliminary results discussed in the following chapter. In the next Chapter 4, our goal is to study the enhancement of energy and coherence by the means of the protocol, that employs a global measurement over a simplified case of a pair of TLS. After a brief characterisation of the latter, we probe the validity of our results under decoherence processes, namely, spontaneous emission and dephasing. Further, we illustrate our findings for the optimisations of the protocol with the help of projector-valued operator measures. To conclude the chapter, we study generalisations of the global protocol to many copies of TLS. Then in the following Chapter 5, we move away from a single measurement over all TLS constituting the system and instead consider to the measurements over pairs of TLS. We begin by introducing the pairwise protocol assuming the system to be in a pure state. Then we present approximations of the values of quantities of interest as their analytical full-form counterparts are cumbersome. Equipped with this knowledge we shift our focus to protocol optimisations and propose two methods on how to improve the disadvantages of the pairwise protocol. In addition, we study how two dephasing processes before and after measurement affect the results. Lastly, in Chapter 6, we conclude the thesis with a final discussion of our results and an outlook for future investigations.

1.3 Publications covering thesis

The thesis is based on the following published papers:

- *Gumberidze, M., Kolář, M. and Filip, R. Measurement Induced Synthesis of Coherent Quantum Batteries. Sci Rep 9, 19628 (2019). https://doi.org/10.1038/s41598-019-56158-8 (Impact Factor: 3.998);*

- *Gumberidze, M., Kolář, M. and Filip, R. Pairwise-measurement- induced synthesis of quantum coherence. Phys. Rev. A 105, 012401 (3 Jan.2022). https://link.aps.org/doi/10.1103/PhysRevA.105.012401 (Impact Factor: 3.14).*

The first article, presented in the thesis, was motivated by a process of charging quantum batteries as a possible particular application. However, in the consecutive research, i.e., the second article, we generalized our aim to quantum coherence manipulations.

Chapter 2

Methods

This chapter introduces the essential theoretical tools used in the thesis. At first, we recall the effect of the measurement of the system with the help of projective, Sec. 2.1, and other types of generalized measurements, Sec. 2.2. In addition, we introduce the coherence notion, Sec. 2.3, and provide a chosen measure quantifying it in the current research, Sec. 2.4. Moreover, we introduce a relatively new measure of mutual coherence, Sec. 2.5, that will be employed in the second part of the thesis.

2.1 Projective measurements

Quantum measurement allows us not only to learn about the phenomena in microworld, but also to affect them and manipulate states of quantum systems. Projective measurements [9], shortly projections, in quantum mechanics are usually described by an observable

$$\hat{M} = \sum_m m\hat{P}_m \tag{2.1}$$

where m are the possible outcomes of the measurement corresponding to the projective operator $\hat{P}_m$.

As any other type of a generalised measurement, projections satisfy the completeness relation:

$$\sum_i \hat{P}_i = \hat{I}. \tag{2.2}$$

However, projections have several properties that distinguish them from other types of generalised measurements, namely they are mutually orthogonal

$$\hat{P}_i \hat{P}_j = \hat{P}_i \delta_{ij}, \tag{2.3}$$

and, therefore, repeatable $\hat{P}_m \hat{P}_m = \hat{P}_m$.

The projective measurement is called selective [54] if the specific outcome with a concrete eigenvalue is observed.

Let's assume the system we measure is in a pure state $|\psi\rangle$. A selective measurement would give a concrete outcome with an eigenvalue m and a resulting post-measurement state

$$|\psi'\rangle = \frac{\hat{P}_m |\psi\rangle}{\sqrt{\langle\psi| \hat{P}_m |\psi\rangle}}. \tag{2.4}$$

It is a probabilistic operation with a probability of success, dictated by Born's rule,

$$p_m = \langle\psi| \hat{P}_m |\psi\rangle , \tag{2.5}$$

that is a re-normalization factor in the denominator of Eq. (2.4).

Employing

$$\hat{\rho} = |\psi\rangle \langle\psi| \tag{2.6}$$

the post-measurement state can be reformulated in terms of the density matrices:

$$\hat{\rho}' = \frac{\hat{P}_m \hat{\rho} \hat{P}_m}{\mathrm{Tr}[\hat{P}_m \hat{\rho} \hat{P}_m]}, \tag{2.7}$$

where

$$p_m = \mathrm{Tr}[\hat{P}_m \hat{\rho}]. \tag{2.8}$$

is the probability of obtaining the result m, where the properties of projectors were used.

If no selection is performed, the resulting state of the system after measurement represents a convex combination of all possible outcomes (called non-selective measurement)

$$\hat{\rho}'' = \sum_m \hat{P}_m \hat{\rho} \hat{P}_m. \tag{2.9}$$

This is a negative back action of any quantum measurement, however, the selection of some measurements events can bring an useful conditional transformations of the state.

The following example shows how selective measurement can make a superposition more balanced. Let's assume we have a two-level system in a ground state $|g\rangle$. We can apply to it the coherent projector defined in the energy basis $\{|g\rangle, |e\rangle\}$ as

$$\hat{P} = \frac{1}{2}(|g\rangle\langle g| + |g\rangle\langle e| + |e\rangle\langle g| + |e\rangle\langle e|). \tag{2.10}$$

According to (2.4) we get the post-measurement state

$$|\tilde{\psi}\rangle = \sqrt{\frac{1}{2}}(|g\rangle + |e\rangle). \tag{2.11}$$

Clearly, the measurement mapped the incoherent state to the maximally coherent state, corresponding to the equator on the Bloch sphere. To conclude, the application of proper measurement with further subselection of the states can increase the coherence of the state of a system. This fact will be used as a an important observation further in a thesis.

2.2 POVM

In some cases, we are more interested in the measurement statistics itself, namely, the set of eigenvalues $\{m\}, m = 1, ..., N$ rather than the final state of the system after the measurement. For this purpose, general measurements without a requirement of the repeatability could be employed.

Positive operator valued measures, or POVMs [9], represent this type of measurements. Their simplest application is in the task of unambiguous distinguishing between non-orthogonal quantum states [9, 55]. Particularly, in this thesis POVMs are considered as an alternative to projections for optimisation purposes.

They are defined as a set of operators $\{E_m\}$ called POVM elements, that satisfy the completness relation

$$\sum_m \hat{E}_m = \hat{I}, \tag{2.12}$$

with the probability of m-th outcome

$$p_m = \langle\psi| \hat{E}_m |\psi\rangle . \tag{2.13}$$

We can define the measurement operators $\hat{M}_m = \sqrt{\hat{E}_m}$ to be able to have a knowledge about the post-measurement state

$$\hat{\tilde{\rho}} = \frac{\hat{M}_m \hat{\rho} \hat{M}_m^\dagger}{\mathrm{Tr}[\hat{M}_m \hat{\rho} \hat{M}_m^\dagger]}, \tag{2.14}$$

where $\hat{M}_m \hat{M}_m \neq \hat{M}_m$ as operators $\hat{M}_m$ are non-orthogonal, therefore, unrepeatable in distinction to projectors $\hat{P}_m$. In addition, the requirement of positivity is introduced $\hat{E}_m \geqslant 0$, namely, for every state $|\psi\rangle$

$$\langle\psi| \hat{E}_m |\psi\rangle \geqslant 0. \tag{2.15}$$

2.3 Quantum coherence

Quantum coherence is defined by non-zero off-diagonal terms of the density matrix in a predetermined basis and stems from a principle of existence of coherent superposition in quantum mechanics [14]. This measure is established with respect to a fixed basis, otherwise, it has no meaning. The choice of basis depends on physical context and, precisely, on the context of the task; we prefer energy basis due to closeness of our approach to ideas of quantum thermodynamics. Suppose we have a two-level system (TLS) in a pure state

$$|\psi\rangle = \sqrt{p}\ |e\rangle + e^{i\phi}\sqrt{1-p}\ |g\rangle\,, \tag{2.16}$$

where ϕ denotes the phase.

We can write down the density matrix in the basis $\{|g\rangle\,, |e\rangle\}$ as

$$\hat{\rho} = |\psi_j\rangle\langle\psi_j| = \begin{pmatrix} 1-p & e^{i\phi}\sqrt{p(1-p)} \\ e^{-i\phi}\sqrt{p(1-p)} & p \end{pmatrix}. \tag{2.17}$$

Clearly, in classical approximation the density matrix would have only diagonal terms as we can observe a system only in a statistical mixture of ground $|g\rangle$ or excited $|g\rangle$ states. However, in quantum scenario it can be superposition of both, hence, states can interfere bringing off-diagonal terms to the density matrix. The off-diagonal elements are generally complex numbers and depend on phase, therefore, multiple interferometric measurements are needed to find their absolute values. Nevertheless, further in the thesis without losing the generality we consider all off-diagonal elements to be same and real. Quantum coherence is hard to observe in macroscopic world. Moreover, even at micro-level it is fragile and can be easily destroyed by the environment influence, leading to the diminishing

off-diagonal entries in Eq. (2.17). Therefore, it is important to verify the stability of all quantum coherence effects and procedures with regard to this process called decoherence, its effect is explored in Sec. 4.2 and Sec. 5.5.

2.4 Relative entropy of coherence

The choice of the relative entropy of coherence, Eq. (2.18), as our measure is definitely not unique. As an alternative, we may use as well the l_1-norm based measure [14]. Although both are proper coherence measures, we prefer relative entropy of coherence. Such preference is motivated by the recognized connection of $C(\hat{\rho})$ with thermodynamic quantities [56] and the notion of von Neumann entropy, naturally connecting this measure and thermodynamics in much broader sense [57].

In the remainder of thesis we will use terms coherence and relative entropy of coherence interchangeably. The latter is defined as

$$S(\hat{\rho}||\hat{\sigma}) = \mathrm{Tr}(\hat{\rho}\ln\hat{\rho}) - \mathrm{Tr}(\hat{\rho}\ln\hat{\sigma}), \tag{2.18}$$

where $\hat{\sigma} \equiv \hat{\rho}^{diag}$ is the *diagonal* version of the state $\hat{\rho}$ with respect to the *energy* basis. This definition is frequent in the literature, however, we will also use further its equivalent form, Eq. (3.6), obtained with respect to our system of interest.

One should note that the maximally coherent state in a d-dimensional space would be

$$|\psi_d\rangle = \frac{1}{\sqrt{d}}\sum_{i=1}^{d}|i\rangle \tag{2.19}$$

and it will have the maximal relative entropy of coherence

$$C(|\psi_d\rangle\langle\psi_d|) = \ln d. \tag{2.20}$$

For any state $|\psi\rangle$ the following general inequality holds

$$C(|\psi\rangle\langle\psi|) \leqslant \ln d, \tag{2.21}$$

however, it is more difficult to reach this upper bound as d increases in experiments.

2.5 Mutual coherence

The relative entropy of coherence is useful while determining the coherence gain of the system however, for compound systems consisting of subsystems, it does not take into account the global and local contributions to an overall quantum coherence of the system. By local coherence we mean the coherence of the subsystems themselves and by global counterpart we define the coherence of the joint system as a whole. Hence, the part of coherence that constitutes the difference between these two will be explored in this thesis denoted as mutual coherence.

Therefore, for the sake of distinguishing between local and global coherence, we introduce a quantity called *mutual relative entropy of coherence* [53]. It represents

$$C_m(\hat{\rho}) = S(\hat{\rho}||\bigotimes_i \hat{\rho}_i) - S(\hat{\rho}^{diag}||\bigotimes_i \hat{\rho}_i^{diag}) \tag{2.22}$$

where $\hat{\rho}$, $\hat{\rho}_i = \mathrm{Tr}_{\forall j\neq i}(\hat{\rho})$ denote the total state of the system and the local states of its constituents, respectively, whereas $\hat{\rho}^{diag}$, $\hat{\rho}_i^{diag}$ are the diagonal (or fully dephased) versions of states. In analogy to the relative entropy of coherence $C(\hat{\rho})$, (2.18), this measure is also always positive, $C_m(\hat{\rho}) \geqslant 0$.

The mutual coherence thus specifies how much the distance (characterized by the relative entropy, however, not in a strict sense as it does not

have properties of distance) of the state $\hat{\rho}$ with respect to the corresponding product of local states $\bigotimes_{i=1}^{N} \hat{\rho}_i$ increases compared to distance between diagonal (fully dephased) versions of that states. The RHS of Eq. (2.22) can be, after some algebra, simplified to

$$C_m(\hat{\rho}) = C(\hat{\rho}) - C^{loc}(\hat{\rho}), \tag{2.23}$$

where $C^{loc}(\hat{\rho}) \equiv \sum_i C(\hat{\rho}_i)$, with the local states $\hat{\rho}_i$ defined as in (2.22). The mutual coherence, Eq. (2.23), quantifies as well the difference in work extracted [56] within certain thermodynamic process from a coherent state $\hat{\rho}$, if the extraction is performed globally (with the total state) or locally (using the marginal states only). Such quantity is, by definition, insensitive to the state transformations which increase only the local coherence. This property will be of a particular use for the purposes of this thesis outlined in the next chapter.

Chapter 3

Basic notions

In this section we introduce the aim of the thesis and proceed with the description of the system of interest, Sec. 3.1 together with measurement made on it, namely, the application of the projector filtering out the total ground state population of the system, Sec. 3.2. The chapter concludes with variables of interest, namely, energy and coherence, Sec. 3.3.

In this thesis we aim to coherently charge and synthesise a system comprised of many TLS by the means of projective measurements. Mainly, we are interested not only in increase in energy, as would be sufficient for many thermodynamics discussions, but simultaneously a quantum coherence as well. As they are complementary even in a case of single TLS, their simultaneous enhancement and synthesis is an attractive fundamental problem. The benefits of energy gain is clear from the point of view of thermodynamics as we get charging device or a battery. Why coherence of the system constitutes such a great importance for us? Latest articles and research shows that quantum coherence is a useful resource especially the coherence between non-degenerate energy eigenstates. These could be extracting larger average amount of energy from a quantum system [58],

increasing the potential usefulness of the thermal reservoirs [59, 60] or increase in the power output of thermal machines [61], [62], even with experimental demonstration [63]. These more basic and flexible cases stem from more complex physical processes in cavity quantum electrodynamics [64], trapped ion experiments [65] and superconducting circuits [66].

Hence, we can merge two described goals into simultaneous synthesis of energy and quantum coherence, that could be in terms of application suitable for quantum batteries, see Sec. 1.1. Proposed protocols fulfilling this goal would be described in the following chapters.

3.1 System of interest

As a simplified system, at first, we consider two independent copies of TLS, denoted 1 and 2, with a non-zero energy gap E between the states. The preferred basis of the pair of TLSs, which we will uniquely refer to throughout the thesis, will be given by the TLS energy eigenstates labeling the ground and excited state, respectively, $\{|g_j\rangle, |e_j\rangle\}$, for both subsystems $j = 1, 2$. The Hamiltonians defining these states read

$$\hat{H}_j = \frac{E}{2}\left(|e_j\rangle\langle e_j| - |g_j\rangle\langle g_j|\right), \quad j = 1, 2, \tag{3.1}$$

yielding the Hamiltonian of the total system

$$\hat{H} = \hat{H}_1 \otimes \hat{1}_2 + \hat{1}_1 \otimes \hat{H}_2. \tag{3.2}$$

From an energetic point of view, the Hamiltonian (3.2) represents a four-level system with the following energy eigenstates: $|g_1 g_2\rangle$ ground state with energy $-E$, doubly degenerate first excited states $\{|e_1 g_2\rangle, |g_1 e_2\rangle\}$ with zero energy, and $|e_1 e_2\rangle$ with energy $+E$. We use definition (3.1) for a convenience to recognize the inverse of the population. It brings a negative en-

ergy values, however, all the results can be always equivalently re-scaled to have a positive energy.

In general, our system may consist of an arbitrary number N of TLS. The Hamiltonian of the total system would be then

$$\hat{H}^{(N)} = \sum_{j=1}^{N} \hat{H}_j \bigotimes_{\substack{k=1 \\ k\neq j}}^{N} \hat{\mathbb{1}}^{(k)}, \tag{3.3}$$

where the Hamiltonian of a single TLS is given by (3.1).

3.2 Universal measurement

In this section we introduce a basic universal measurement employed in the thesis to synthesise larger coherence and energy from the individual TLS. Universality means that our measurement does not depend on the states or the system or their number. For this purpose, let us consider a simplified version of a pair of TLS denoted as 1 and 2. We can map it to a 4-dimensional total system schematically shown in Fig. 3.1. The measurement made on the system is selective, it filters out the total ground states $|g_1 g_2\rangle$, admitting all other possible state combinations, i.e. $|g_1 e_2\rangle, |e_1 g_2\rangle, |e_1 e_1\rangle$. In other words, we eliminate a case when both TLS are in ground states. Projector realizing such a measurement is of the form

$$\hat{P} = \hat{\mathbb{1}} - |g_1 g_2\rangle \langle g_1 g_2|, \tag{3.4}$$

where $\hat{\mathbb{1}}$ denotes the identity matrix. Apparently, such a measurement only conclusively distinguishes when both TLSs are simultaneously in the ground states, other states remain indistinguishable. Fig. 3.1 shows visually the action of a projector filtering out the ground state population of a pair of TLS.

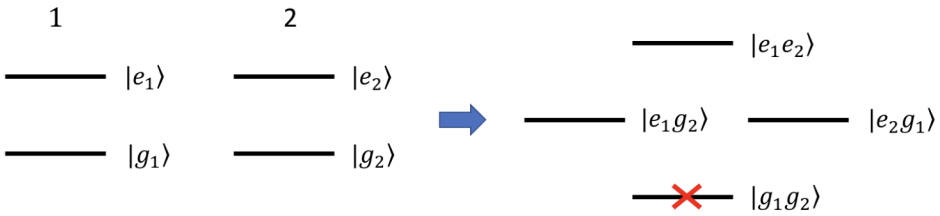

Figure 3.1: The scheme of mapping initially a pair of independent TLS, denoted as 1 and 2, to the 4- dimensional space with the means of application a global projector wiping out a total ground state population of the system. Hence, the system after the measurement could be in any state of the 3-dimensional successful subspace except of the ground state.

Technically, the projective operator used in the thesis, is wiping out the total ground state of the system. For instance, if we map our two TLS system to a 4 - dimensional space, based on the differences of energy level values we will get a system pictured in Fig. 3.1. There are 4 possible total states corresponding to different outcomes of measurement: both TLS are in the ground states $|g_1g_2\rangle$, one of TLS is in the ground state and the other one is in the excited state $|g_1e_2\rangle$ or $|e_1g_2\rangle$ (they are symmetrical), both TLS are in the excited states $|e_1e_2\rangle$. Obviously, the case when both TLS are in the ground state corresponds to the lowest energy. Consequently, our choice of the projective operator is not random as it eliminates the state $|g_1g_2\rangle$ with low energy, therefore, bringing it to higher energy three dimensional subspace $\{|g_1e_2\rangle, |e_1g_2\rangle, |e_1e_2\rangle\}$. The question arises if a quantum coherence can be conditionally increased as well. The answer is positive and will be explicated in the following chapters.

3.3 Energy and coherence

The average energy and the variance of energy of any quantum state of our system is determined in a standard way as

$$\langle E\rangle = \mathrm{Tr}(\hat{\rho}\hat{H}), \quad \langle \Delta E^2\rangle = \mathrm{Tr}(\hat{\rho}\hat{H}^2) - \langle E\rangle^2. \tag{3.5}$$

To quantify coherence of the state, we use the relative entropy of coherence (denoted simply "coherence" from now on) defined as [14]

$$C(\hat{\rho}) = S(\hat{\rho}_{diag}) - S(\hat{\rho}), \tag{3.6}$$

where $S(\hat{\rho}) = -\mathrm{Tr}(\hat{\rho}\ln\hat{\rho})$ is von Neumann entropy and $S(\hat{\rho}_{diag})$ is the entropy of the *diagonal* version of the state with respect to the *energy* basis. Thus, the latter effectively amounts to the Shannon entropy of state $\hat{\rho}$ concerning energy eigenbasis. In the derivation the following was assumed $\mathrm{Tr}(\hat{\sigma}\ln\hat{\sigma}) = \mathrm{Tr}(\hat{\rho}\ln\hat{\sigma})$, where $\hat{\sigma} \equiv \hat{\rho}^{diag}$, see Eq. (2.18). The maximum value of coherence C depends on the dimension D of the system Hilbert space. For any system $0 \leq C \leq \ln D$ holds [14], thus, e.g., for a single TLS it is upper bounded by $C = \ln 2$.

As we are interested in changes of the battery energy and coherence, we focus on the behavior of the energy difference

$$\Delta E = E_f - E_0, \quad E_f \equiv \mathrm{Tr}(\hat{\rho}_f\hat{H}), \quad E_0 \equiv \mathrm{Tr}(\hat{\rho}_0\hat{H}), \tag{3.7}$$

between the final energy after the charging and the initial energy before the charging process, respectively. Similarly, we focus on the change of the coherence

$$\Delta C = C_f - C_0, \quad C_f \equiv C(\hat{\rho}_f), \quad C_0 \equiv C(\hat{\rho}_0), \tag{3.8}$$

of the battery state.

By advancing substantially presentation of the results, we can see the opening result of the next Chapter 4 plotted in Fig. 3.2. The plot shows the simultaneous increase in the energy $\Delta E > 0$ and coherence $\Delta C > 0$ of the battery after charging process with non-negligible probability of success p_s. More details could be found in the following Chapter 4.

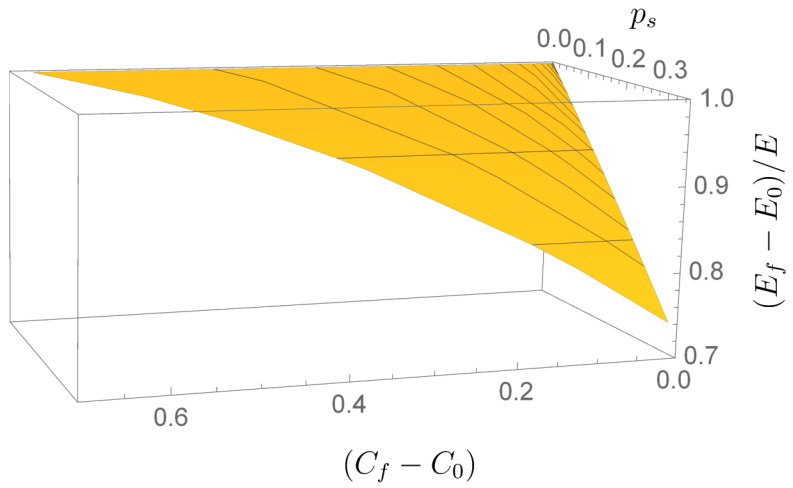

Figure 3.2: Parametric 3D plot of the relative entropy of coherence difference ΔC, Eq. (3.8), on x-axis, the normalized average energy difference $\Delta E/E$, Eq. (3.7), on z-axis and single run probability of success p_s on y-axis. It demonstrates the basic result of the global protocol, Chap. 4, for a pair of TLS: simultaneous increase in the energy and coherence of the battery (after the charging process) with sufficient probability of success.

The thesis will cover two different approaches of coherent increase of the energy. First, the global protocol, see Chap. 4, will be introduced with its main distinctive feature of a single projective measurement over all TLS constituting the system of interest. Subsequently, more feasible pairwise

protocol, see Chap. 5, will be presented with the following upgrade: it will consist of measurements over pairs of TLS in an arbitrary order. Both protocols are aimed to synthesize from independent TLS the larger correlated system with simultaneously increased energy and coherence.

Chapter 4

Energy and coherence synthesis by a global protocol

In this chapter, we propose a strategy which is coherently synthesizing excited two-level systems to a larger coherent system by the *collective* universal quantum measurement with elements diagonal in the energy basis. Such synthesizing unifies the battery build-up and charging process. Our main result shows the possibility of elementary coherent energy synthesizing, i.e., the increase of both the initial energy and coherence [14] (both small but nonzero) employing global quantum measurement on the system. This result is quantitatively presented in Fig. 3.2. Such energy and coherence increasing measurement can be extended and optimized further, as we subsequently propose, to reach maximal coherent energy of the battery. Although this charging stage is, in a single protocol run, conditional with a limited probability of success p_s, it can be repeated until it succeeds and TLS are synthesized and coherently charged with the overall success probability arbitrarily close to one. Our work [67] represents a bottom-to-top approach and analyzes only the basic recycling strategy. We

generalize the protocol to higher number N of TLS, although sticking with the general idea of global measurement on these copies, and open the road for future numerical optimization in this direction, as well. Top-to-bottom numerical approach based purely on numerical optimization requires the insight presented here anyway.

4.1 Pure states

Before we analyze more realistic cases of TLS in mixed states, we discuss the ideal case showing the main idea of the protocol. For instance, let us assume the charging of a battery consisting of a pair of TLS in pure states

$$|\psi_j\rangle = \sqrt{p}\ |e_j\rangle + \sqrt{1-p}\ |g_j\rangle\,, \quad j = 1, 2, \tag{4.1}$$

where the Hamiltonians defining the respective energy eigenstates are in Eq. (3.1). This type of state can be, in principle, a steady state of TLS, originating from a certain type of interaction with a thermal bath [68, 69, 70, 71, 72]. This bath can increase the TLS energy *and* coherence with respect to its ground state $|g\rangle$. Such case will serve below as an optimization target for harnessing of coherent energy from the environment. Hence the total state of the system will be the direct product of two single TLS states

$$|\Psi_i\rangle = |\psi_1\rangle \otimes |\psi_2\rangle = p\,|e_1e_2\rangle + \sqrt{p(1-p)}\,(|e_1g_2\rangle + |g_1e_2\rangle) + \\ +(1-p)\,|g_1g_2\rangle\,. \tag{4.2}$$

Such a system has the following initial average energy and coherence equal to

$$E_0 = \langle\Psi_i|\,\hat{H}\,|\Psi_i\rangle = (2p-1)E, \tag{4.3}$$

$$C_0 = -2\left[p\ln p + (1-p)\ln(1-p)\right], \tag{4.4}$$

with respect to Hamiltonian (3.2).

Projective measurements are known to change the state of the system closer to a desired one. We want to choose such measurement that will charge the battery, i.e., increase its energy but also coherence, if possible. Moreover, we want to achieve this goal without using projectors on states with any coherence with respect to the energy eigenbasis of the Hamiltonian (3.2).

If we project on the superposition of energy eigenstates, coherence can be induced by the measurement itself. Therefore, only projectors diagonal in the measurement basis are allowed. Namely, we choose the pair of two complementary projective operators $\{\hat{P}_0, \hat{P}_1 = \hat{1} - \hat{P}_0\}$, with

$$\hat{P}_0 = |g_1 g_2\rangle\langle g_1 g_2|, \quad \hat{P}_1 = \hat{1} - |g_1 g_2\rangle\langle g_1 g_2|. \tag{4.5}$$

It should be mentioned, that the measurement $\hat{P}_0$ can not be decomposed to local measurements of the ground state of each TLS. Moreover, $\hat{P}_1$ is not principally capable to distinguish between other states.

The final state of the system after application of the pair (4.5) will be of the form

$$|\Psi_0\rangle = \frac{\hat{P}_0|\Psi_i\rangle}{\sqrt{1-p_s}} = |g_1 g_2\rangle, \tag{4.6}$$

$$|\Psi_f\rangle = \frac{\hat{P}_1|\Psi_i\rangle}{\sqrt{p_s}} = \frac{p|e_1 e_2\rangle + \sqrt{p(1-p)}\left(|e_1 g_2\rangle + |g_1 e_2\rangle\right)}{\sqrt{p(2-p)}}, \quad p \neq 0, \tag{4.7}$$

where we are more interested into the state $|\Psi_f\rangle$ as it represents the successful outcome of the measurement process. The probability to obtain it equals to

$$p_s = p(2-p), \tag{4.8}$$

that constitutes a re-normalisation factor of *final* state, Eq. (4.7) after *successful* round of the battery charging process.

If we consider the pair of our TLS as a battery to be charged then the procedure described before would serve as a probabilistic protocol of charging. According to Fig. 4.1 we could simultaneously charge and synthesize a battery in three steps: in the first step, we assume that a pair of TLS is prepared with the help of cold coherence-creating bath [68, 69, 70, 71, 72]. Such bath enables, due to the structure of the system-bath interaction Hamiltonian, the formation of coherence in energy basis of a generic two-level system, independently of its initial state. In the step 2, we make a projective measurement over a pair of TLS and, finally, in the step 3, we either get a success and the pair of TLS is charged or failure, when both TLS end up in ground states and, therefore, are returned back to the bath for recycling purpose. This strategy involves repeat until success (RUS) cycle, in other words, we can recycle our TLS as many times as needed to reach the successful outcome of the measurement. In the inset of the plot one can see that the probability of failure with the number of repetitions of the recycling goes down. It means that with a certain number of repetitions the probability of success increases almost to 1.

In the case of the success, we fuse the initially independent pair of TLS into a larger superposition, thus creating and coherently charging the battery simultaneously. The failure of the protocol results in reducing the initial energy and coherence to zero, by bringing the TLS pair to the energetic ground state. Thus, these pairs (failed to be charged) can be used once more to harness a partial coherence from the environment. If such a strategy is repeated, the probability of failure after R independent repetitions (meaning that the battery will be not charged even in a single event)

decreases as

$$p_f^{(R)} = (1 - p_s)^R = (1 - p)^{2R}, \quad R \geq 1, \tag{4.9}$$

with p the probability of single TLS excitation, Eq. (4.1). As illustrated in the inset of Fig. 4.1, such event becomes almost impossible at an exponential rate.

The final energy and coherence of the state are

$$E_f = \langle \Psi_f | \hat{H} | \Psi_f \rangle = \frac{pE}{2 - p}, \tag{4.10}$$

$$C_f = \ln(2 - p) - \frac{2(1 - p)}{2 - p} \ln(1 - p) - \frac{p}{2 - p} \ln p. \tag{4.11}$$

The formulas (4.10), (4.11) yield the increase in both of the quantities

$$\Delta E = \frac{2(1 - p)^2}{2 - p} E, \tag{4.12}$$

$$\Delta C = \ln(2 - p) + \frac{2(1 - p)^2}{2 - p} \ln(1 - p) + \frac{(3 - 2p)p}{2 - p} \ln p. \tag{4.13}$$

pictured in the plots Fig. 4.2. One can see that coherence is increased in the lower range of values of the probability of excitation p of a single TLS. Whereas the energy gain is positive throughout the whole range of probability p with largest value in its lowest part. The maximal possible gain of energy equals to the value of a gap E between ground and excited states of a single TLS.

If the single basic step of the protocol increases both coherence and energy, this result would constitute a prerequisite to use such coherent energy for an iterative procedure on many TLS, see Sec. 4.4.

The exact value $p_0 \approx 0.18$, at which the final coherence is equal to initial, is the solution of the transcendent equation $C_f(p) = C_0(p)$, not solvable analytically. The value of coherence $\tilde{C}_0 \equiv C_f(p_0) = C_0(p_0) \approx 0.96$. If

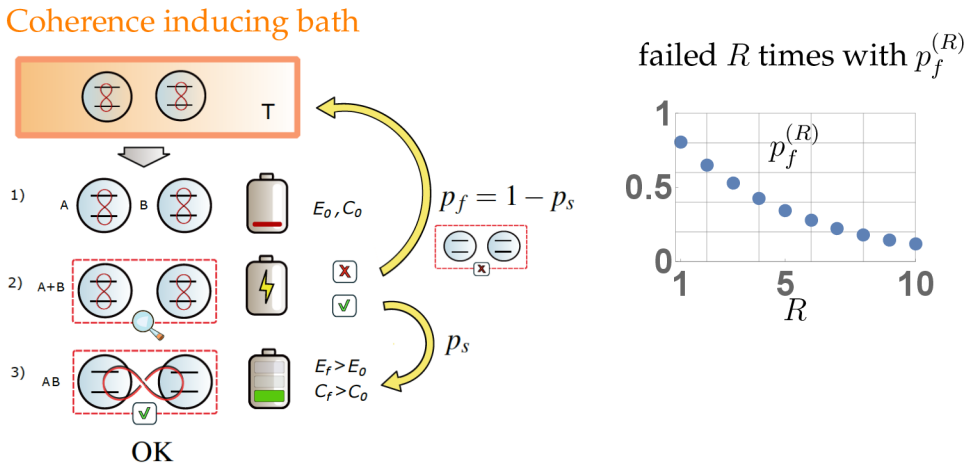

Figure 4.1: Schematics showing the idea of the 2-TLS battery charging process in three steps and (inset) the total probability of failure $p_f^{(R)}$ after R unsuccessful repetitions. In the initial step 1) the pair of TLS leaves the cold coherence inducing bath [68] and enters the process, assumed to be almost discharged with low initial energy E_0 and coherence C_0 (red loops connecting the levels). Step 2) represents the *conditional* stage of the charging operation. If the outcome of this step is successful (see step 3) with the single run probability of success p_s, the battery is made more coherent and simultaneously charged, i.e., has higher energy $E_f > E_0$ and increased coherence $C_f > C_0$ as well, both with respect to the eigenbasis of Hamiltonian (3.2). If the charging fails, with the single run probability $p_f = (1 - p_s)$ in step 2), the battery is completely discharged and incoherent. In principle it can be recycled by bringing it in contact with the bath again and the protocol is repeated until success (RUS). If the charging does not successfully occur in R recycling runs, the total probability of failure, $p_f^{(R)} = (1 - p_s)^R$, is exponentially converging to zero with the number of repetitions, see the inset for a typical behavior.

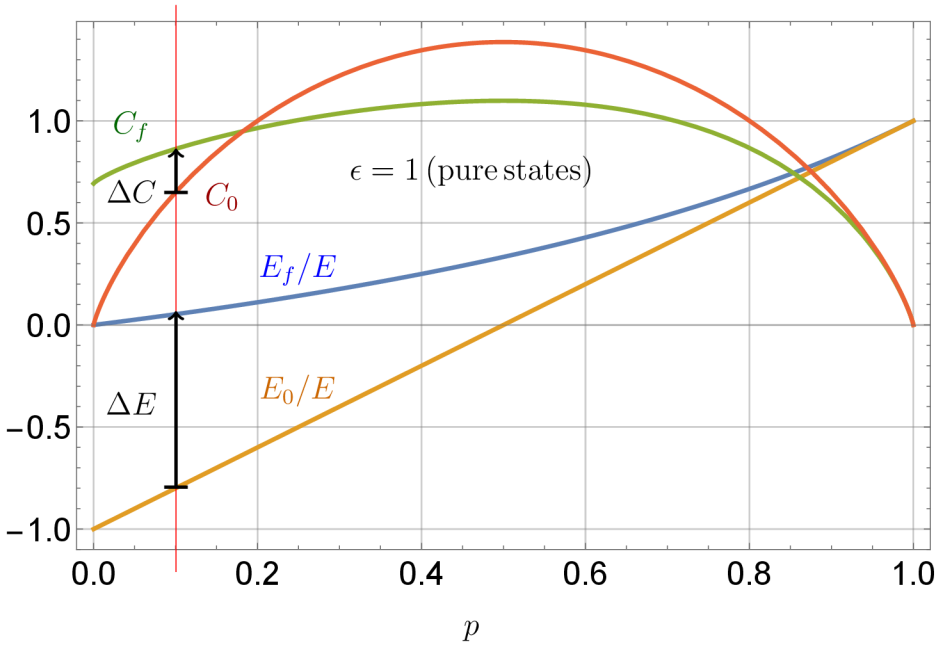

Figure 4.2: The plot of the normalized average energy E_f/E, E_0/E and the relative entropy of coherence C_f, C_0 for the final state $|\Psi_f\rangle$, Eq. (4.7), and the initial state $|\Psi_i\rangle$, Eq. (4.2), for a pair of TLS in pure states. The values are plotted vesrus the TLS excitation probability p, Eq. (4.1), with the red vertical line guiding the eye for the value $p = 0.1$ and black arrows expressing the coherence and energy increase. The conditional increase of the final energy over the initial one, $(E_f - E_0)/E > 0$, is achieved with maximum in the region of small p. The final entropy of coherence can be conditionally increased above the initial one in a region of small excitation probabilities p, up to the point $\tilde{C}_0 \approx 0.96$.

we derive the final coherence in terms of initial one we get

$$C_f \approx \ln 2 \left(\frac{2}{5} C_0 + 1 \right). \tag{4.14}$$

It is straightforward to see $\lim_{C_0 \to 0} C_f = \ln 2$, that indicates the maximum possible coherence gain. The relation (4.14) captures the linear transformation "amplifying" $C_0 \to C_f$ up to the boundary value $C_f = \tilde{C}_0 \approx 0.96$. This represents the value of the initial/final coherence where the curves C_f and C_0 cross each other. As such, $\tilde{C}_0$ represents the maximum value of the coherence attainable, if coherence *increase* is required.

In addition, we calculated the variance of energy of initial (4.2) and final (4.7) states, respectively,

$$\langle \Delta E_0^2 \rangle = 2p(1-p)E^2, \tag{4.15}$$

$$\langle \Delta E_f^2 \rangle = \frac{2p(1-p)E^2}{2-p}, \quad p \neq 0. \tag{4.16}$$

Clearly, sorting of the total ensemble of states $|\Psi_i\rangle$ increases the energy conditionally on the subensemble of states $|\Psi_f\rangle$, resulting in $\Delta E > 0$, cf. Eq. (3.7). We emphasize the fact, that $E_f \geq E_0$ for *all* excitation probabilities p with the largest increase in the region $p \ll 1$, together with the decrease of the energy variance $\langle \Delta E_f^2 \rangle < \langle \Delta E_0^2 \rangle$ for all $0 < p < 1$. We can explain this effect by noting that the successful charging procedure cuts-off the lowest energy contribution $(-E)$, weighted by the ground state probability $(1-p)^2$. This amounts to new conditional populations of the energy eigenstates, Eq. (4.7), the shift of the average energy $E_0 \to E_f$, and lowering of the energy variance $\langle \Delta E_f^2 \rangle < \langle \Delta E_0^2 \rangle$, c.f. Eqs. (4.10) and (4.3), hence concentrating the energy distribution of the final battery. Together with the fact, that the average value of energy is increased by the protocol, $E_f > E_0$, one can understand the situation as an increase in the quality

of coherent energy. Simultaneously, the projective measurement does not distinguish the states $|e_1e_2\rangle, |e_1g_2\rangle, |g_1e_2\rangle$ and therefore it allows not only to keep the initial coherence, but even to increase it.

It is interesting to observe how the energy ΔE and coherence ΔC increase are related to the probability of success p_s in Fig. 3.2 parameterised by the excitation probability of a single TLS p. One can notice that larger amount of energy and coherence can be gained within the range of lower half of values of probability of success. However, the gain of energy and coherence are positive throughout all the range of probability of success p_s, therefore, the result of charging procedure on average is positive.

We would like to stress that our protocol basically decomposes any initial state Eq. (4.2) into component in the one dimensional $|g_1g_2\rangle$ subspace and its orthogonal complement from three dimensional subspace spanned by $\{|g_1e_2\rangle, |e_1g_2\rangle, |e_1e_2\rangle\}$. The validity of the values ΔC and ΔE directly stems from the validity of the form of post-measurement state in Eq. (4.7) *only* for $p \neq 0$. The initial state $|\Psi_i\rangle$, Eq. (4.2), either has a non-zero component in the above mentioned 3D subspace (for $p > 0$), or does not have it (for $p = 0$) in which case there is no increase of the energy and coherence after the successful measurement, causing the discontinuity of the values at $p = 0$. This fact is taken into account in all our derivations and is stressed by the condition $p \neq 0$ in Eq. (4.7) and the following.

In addition, we do not consider a single TLS model at all for the sake of its simplicity. If we aimed to maximize energy only and coherence would be irrelevant, the conditional measurement strategy would work well for a single TLS, with the successful outcome $P_1 = |e_1\rangle\langle e_1|$. This strategy, however, removes all initial coherence of the TLS, therefore we coin it as "incoherent" in the following. If applied in parallel to a pair of TLS, two

independent successful events will project the pair into the state $|\Psi_f\rangle = |e_1 e_2\rangle$, with the success probability $p_{s,\text{incoherent}} = p^2$. It would be, once more, an incoherent strategy, erasing all initial coherence of the TLSs. Moreover, such success probability is, in the range of small excitation probabilities $p \ll 1$, remarkably smaller compared to $p_{s,\text{coherent}} = p(2-p)$, Eq. (4.8). If projector described in 3.2 is applied to a single TLS, it forces the state of a system to collapse to the excited state, thus increasing the energy of it however the coherence is lost in the process. It does not coin with the accomplishment of our aim, namely, the increase of coherence together with the energy of the system.

4.2 Dephasing and spontaneous emission

To test the robustness of the proposed protocol, we consider decoherence effects on our system to find out if the result of the previous section holds when imperfections of the system are encountered. Namely, in this section, we will consider the effects of spontaneous emission and pure dephasing processes on a system. Both of them lead to states with partial coherence described by reduction of the off-diagonal terms $Tr(\hat{\rho}^2) < 1$ and will be explored consequently in this section.

At first, we take into consideration the pure dephasing process [9, 73, 15] of TLSs constituting the system. It is the fast process resulting in the decay of the phase of the state of the system. The initial state, in this case, will be of the form

$$\begin{aligned}\hat{\rho}_j = p\,|e_j\rangle\langle e_j| + \epsilon\sqrt{p(1-p)}(|e_j\rangle\langle g_j| + |g_j\rangle\langle e_j|) + \\ +(1-p)\,|g_j\rangle\langle g_j|\,, \quad j = 1,2,\end{aligned} \tag{4.17}$$

where $0 \leq \epsilon < 1$ is the dephasing rate of the state of the system. The total

initial density matrix will be the direct product $\hat{\rho}_i = \hat{\rho}_1 \otimes \hat{\rho}_2$.

Application of the projector-based measurement statistics $\{\hat{P}_0, \hat{P}_1 = \hat{1} - \hat{P}_0\}$, (4.5) gives us following resulting states

$$\hat{\rho}_0 = \frac{\hat{P}_0 \hat{\rho}_i \hat{P}_0}{\sqrt{1-p_s}} = |gg\rangle \langle gg| , \tag{4.18}$$

$$\hat{\rho}_f = \frac{\hat{P}_1 \hat{\rho}_i \hat{P}_1}{p_s}, \quad p_s = p(2-p) \neq 0, \tag{4.19}$$

respectively, where the probability of success p_s of the dephased state equals to the probability of success of the pure state (4.8), independent of ϵ.

As dephasing affects only off-diagonal terms of the density matrix, the final energy of the resulting successful state is going to be similar to the case of pure state, Eq. (4.10).

On the other hand, the initial and final coherence of the state will be affected distinctly. The values of initial coherence $C_0 = C(\hat{\rho}_i) = \sum_j C(\hat{\rho}_j)$, Eq. (4.17) and final $C_f = C(\hat{\rho}_f)$, Eq. (4.19) are going to decrease resulting in the change of their difference $\Delta C = C_f - C_0$. The latter expressed in terms of initial coherence can be written as

$$\Delta C \approx \left(\frac{5-\epsilon}{10} \ln 2 - 1 \right) C_0 + \epsilon^2 \operatorname{arctanh} \epsilon^2 + \ln \sqrt{1-\epsilon^4}. \tag{4.20}$$

Following the same logic as in the previous section, we can find a value of coherence corresponding to $\Delta C = 0$

$$\tilde{C}_0 = \frac{\epsilon^2 \operatorname{arctanh} \epsilon^2 + \ln \sqrt{1-\epsilon^4}}{1 - \ln 2 \left(5-\epsilon\right)/10} \approx \frac{\epsilon^4}{2\left[1 - \ln 2 \left(5-\epsilon\right)/10\right]}, \tag{4.21}$$

where the last approximation stems form the fact that the numerator of the middle fraction can be well approximated by the function $\epsilon^4/2$ up to $\epsilon \approx 0.8$. We see, Fig. 4.3, that for decreasing ϵ the maximum value of coherence $\tilde{C}_0$ shifts to *lower* values of p.

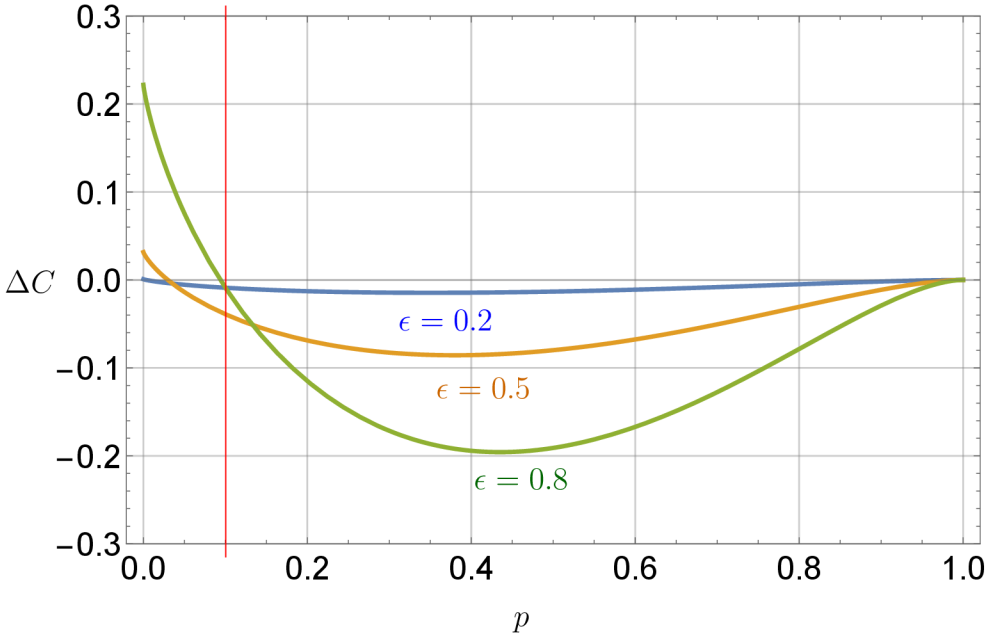

Figure 4.3: Plot of the difference between the final and initial relative entropy of coherence, $\Delta C = C_f - C_0$, Eq. (4.20), for a pair of TLS in partially-coherent states with different values of ϵ. The values are plotted versus the TLS excitation probability p, Eq. (4.17), again the red vertical line guides the eye for the value $p = 0.1$, as in Fig. 4.2. The final entropy of coherence can be conditionally increased above the initial one in a region of small excitation probabilities p, up to the point $\tilde{C}_0(\epsilon)$, cf. Eq. (4.21). The final and initial energy, E_f/E and E_0/E of the system are identical to the case of pure states, cf. Fig. 4.2, as energy is determined by diagonal terms of density matrix $\hat{\rho}$ only and is independent of ϵ.

Now we switch our attention to the other type of decoherence, namely, spontaneous emission [9, 73, 15]. As it affects an amplitude of the pure state, therefore, the state of the system (4.17) will change to

$$\overline{\hat{\rho}}_i = \Big\{ [(1-p)+\eta p]\,|g_1\rangle\langle g_1| + \sqrt{1-\eta}\sqrt{p(1-p)}(|g_1\rangle\langle e_1| + |e_1\rangle\langle g_1|) + \\ +(1-\eta)p\,|e_1\rangle\langle e_1| \Big\} \otimes \Big\{ [(1-p)+\eta p]\,|g_2\rangle\langle g_2| + \sqrt{1-\eta}\sqrt{p(1-p)}(|g_2\rangle\langle e_2| + \\ + |e_2\rangle\langle g_2|) + (1-\eta)p\,|e_2\rangle\langle e_2| \Big\}, \quad 0 \le \eta \le 1. \tag{4.22}$$

where η is the probability of the emission process.

Subjecting this state to the projector based charging procedure $\{\hat{P}_0, \hat{P}_1 = \hat{1} - \hat{P}_0\}$, Eq. (4.5), yields successful post-measurement state

$$\overline{\hat{\rho}}_f = \frac{\hat{P}_1 \overline{\hat{\rho}}_i \hat{P}_1}{\overline{p}_s}, \quad \overline{p}_s = (1-\eta)p[2-p(1-\eta)] \neq 0. \tag{4.23}$$

where $\overline{p}_s$ is the updated probability of success for the amplitude-damped state.

As in this case, even the diagonal terms are affected by spontaneous emission, therefore, the initial and final energy will change accordingly

$$\overline{E}_0 = E\,[2p(1-\eta)-1]\,, \tag{4.24}$$

$$\overline{E}_f = E\left[\frac{2}{p(\eta-1)+2} - 1\right]. \tag{4.25}$$

The plot of the above mentioned values can be found in a Fig. 4.4.

As in the previous lines it is more useful to show the approximate result for coherence change ΔC, Eq. (3.8), than the individual summands, yielding

$$\Delta\overline{C} \approx \left[\frac{2\ln 2}{5}\left(1+\frac{5}{2}\eta\right) - 1\right]\overline{C}_0 + \ln 2, \tag{4.26}$$

a good approximation for $0 \le \eta \le 1/3$. The interesting fact that $\Delta\overline{C}$ increases with η stems from the different speed at which $\overline{C}_0$ and $\overline{C}_f$ decrease with η. This opens the gap $\Delta\overline{C}$ between them and simultaneously

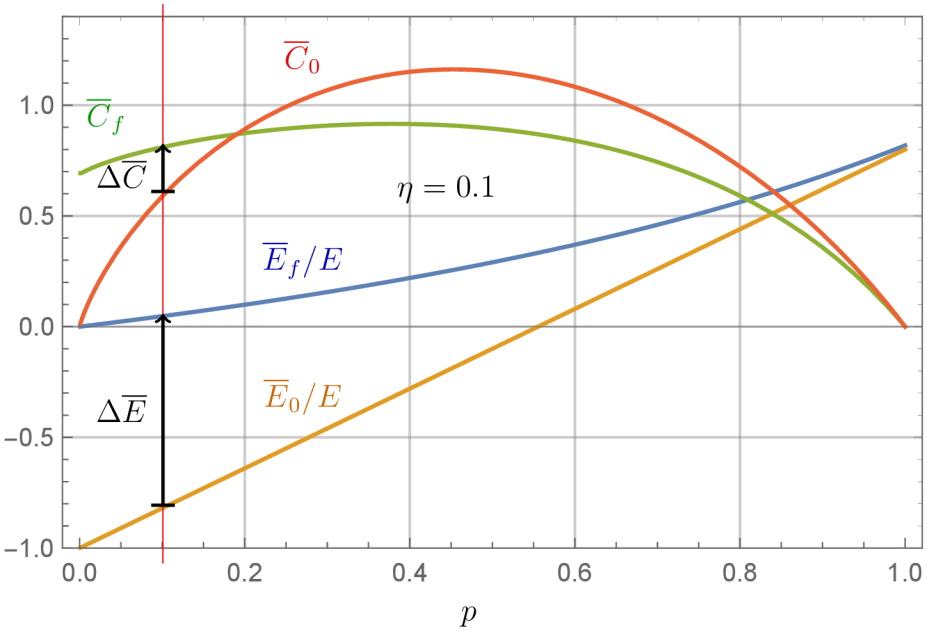

Figure 4.4: The plot of the normalized average energy $\overline{E}_f/E$, $\overline{E}_0/E$ and the relative entropy of coherence $\overline{C}_f$, $\overline{C}_0$ for the final state $\overline{\hat{\rho}}_f$, Eq. (4.23), and the initial state $\overline{\hat{\rho}}_i$, Eq. (4.22), with spontaneous emission probability $\eta = 0.1$. The values are plotted versus the TLS excitation probability p, Eq. (4.1), the red vertical line guides the eye for the value $p = 0.1$, and the blue arrows express the coherence and energy increase. The conditional increase of the final energy over the initial one, $(\overline{E}_f - \overline{E}_0)/E > 0$, is achieved with maximum in the region of small p. The final coherence can be conditionally increased above the initial one in a region with η dependent boundary.

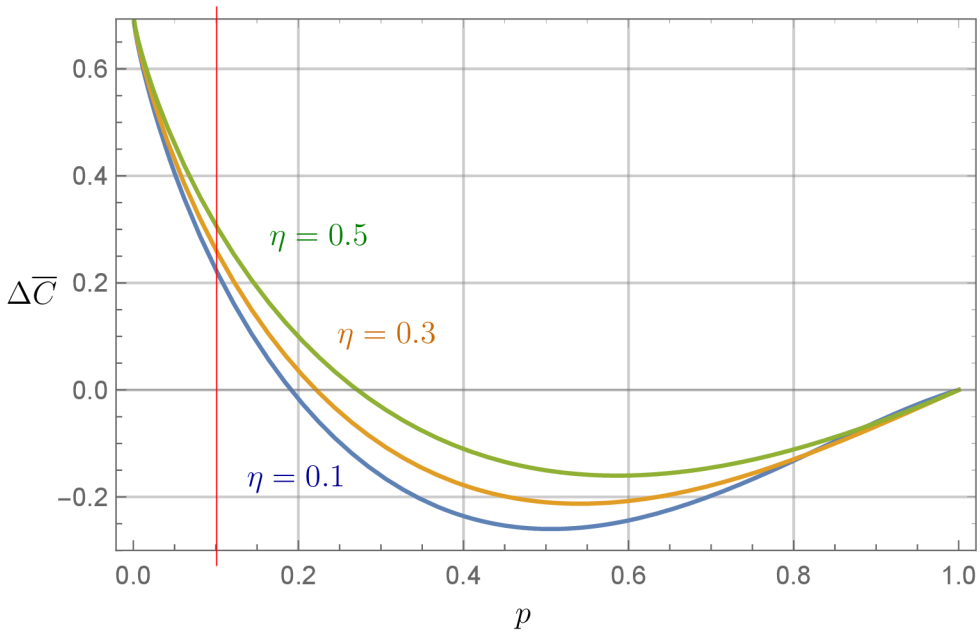

Figure 4.5: The plot of the difference between the final and initial coherence, $\Delta\overline{C} = \overline{C}_f - \overline{C}_0$, Eq. (4.26), for a pair of TLS in states after spontaneous emission with different values of η. For $\eta \ll 1$ one finds the increase in the region of small excitation probabilities p (the red vertical line guides the eye for the value $p = 0.1$) up to the point $\tilde{C}_0$, Eq. (4.27). Remarkably, for increasing η, $\Delta\overline{C}$ increases as well, which comes at the expense of the corresponding probability of success p_s, Eq. (4.23).

increases the lower-value crossing point, $C_f = C_0$, in which the charging protocol stops increasing the coherence. This value reads (if such point of coincidence exists), see Fig. 4.5,

$$\tilde{C}_0 \approx \ln 2 \left[1 - \frac{2\ln 2}{5}\left(1 + \frac{5}{2}\eta\right)\right]^{-1}. \tag{4.27}$$

Comparison of Eqs. (4.21) and (4.27) reveals one striking difference. Although both processes (dephasing and spontaneous emission) of the initial states decrease the initial value of coherence C_0 in a similar way, the effect of charging yields results with qualitatively opposite behavior. Whereas lowering ϵ, Eq. (4.17), quickly *decreases* $\tilde{C}_0$ (Fig. 4.3), the increase of η, Eq. (4.22), leads to the *increase* of $\tilde{C}_0$ (Fig. 4.5).

4.3 Protocol optimisations by POVM

In this section, we generalise the projector-based measurement protocol to POVM-based one. This is done in order to optimize the results obtained by the usage of projective measurement, namely the simultaneous coherence and energy gains ΔC and ΔE. It is known that generalized measurements, positive-operator-valued-measures (POVMs), can be useful if a compromise between incompatible features has to be found.Due to fundamentally different properties of POVMs [9] (see Sec. 2.2), namely, their unrepeatability $\hat{M}\hat{M} \neq \hat{M}$, we can expect our results to be improved.

To check our expectations, we numerically generalize and optimize the charging protocol for the use of generalized measurement elements, c.f. Eq. (4.5), of the form $\{\hat{M}_0, \hat{M}_1 = \hat{1} - \hat{M}_0\}$ with

$$\hat{M}_0 = a\,|g_1g_2\rangle\langle g_1g_2| + b\,(|g_1e_2\rangle\langle g_1e_2| + |e_1g_2\rangle\langle e_1g_2|), \quad 0 \leq a, b \leq 1, \tag{4.28}$$

applied to the pure initial state, Eq. (4.2).

We can observe following properties from Eq. (4.28):

1. When substituting $a = 1$, $b = 0$ the generalised measurement collapses to the previous case of projective measurement;

2. In the case $a = 1$, $b = 1$, s clearly an optimal choice for maximizing the final energy, as it results in removing all the populations except those of the state $|e_1 e_2\rangle$, that corresponds to analogy of the successful state (4.7) with maximum energy, but certainly zero coherence in the energy eigenbasis.

It should be stressed that Eq. (4.28) complies with the requirement of being diagonal in the energy eigenbasis, hence, representing a justified generalisation to the case of POVM.

Note, if $a = b^2$ there is one more interesting feature of POVM (4.28), it can be rewritten as

$$\hat{M}_0 = \hat{M}_0^{(1)} \otimes \hat{M}_0^{(2)} \tag{4.29}$$

a product of a POVM acting on a single TLS [74]. In other words, the final state after the action of the POVM is also separable. Therefore, (4.28) in this case it increases coherences locally on each TLS resulting into the $\Delta C_m = 0$ (this discovery was a springboard for usage a measure of mutual entropy in further work, see Chap. 5). As a conclusion, in order to increase coherence globally we need non-separable type of generalised measurements, Sec. 2.2.

The results were calculated numerically and due to their cumbersome form we present them only graphically. They present the optimized values of final coherence and energy versus the probability of excitation p. The optimisation was done over a certain range of parameters a, b.

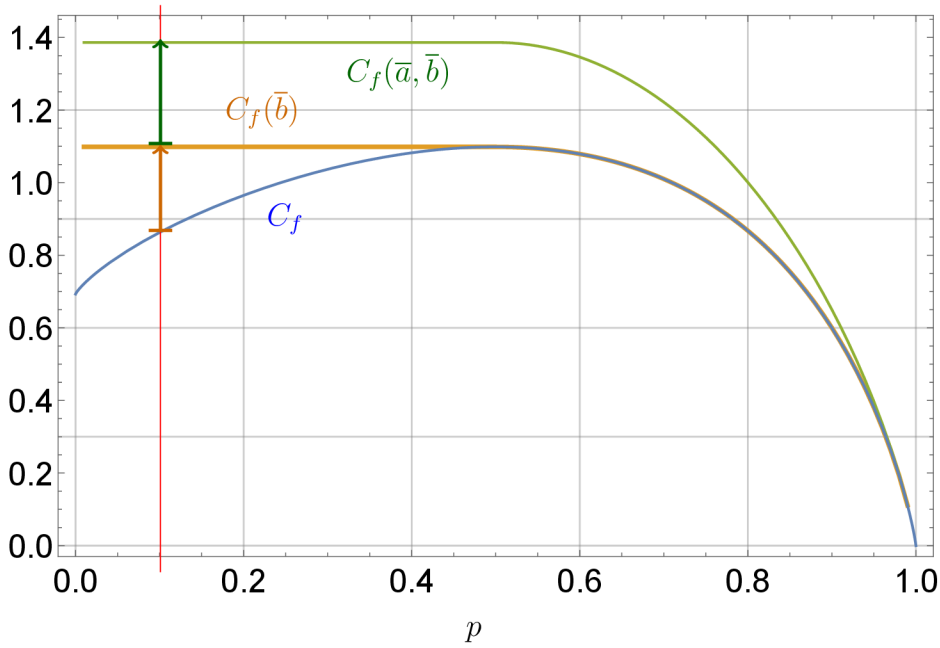

Figure 4.6: Plots of the optimal coherence after the charging for general POVM (green), cf. Eq. (4.28), and its restricted class with $a = 1$ (orange), applied to the initial state $|\Psi_i\rangle$, Eq. (4.2). These are compared to blue line C_f from Fig. 4.2, respectively. The relation of optimal values of parameters $\overline{a}$ and $\overline{b}$ for which the final coherences $C_f(\overline{b})$ and $C_f(\overline{a},\overline{b})$ are maximized is given as $\overline{b} = 1-\sqrt{1-\overline{a}}$. The coherence $C_f(\overline{a},\overline{b})$ (green line), for the general type of POVM, shows substantial increase over the whole range of p (e.g., green arrow for $p = 0.2$ in Fig. 4.6). The result for restricted type of POVM (orange line) show increase of the coherence values (e.g., orange arrow for $p = 0.2$ in Fig. 4.6) over the interval of $p < 1/2$, with respect to the simple projector case, Eq. (4.5).

Figures 4.7 and 4.6 represent the results for two specific types of POVMs: the first one, determined by the arbitrary values of $0 \leq a, b \leq 1$ and, therefore, dubbed as a general; the second with $a = 1$, $0 \leq b \leq 1$, dubbed as a restricted one. The choice was dictated by the values to be optimized, whether it is a coherence only or an advantageous ratio between the coherence and energy gains. Both types of POVMs are compared to projector case $a = 1$, $b = 0$.

The optimisation process for both types of protocol was made with respect to the final coherence value C_f, Eq. (3.6). Therefore, the general type of POVM, Eq. (4.28), was optimized over parameters a, b, resulting into the most advantageous option $C_f(\overline{a}, \overline{b})$, where the relation between parameters $\overline{a}$ and $\overline{b}$ is defined as $\overline{b} = 1 - \sqrt{1 - \overline{a}}$. Substituting latter to the general form of POVM, Eq. (4.28), we get the coherence-maximising POVM

$$\hat{K_0} = \overline{a} \left|g_1 g_2\right\rangle \left\langle g_1 g_2\right| + (1 - \sqrt{1 - \overline{a}}) \left(\left|g_1 e_2\right\rangle \left\langle g_1 e_2\right| + \right.$$
$$\left. + \left|e_1 g_2\right\rangle \left\langle e_1 g_2\right|\right), \quad 0 \leq \overline{a} \leq 1, \tag{4.30}$$

whereas the relationship between the optimal value $\overline{a}$ and the excitation probability p can be well approximated by the polynomial dependence $\overline{a} \approx 1 - 3/2p^2 - 8p^4$ in the interval $0 \leq p \leq 2/5$. Similarly, the second type of POVM was optimized over a single parameter b to reach the corresponding maximal final coherence value $C_f(\overline{b})$ with the parameter $\overline{b}$.

The result for the general type of POVM gives the maximum increase of the coherence equal to $C_f(\overline{a}, \overline{b}) \approx \ln 4$. The corresponding final energy for these parameters is plotted in Fig. 4.6 and is noticeably smaller than in the case of the projector, c.f. 4.2. On the other hand, the restricted type of POVM result shows a distinguishable increase of both final energy and coherence over the projector case, therefore, constituting a compromise

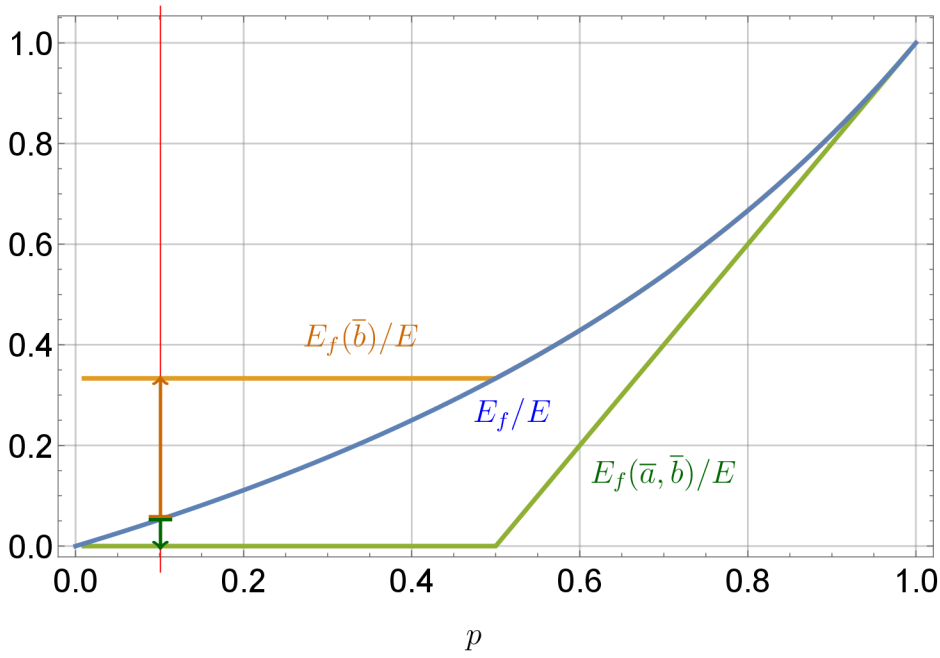

Figure 4.7: Plots of the optimal energy after the charging for general POVM (green), cf. Eq. (4.28), and its restricted class with $a = 1$ (orange), applied to the initial state $|\Psi_i\rangle$, Eq. (4.2). These are compared to blue lines showing E_f/E from Fig. 4.2, respectively. The energy values are given for optimal values of parameters $\overline{a}$ and $\overline{b}$ for which the final coherences $C_f(\overline{b})$ and $C_f(\overline{a},\overline{b})$ are maximized. The highest coherence $C_f(\overline{a},\overline{b})$ value (see green line in Fig. 4.6) is compensated by smaller increase in the energy compared to the simple projection, Eq. (4.5) (e.g., green arrow for $p = 0.2$ in Fig. 4.7). The result for restricted type of POVM (see orange line in Fig. 4.6) with the coherence $C_f(\overline{b})$ shows simultaneous improvement of the post measurement energy values (e.g., orange arrow for $p = 0.2$ in Fig. 4.7) on the same interval of p, with respect to the simple projector case, Eq. (4.5).

optimisation. The final coherence value in this case reaches $C_f(\overline{b}) = \ln 3 < \ln 4$. Both final energy and coherence are increased in the range of small excitation probability range $0 \leq p \leq 1/2$.

Additionally, it is worth to mention that although we are interested in increasing coherence of the *total* system (pair of TLS) for certain values of parameters a, b the individual (local) coherence of each TLS is increased as well. However, the comparison of local and global coherences is more relevant and explored in the next chapter with pairwise protocol, see Chap. 5.

To summarize this section, we found that due to the presence of additional free parameters a, b, Eq. (4.28) allows for subsequent optimization and, therefore, POVM based strategy offers more advantageous options compared to the simple projector based protocol. We have presented two different types of results. Depending on the aim of the optimisation, POVM can allow for increase of both $E_f(\overline{b})$ and $C_f(\overline{b})$ over the corresponding projector values or the final coherence $C_f(\overline{a}, \overline{b})$ above the projector value C_f only, however drawn back with simultaneous decrease of $E_f(\overline{a}, \overline{b})$ below E_f, see Fig. 4.7. We would like to note, that although POVMs have a similar positive effect (increased average energy and coherence) as the projectors, they may on the other hand increase the variance of energy. This fact underlines the qualitatively different nature of POVMs compared to projection measurements.

4.4 Generalisation to N-TLS

In this section, we generalise the result to N TLS system. For simplicity, we consider them in pure states, Eq. (4.1), yielding the total initial state of

the system

$$|\Psi_i^{(N)}\rangle = \bigotimes_{j=1}^{N} |\psi_j\rangle, \tag{4.31}$$

where $j = 1, \cdots, N$ labels the copies of TLS.

The Hamiltonian of the system comprises the Hamiltonians of independent TLS, Eq. (3.1), and equals to Eq. (3.3).

Subsequently, the initial energy of the system is given by a straightforward due to its additivity generalization of Eq. (4.3), yielding

$$E_0^{(N)} = \frac{NE_0}{2} = \frac{NE}{2}(2p-1). \tag{4.32}$$

The charging process in the same way as in the previous sections consists of application of a pair of global projectors
$\{\hat{P}_0^{(N)},\ \hat{P}_1^{(N)} = \hat{1} - \hat{P}_0^{(N)}\}$, where

$$\hat{P}_0^{(N)} = \bigotimes_{j=1}^{N} |g_j\rangle \langle g_j|, \quad \hat{P}_1^{(N)} = \hat{1} - \hat{P}_0^{(N)}, \tag{4.33}$$

is the projector on the global ground state of the system, cf. Eq. (4.5).

Application of the projector $\hat{P}_1^{(N)}$ to the state (4.31) results in successfully charged state

$$|\Psi_f^{(N)}\rangle = \frac{\hat{P}_1^{(N)} |\Psi_i^{(N)}\rangle}{\sqrt{p_s^{(N)}}}, \tag{4.34}$$

with the probability of success $p_s^{(N)}$

$$p_s^{(N)} = 1 - (1-p)^N \neq 0, \tag{4.35}$$

converging to 1 with N, for any finite $p \neq 0$, and the corresponding energy of the final, successful state

$$E_f^{(N)} = \frac{NE}{2}\left[\frac{2p}{1-(1-p)^N} - 1\right]. \tag{4.36}$$

From these results we obtain an upper bound on the energy increase

$$\Delta E^{(N)} \equiv E_f^{(N)} - E_0^{(N)} = E\left[\frac{Np(1-p)^N}{1-(1-p)^N}\right] \approx E(1-Np) \leq E,$$
$$p \ll 1,\ N \gg 1. \tag{4.37}$$

The final energy $E_f^{(N)}$, Eq. (4.36), after the charging process as a function of p, parameterised by the number N of TLS, is plotted in Fig 4.8 and Fig 4.9, where we present the results for pure initial states of $N = 3$ and $N = 4$ TLS, see Fig. 4.8 and Fig. 4.9, respectively. By comparison to results for a pair of TLS, Fig. 4.2, we can see the behavior of the final energy $E_f^{(N)}$ with the growth of N. The final energy in the case of successful charging is increased for all p, however, the energy gain reads $\Delta E^{(N)} \leq E$, and it is thus upper bounded by the energy gap E for all N. Thus, the goal of the charging protocol (energy increase) is achieved, although the change of the energy *relative* to the total initial energy available, Eq. (4.32), is decreasing as $|\Delta E^{(N)}/E_0^{(N)}| \propto N^{-1}$ in the range $p \ll 1$, where the energy increase is maximum.

The expression for the final coherence $C_f^{(N)}$ for the successful measurement outcome in the case of pure initial state (4.31) (the term corresponding to the von Neumann entropy vanishes) reads

$$C_f^{(N)} = -\sum_{k=1}^{N} \binom{N}{k} \frac{p^k(1-p)^{N-k}}{1-(1-p)^N} \ln\left[\frac{p^k(1-p)^{N-k}}{1-(1-p)^N}\right],$$
$$\lim_{p\to 0} C_f^{(N)} = \ln N, \tag{4.38}$$

and should be compared to the coherence of the initial pure state, Eq. (4.31),

$$C_0^{(N)} = -\sum_{k=0}^{N} \binom{N}{k} p^k(1-p)^{N-k} \ln\left[p^k(1-p)^{N-k}\right]. \tag{4.39}$$

The examples of coherence, $C_f^{(N)}$ and $C_0^{(N)}$, are plotted in Fig. 4.8 and Fig. 4.9. Their difference increases with N, contrary to the behavior of

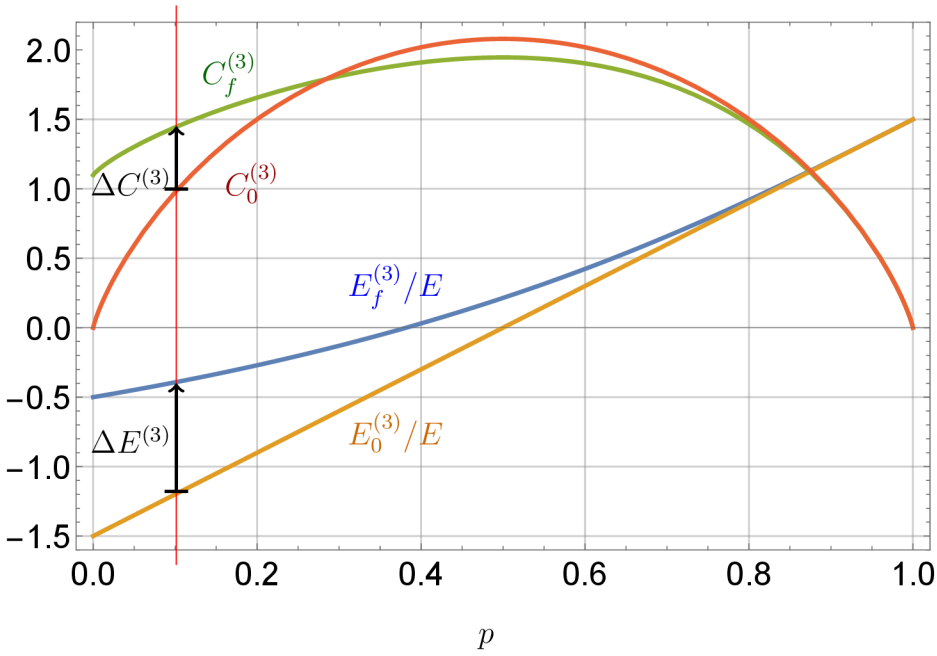

Figure 4.8: The plot of the normalized average energy $E_f^{(N)}/E$ (4.36), $E_0^{(N)}/E$ (4.32), and the relative entropy of coherence $C_f^{(N)}$ (4.38), $C_0^{(N)}$ (4.39), for the final state $|\Psi_f^{(N)}\rangle$, Eq. (4.34), and the initial state $|\Psi_i^{(N)}\rangle$, Eq. (4.31), for $N = 3$ TLS. The values are plotted versus the higher level excitation probability p, Eq. (4.1). The average energy gain, $0 \leq E_f^{(N)} - E_0^{(N)}$, is achieved with maximum for $p \to 0$. The final entropy of coherence $C_f^{(N)}$ can be conditionally increased above the initial one $C_0^{(N)}$ in a region of small excitation probabilities p. The red vertical line is a guide for the eye at $p = 0.1$ and the black arrows indicate the energy and coherence increase for each respective N.

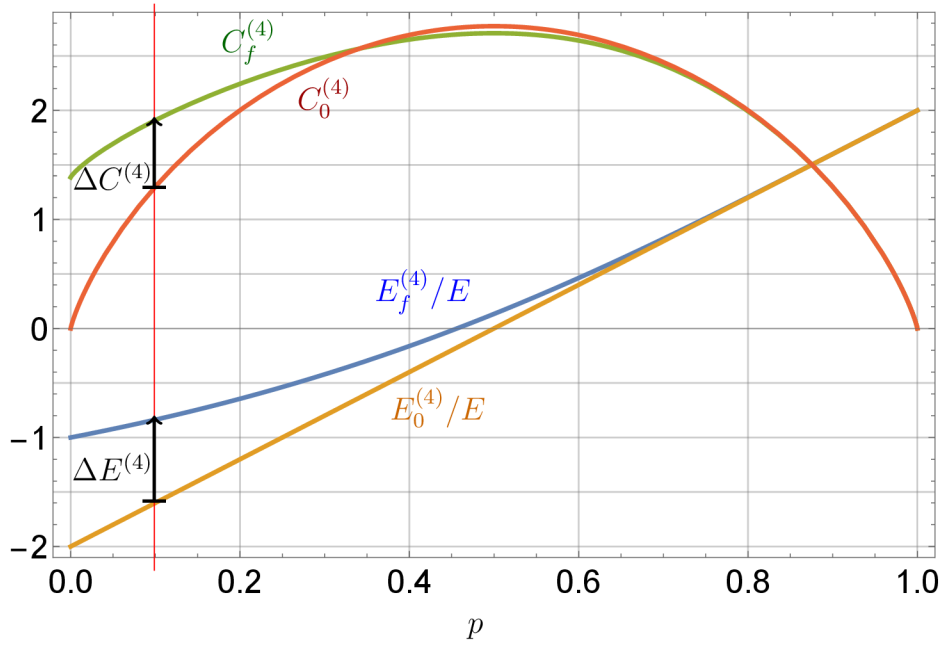

Figure 4.9: The plot of the normalized average energy $E_f^{(N)}/E$ (4.36), $E_0^{(N)}/E$ (4.32), and the relative entropy of coherence $C_f^{(N)}$ (4.38), $C_0^{(N)}$ (4.39), for the final state $|\Psi_f^{(N)}\rangle$, Eq. (4.34), and the initial state $|\Psi_i^{(N)}\rangle$, Eq. (4.31), for $N = 4$ TLS. The values are plotted versus the higher level excitation probability p, Eq. (4.1). The gain of coherence $\Delta C^{(4)} > \Delta C^{(3)} > \Delta C^{(2)}$ increases with the number N of TLS constituting the battery, whereas the energy gain is limited by $E_f^{(N)} - E_0^{(N)} \leq E$ for every N, see Eq. (4.37). The red vertical line is a guide for the eye at $p = 0.1$ and the black arrows indicate the energy and coherence increase for each respective N.

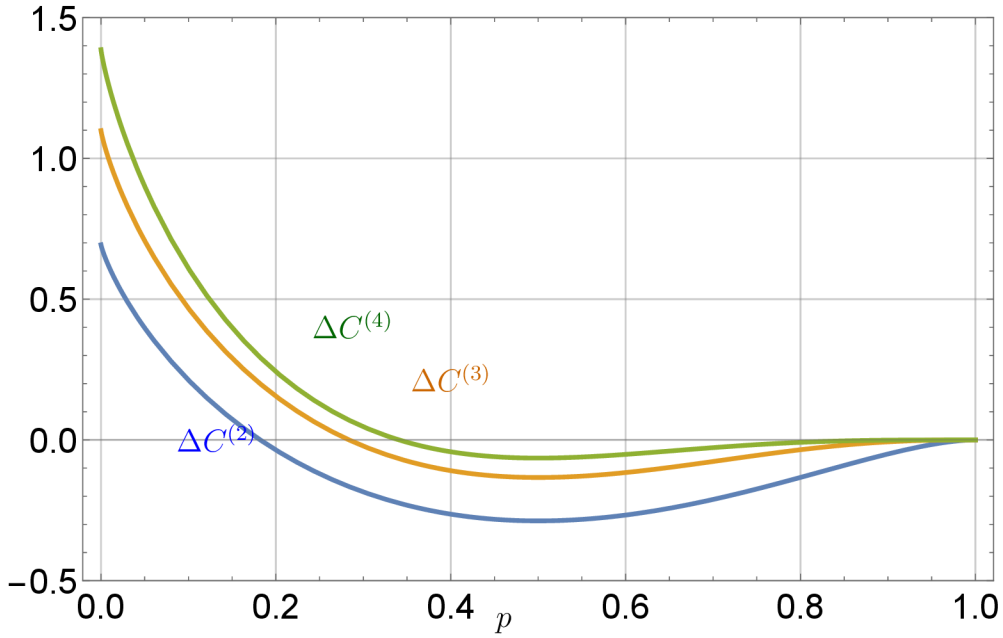

Figure 4.10: The gain of coherence $\Delta C^{(4)} > \Delta C^{(3)} > \Delta C^{(2)}$ increasing with the number N of TLS constituting the battery.

$\Delta E^{(N)}$, as well as the range of the excitation probabilities p in which $\Delta C^{(N)} \equiv C_f^{(N)} - C_0^{(N)} \geq 0$. Notably, this last property is positive due to the fact that the higher N we use, the less we are restricted by the choice of parameters for which we observe the positive effect of the charging protocol, i.e., the energy $E_f^{(N)}$ *and* coherence $C_f^{(N)}$ increase, over the respective initial values. Moreover, it follows from Eqs. (4.38)-(4.39) that for fixed initial state excitation probability p, Eq. (4.1), we obtain

$$\Delta C^{(N)} > \cdots > \Delta C^{(3)} > \Delta C^{(2)}, \tag{4.40}$$

and the crossing points $\Delta C^{(N)} = 0$ are shifting towards larger excitation probabilities p, see Fig. 4.10. It is worth noting, that $\lim_{p\to 0} C_f^{(N)}(p) = \ln N$ is monotonically increasing with the number of TLS. However, taken relative to the maximum achievable coherence in the system of N TLS, $C_{\max}^{(N)} =$

$N \ln 2$, the ratio $C_f^{(N)}(0)/C_{\max}^{(N)}$ approaches zero for increasing N. This result can be interpreted as the inability to fully exploit the values of coherence offered by increasing the dimension of our system with the present protocol in the region of $p \ll 1$. On the other hand, in the region $p \approx 1/2$ the post-measurement coherence value $C_f^{(N)}(1/2)$ approaches monotonically the value $C_{\max}^{(N)}$ with increasing N, c.f. Fig 4.8 and Fig 4.9.

4.5 Conclusions

We have presented a protocol for the repeat-until-success charging and synthesizing of the quantum battery by means of a global quantum measurement diagonal in the energy basis. The building blocks of our battery are factorized copies of identical two-level systems (TLS) with nonzero, although possibly very small, population of the excited state, and some small residual coherence that can be achieved by a suitable interaction with a sufficiently cold thermal bath [68, 69, 70, 71, 72]. A pair of TLS subsequently undergoes a global, unity-resolving measurement with two possible outcomes, each represented by an operator diagonal in the TLS energy basis.

If the protocol succeeds, we synthesize the initially independent pair of TLS into a system with non-factorized state and higher coherent energy, thus creating and charging the battery simultaneously. The failure of the protocol results in reducing the initial energy and coherence to zero. These two possibilities represent the outcomes of the inherently conditional protocol, however with the possibility of increasing the success probability arbitrarily close to one (using repeat-until-success strategy), making the protocol effectively approach to a deterministic one. Our results show that

the dephasing and/or spontaneous emission of the energy of the initial state decreases the positive effect of the charging, but does not prevent the charging in principle. The variance of energy is alos positively decreased in this type of charging protocol.

The results of the projector-based charging protocol were generalized to the case of using N-TLS, either in a global or pairwise measurement approach. The final value of the coherent energy can be increased even more, due to optimization, if the measurement consists of POVM elements. Such protocol is superior in the value of coherence and energy with respect to the results of the projective measurement. The results stimulated proof-of-principle experimental verification of such energy synthesizing using controlled quantum systems[74] in Olomouc Quantum Laboratory. To verify the observability of simultaneous energy and coherence increase, experimental tests can be further implemented using photons [75, 76, 77, 78], employing such optical toolbox also with atoms [79, 80, 81], or solid-state systems [82, 83]. The implementation of measurement strategy for another experimental platforms is under development. This optical experimental tests would stimulate quantum thermodynamic analysis [56, 84] of such synthesis, already used to analyze energy manipulations [85, 86, 87].

We have verified that many paths are open to synthesize energy in coherent quantum battery for further optimization. This optimization is a demanding top-to-bottom task, therefore, it has to be solved numerically, with taking into account the details of particular experiment. This was confirmed in the first experimental test [74].

Chapter 5

Energy and coherence synthesis by a pairwise protocol

A global protocol, presented in the previous chapter has several drawbacks, few of the main described below:

- independent of the number N of TLS constituting a battery the amount of possible increase of energy is limited by the energy gap E of a single TLS;
- the protocol requires a single global projective measurement over a system that can be challenging to implement experimentally for large N TLS;

therefore, to improve these downsides in the current chapter we present a modified approach with multiple measurements of TLS over pairs named as pairwise protocol [88].

We substantially increase the protocol feasibility by changing the universal projection-based protocol globally applied to the system of N weakly coherent, non interacting TLS (inspired by [35, 89], where all TLS are con-

sidered initially almost in their ground states [67]), to many pairwise projections on the same TLSs. Moreover, we focus on keeping the universal protocol character mentioned in the previous paragraph. These are applied in a sequential manner, synthesizing factorized TLS into a higher-dimensional coherent system, while increasing its energy and coherence jointly. The pairwise approach is experimentally accessible, as no complex, multi TLS projection is needed. Notably, the simultaneous energy and coherence (with respect to energy eigenbasis) increase, is universally gained by using diagonal pairwise projectors independently of the input weakly excited states. We consider the choice of energy eigenbasis as a natural reference for coherence evaluation, being inspired, e.g., by works on quantum batteries [35, 89], which are originally the energy storage devices. As such, their quantum mechanical properties should be studied with respect to this basis as well. Other methods employ the projection-based manipulations as well, but utilize them for different purposes, such as, e.g., the stabilization process of an open quantum battery [51].

Our simultaneous study of energy and coherence gain is complemented by the interest in the behavior of *mutual (correlated) coherence* [53, 90, 91, 92, 93]. The mutual coherence allows us to distinguish the contributions to the coherence from the global (N-partite) state of our system and the individual contributions originating from all local states, obtained by partial tracing-out of the remaining TLS. From a thermodynamic perspective, mutual coherence also quantifies the difference in work extracted from a given state globally vs. locally if certain thermodynamic process is performed [56]. By virtue of using such quantity, we show that our conditional protocol is (in the case of successful outcome) capable of *simultaneous* increase of the system energy, coherence, and, remarkably, also a

mutual coherence. Thus, it transforms the factorized initial state of the system into a more coherent, non-factorizable final state. The coherence gain scales (for low excitation) as an increasing logarithmic function of N, while energy increases with N linearly for the pairwise protocol studied here.

We test as well, if the protocol retains its function while the effect of local dephasing reduces the coherence of the initial system state progressively. The same test is performed regarding the effect of dephasing on the final (resulting) state of the protocol. In both cases the results suggest that the protocol function sustains such effect of environment.

However, here we skip a full analysis of a simple scenario of a pair of TLS as it was thoroughly analyzed in the previous chapter and the results hold for current pairwise protocol as well. Hence, we move directly to the system of N copies of TLS.

5.1 Pure states

For the sake of avoiding repeating the same information, we start with a system of N copies of TLS in pure states, described in the last section 4.4 of the previous chapter.

The main difference constitutes the measurement process, namely, in this case we have repeated projective measurements over pairs of TLS. Therefore, we denote the pair of complementary projectors $\{\hat{P}_0^{(j,k)},\ \hat{P}_1^{(j,k)}\}$

$$\hat{P}_0^{(j,k)} = |g_j g_k\rangle \langle g_j g_k|, \quad \hat{P}_1^{(j,k)} = \hat{1} - \hat{P}_0^{(j,k)}, \tag{5.1}$$

where subscripts “0” and “1” stand for failure and success, respectively. These projectors act on a pair of j-th and k-th TLS.

There is no specific requirement on the sequence of measuring of TLS, hence, they can paired in an arbitrary fashion. However, for the sake of simplicity we consider the general case of measuring TLS in successive pair sequence, i.e., the first and the second TLS, then the second and the third, etc (see Fig. 5.1).

In any scenario, the total projector on N-TLS, $\hat{P}_1^{(N)}$, is invariant with respect to completely successful measurement sequence and constitutes the product of local projectors $\hat{P}_1^{(j,k)}$

$$\hat{P}_1^{(N)} = \prod_{\substack{j=1 \\ k=j+1}}^{N} \hat{P}_1^{(j,k)}, \quad \hat{P}_0^{(N)} = \hat{1} - \hat{P}_1^{(N)}. \tag{5.2}$$

On the other hand, the projector $\hat{P}_0^{(N)}$ corresponds to an unsuccessful scenario, where either at least one measurement or all of the measurements of pairs failed.

In other words, the order in which we measure the pairs of TLS does not play any role as in the end it will not affect the final state of the system, as the different projectors (5.1) commute.

Application of the projector $\hat{P}_1^{(N)}$ to the state (4.31) results in the successfully charged state

$$|\Psi_f^{(N)}\rangle = \frac{\hat{P}_1^{(N)} |\Psi_i^{(N)}\rangle}{\sqrt{p_s^{(N)}}}, \tag{5.3}$$

with the following probability of success $p_s^{(N)}$, corresponding final energy $E_f^{(N)}$, and final coherence $C_f^{(N)}$ of the state, respectively

$$\begin{aligned} p_s^{(N)} = &\sum_{k=0}^{1} \binom{N}{k} p^{N-k} (1-p)^k \\ &+ \sum_{k=2}^{t} \binom{N-k+1}{k} p^{N-k} (1-p)^k \neq 0, \end{aligned} \tag{5.4}$$

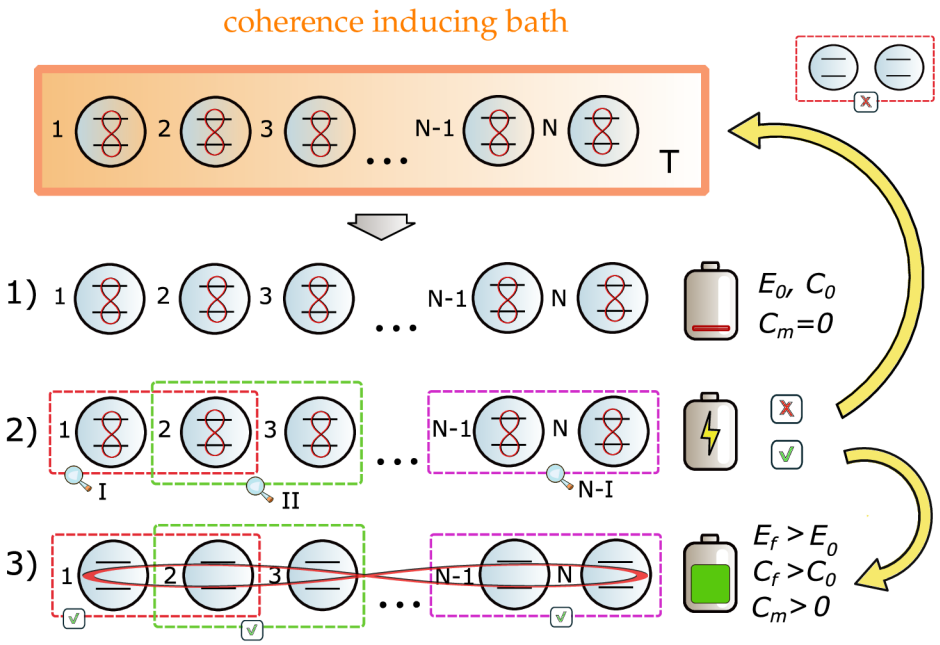

Figure 5.1: Schematics showing the idea of N-TLS coherence synthesis in three steps. **1)** TLS leave a low-coherence inducing bath [68] assumed to be almost discharged with low initial energy $E_0^{(N)}$ and coherence $C_0^{(N)}$ (marked by red loops connecting the levels). **2)** *Conditional* stage of the synthesis operation where measurements on pairs of TLS in a sequence marked by $\{\mathrm{I}, \mathrm{II}, ...\}$ are performed. If all of them are successful with the single run probability of success $p_s^{(N)}$, the coherence is synthesized $C_f^{(N)} > C_0^{(N)}$ and the system has higher energy $E_f^{(N)} > E_0^{(N)}$ as well, both with respect to the eigenbasis of Hamiltonian (3.3). **3)** TLS constituting the system become correlated (represented by a large red loop in step 3). Moreover, the mutual coherence, Eq. (2.23), increases, $\Delta C_m^{(N)} > 0$. If the outcome of step 2 is unsuccessful, with the single run probability $p_f^{(N)} = 1 - p_s^{(N)}$, the system is completely discharged and incoherent. To achieve a successful synthesis, TLS can be recycled by bringing them in contact with the bath again and the protocol is *repeated until success* (RUS).

$$E_f^{(N)} = \frac{E}{2\, p_s^{(N)}} \Bigg[\sum_{k=0}^{1} \binom{N}{k} (N-2k)\, p^{N-k}\, (1-p)^k + \sum_{k=2}^{t} \binom{N-k+1}{k} (N-2k)\, p^{N-k}\, (1-p)^k \Bigg], \tag{5.5}$$

$$C_f^{(N)} = -\sum_{k=0}^{1} \binom{N}{k} \frac{p^{N-k}\,(1-p)^k}{p_s^{(N)}} \ln \left[\frac{p^{N-k}\,(1-p)^k}{p_s^{(N)}} \right] - \sum_{k=2}^{t} \binom{N-k+1}{k} \frac{p^{N-k}\,(1-p)^k}{p_s^{(N)}} \ln \left[\frac{p^{N-k}\,(1-p)^k}{p_s^{(N)}} \right], \tag{5.6}$$

where $t = (N+1)/2$ if the number of TLS N is odd and $t = N/2$ if N is even. Due to the complex form of the results (5.4)-(5.6) valid for the pure initial states (4.31) only, we will present an approximate version of these quantities suitable for $p \ll 1$ region, see Sec. 5.2, and provide graphical representation of the results for mixed states dephased due to the presence of environment, see Sec. 5.5.

Further, we inquire whether the protocol (5.2) increases the energy (5.7), $\Delta E^{(N)} > 0$, as well as the coherence (5.8), $\Delta C^{(N)} > 0$. Namely, we are interested in the energy gain, or the difference between the final successful state and initial states, see Eq. (4.32) and Eq. (5.5), respectively,

$$\Delta E^{(N)} \equiv \frac{E_f^{(N)} - E_0^{(N)}}{E}, \tag{5.7}$$

normalised by energy gap E, see Fig. 5.2. Secondly, we take into account the coherence gain, where the expression for the final coherence $C_f^{(N)}$ (5.6) of the successful measurement outcome should be compared to the coherence of the initial pure state (4.4) yielding the definition of the coherence increase

$$\Delta C^{(N)} \equiv C_f^{(N)} - C_0^{(N)}, \tag{5.8}$$

whereas the complete expression is omitted here for the sake of simplicity. It should be mentioned that the term corresponding to the von Neumann entropy vanishes for pure initial states.

Based on observation made by comparison of Fig. 5.3-5.4, we point out one more positive aspect of the proposed protocol. The change of mutual coherence gives an additional information about the protocol's effect on the system coherence. If we compare Fig. 5.3 to Fig. 5.4 we can notice that for larger numbers N of TLS the gain of mutual coherence is larger than corresponding coherence gain. This suggests that the part of global coherence of the system of N TLS is increased. Therefore, not only the charging protocol increases the coherence of the total system, but it also transforms (consumes) the initial coherence (which equals to the sum of local coherences) into qualitatively different global final coherence. More formally, using the definitions in Eq. (2.23) and Eq. (5.8) and labeling the local coherence according to Eq. (2.23) by "$(N)loc$" superscript and all coherences by subscripts "f" and "0" for final and initial state, respectively, we observe

$$\begin{aligned} \Delta C_m^{(N)} &> \Delta C^{(N)} \\ C_f^{(N)} - C_f^{(N)loc} &> C_f^{(N)} - C_0^{(N)} = C_f^{(N)} - C_0^{(N)loc} \\ C_f^{(N)loc} &< C_0^{(N)loc}, \end{aligned} \tag{5.9}$$

where we have used the fact that initial state (4.31) is a product state, hence $C_0^{(N)} = C_0^{(N)loc}$.

As another point, we may note the reversal of the curves' colors in comparing Figs. 5.3 and 5.4. This is caused by their opposite (decreasing vs. increasing) type of p dependence for even N, see Sec. 5.3.

In the following paragraph, we try to explain the essence of the proto-

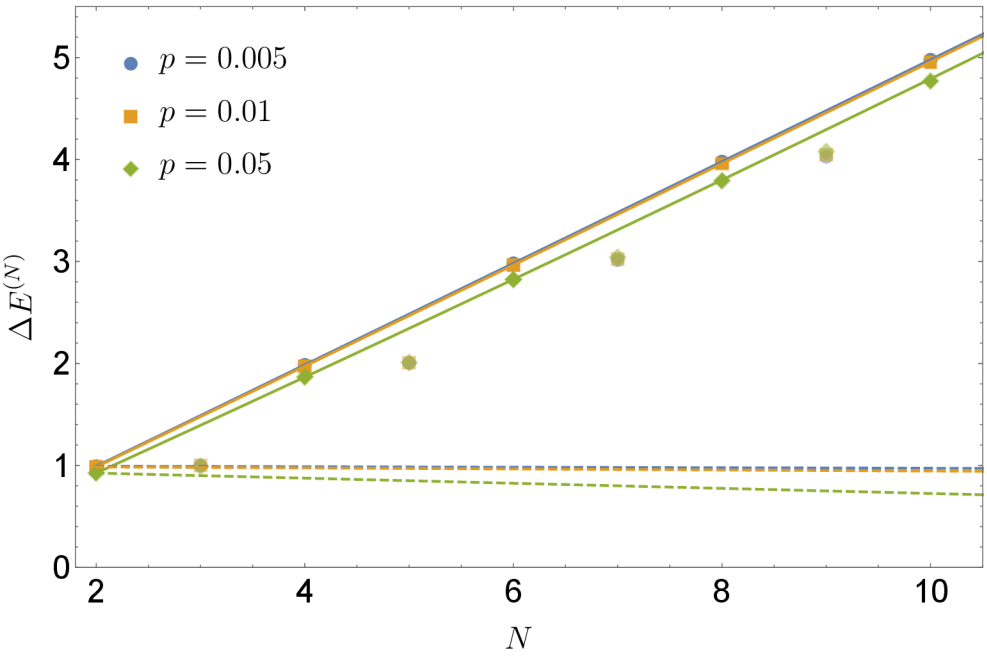

Figure 5.2: Conditional synthesis of energy of N TLS. The plot of the normalized average energy gain $\Delta E^{(N)}$, Eq. (5.7), of N TLS in pure initial state, Eq. (4.31). The values are plotted versus the number of TLS N for different excitation probabilities p, Eq. (4.1). The differently marked discrete points are exact numerical results, full lines are approximate results from Sec. 5.2, and dashed lines remind of the results of global protocol [67]. The energy gain $\Delta E^{(N)}$ increases proportionally to the number N of TLS, however, it is a decreasing function of $p \ll 1$, see Sec. 5.3. Note, the results for $p = 0.005$ and $p = 0.01$ almost coincide.

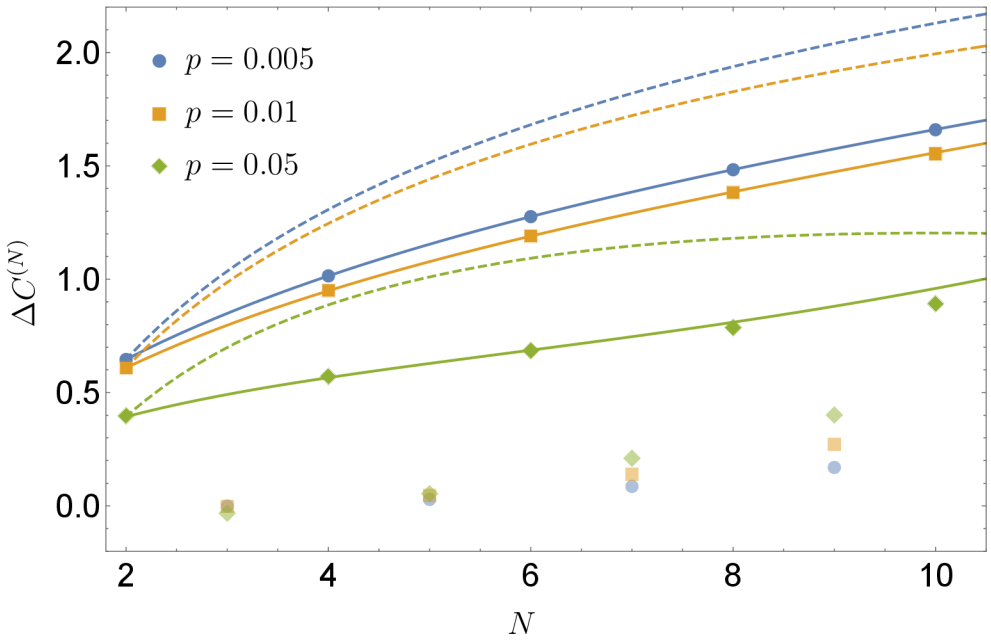

Figure 5.3: Conditional synthesis of coherence of N TLS. The plot of the relative entropy of coherence gain $\Delta C^{(N)}$, Eq. (5.8), of N TLS in pure initial state, Eq. (4.31). The values are plotted versus the number of TLS N for different excitation probabilities p, Eq. (4.1). The differently marked discrete points are exact numerical results, full lines are approximate results from Sec. 5.2, and dashed lines remind of the results of global protocol [67]. The coherence gain $\Delta C^{(N)}$, as energy gain $\Delta E^{(N)}$, c.f. Fig. (5.2), is a decreasing function of $p \ll 1$, see Sec. 5.3. Note, the coherence gain $\Delta C^{(N)}$ differs for odd and even N with a significant advantage for even N.

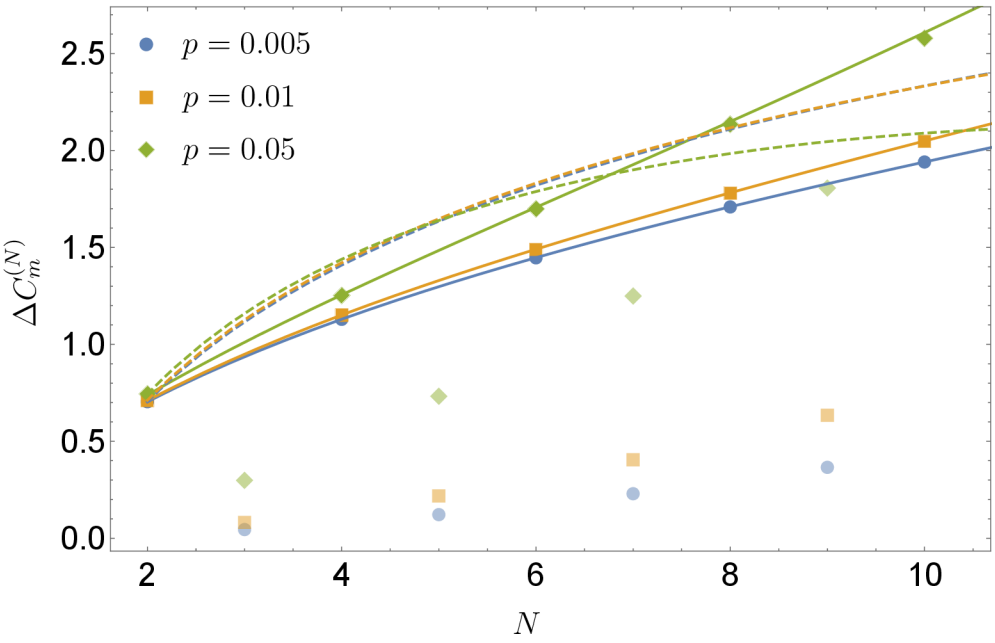

Figure 5.4: Conditional synthesis of mutual coherence of N TLS. The plot of the mutual coherence gain $\Delta C_m^{(N)}$, Eq. (2.23), of N TLS in pure initial state, Eq. (4.31). The values are plotted versus the number of TLS N for different excitation probabilities p, Eq. (4.1). The differently marked discrete points are exact numerical results, full lines are approximate results from Sec. 5.2, and dashed lines remind of the results of global protocol [67]. Note the reversed order of colors of full curves for $\Delta C_m^{(N)}$ and others, reflecting that $\Delta C_m^{(N)}$ is a non-decreasing function of $p \ll 1$, on contrary to $\Delta C^{(N)}$ and $\Delta E^{(N)}$, see Sec. 5.3. Note, the pairwise protocol overcomes the global one, for $N \gtrsim 6$ and $p \gtrsim 0.01$, corresponding to an untypical situation, cf. Fig. 5.2 and Fig. 5.3.

col's working principle. It relies on the fact that for low excitation probability p ($p \ll 1$) of the initial state (4.1) of each TLS, the global state of N TLS, Eq. (4.31), has significant occupation *only* in the lowest-lying energy eigenspaces close to the ground state of the total Hamiltonian (3.3). This occupation typically decreases rapidly (for low p) with the subspace energy eigenvalue, implying low values of the initial state energy $E_0^{(N)}$ and coherence $C_0^{(N)}$. Application of the pairwise protocol completely eliminates occupation of the energy eigenspaces in approximately the lower half of the global energy spectrum of the Hamiltonian (3.3). On contrary, it proportionally increases several occupations of the upper half of the spectrum, keeping the higher-energy level occupations flat distributed with different values in respective energy subspaces. Such redistribution of occupation always (for any p) increases the total average energy. For $p \ll 1$ the protocol increases as well the final state coherence $C_f^{(N)}$ with respect to the initial state, because the initial populations are close to the ground state. For higher p ($p \approx 1/2$) the initial state has populations similar to the (maximally coherent) flat distribution over all the energy eigenspaces. The protocol-induced wipe out of the low-energy populations drives the final state away from the initial high-coherence state (typically to the state that is flat distributed *only* in subspaces of the upper half of the spectrum), causing overall decrease of the final coherence $C_f^{(N)}$ relative to the initial one. Such qualitative picture holds in the case of even number N of TLS entering the protocol. If, on contrary, N is odd and $p \ll 1$, the protocol does wipe out all but a single mid-energy level completely, being responsible for lower $\Delta E^{(N)}$ and $\Delta C^{(N)} \to 0$ gains, cf. Fig. 5.2-5.3.

To enhance the chance to obtain the energy and coherence increase described above, we can employ the repeat until success (RUS) strategy [67].

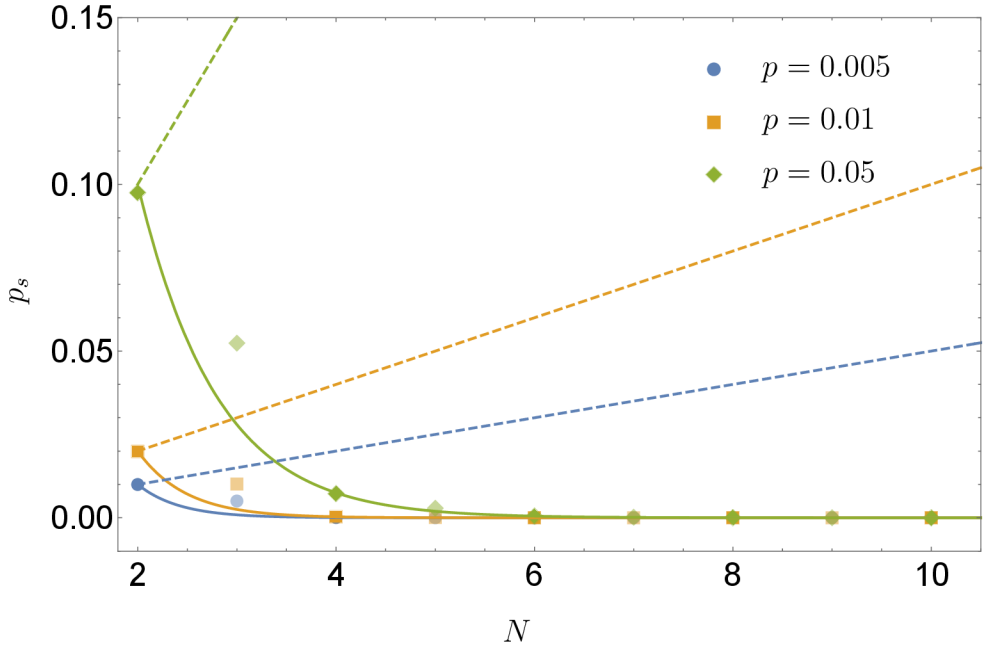

Figure 5.5: Repeat-until-success strategy for coherence synthesis. The plot of probability of success p_s, Eq. (5.4), of the projective measurement $\hat{P}_1^{(N)}$, Eq. (5.2), defined by the successful outcome with the final state $|\Psi_f^{(N)}\rangle$, Eq. (5.3). The values are plotted versus the number of TLS N for different excitation probabilities p, Eq. (4.1). The probability of success $p_s \to 0$ with increasing N. Solid and dashed lines represent approximate expressions, see Sec. 5.2, for even numbers N of TLS for the pairwise and global [67] protocol, respectively. The discrete marked points represent exact numerical results for the pairwise protocol.

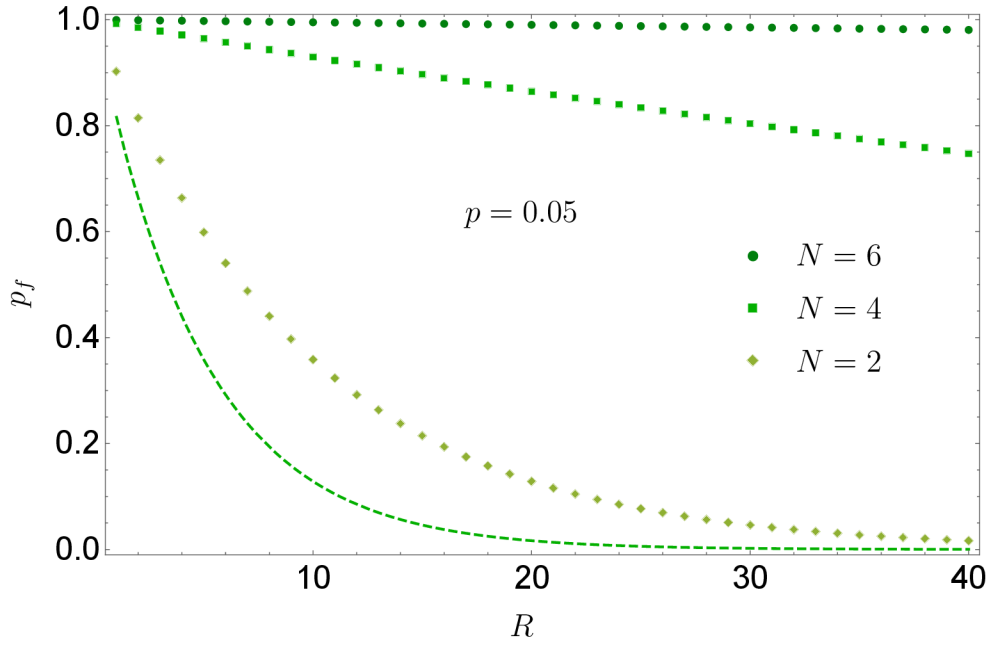

Figure 5.6: Repeat-until-success strategy for coherence synthesis. The dependence of probability of failure p_f in the repeat until success (RUS) strategy, see end of Sec. 5, on the number of repetitions R for $N = \{2, 4, 6\}$ TLS. The values are plotted for an example of the fixed probability of excited state $p = 0.05$. On contrary to the probability of success p_s, probability of failure $p_f \to 1$ with larger number N and smaller excitation probability p. The dashed line represents respective probability of failure of global protocol [67] for $N = 4$ TLS, described in Sec. 5.2.

Such strategy decreases the probability of failure $p_f = (1 - p_s)^R$, with p_s given in Eq. (5.4) and plotted in Fig. 5.5. It relies on the possibility to recycle the TLS that fail to yield the successful outcome after the projector from Eq. (5.1) is applied. In such case all the TLS used for the synthesis can be sent back to the bath and the charging protocol can be reinitialized, see Fig. 5.1, step 2). With increasing number of repetitions R, the total probability of successfully obtaining the final state (4.34) approaches one, cf. Fig. 5.6.

As one can anticipate, creation of exact copies of TLS might be experimentally challenging, therefore we have considered and numerically checked stability of the out-coming $\Delta E^{(N)} > 0$ and $\Delta C^{(N)} > 0$ for a set of N TLS with random initial p sampled from a flat-distributed p-values of the width up to $\Delta p \approx 0.05$. As far as the probabilities of excitation differ from each other by less than few percent, the protocol is still applicable. For differences of the order $\Delta p \gtrsim 0.1$, we have observed detrimental effect on the coherence gain, while the energy gain was still present.

5.2 Approximations

This section aims to translate the cumbersome and complex form of the exact results into a more readable and presentable one. We are going to distinguish between odd and even numbers of TLS explicitly as in our protocol it is preferable to employ *even* numbers N of TLS because it guarantees to reach better outcomes. The qualitative explanation of this fact is highlighted at the end of the previous section, cf. Sec. 5.1. Hence, we will divide the approximation results into two parts: for even and odd numbers of TLS.

The principal interest for us represents the results of pairwise protocol for even numbers of TLS. For this purpose, we limited the range of excitation probability to small values $p \lesssim 0.1$ and the number of TLS constituting the system to $N \lesssim 10$. It was done since the quantities of interest, $\Delta E^{(N)} > 0$, $\Delta C^{(N)} > 0$, mostly have an increase in the region specified before.

The approximations will be made for the central values describing the effect of a pairwise protocol on a system. Namely, starting with the probability of success $p_s^{(N)}$, coherence and energy gains, $\Delta E^{(N)}$ and $\Delta C^{(N)}$, and finishing with the mutual coherence gain $\Delta C_m^{(N)}$. We explore approximations of their dependence on the probability of excitation p and for *even* N the results are following

$$p_s^{(N)} \approx \left(\frac{N}{2}+1\right) p^{\frac{N}{2}}, \tag{5.10}$$

$$\Delta E^{(N)} \approx \frac{N}{2} - \frac{N(20-N)}{24} p, \tag{5.11}$$

$$\Delta C^{(N)} \approx \ln\left(\frac{N}{2}+1\right) - \frac{N(20-N)}{24}(1-\ln p)p, \tag{5.12}$$

$$\begin{aligned}\Delta C_m^{(N)} \equiv C_{m,f}^{(N)} = C_f^{(N)} - C_f^{(N)loc} \approx \ln\left(\frac{N}{2}+1\right) + \frac{N(N+4)}{24}(1-\ln p)p \\ - \ln\left[\frac{3}{2}\left(\frac{N}{2}+1\right)!\right]p.\end{aligned} \tag{5.13}$$

For $p_s^{(N)}$ the accuracy of this approximation is kept within 10%. The expression for $\Delta C_m^{(N)}$, Eq. 5.13, is more precise with a standard deviation percentage $\lesssim 2\%$ and latter is valid in a slightly larger range $p \leqslant 0.12$. In addition, the last term of RHS of $\Delta C_m^{(N)}$, Eq. 5.13, represents the approximation of the local coherence of the system after the measurement. All the results, Eq. 5.10 - Eq. 5.13, are plotted as solid lines in Fig. 5.2, Fig. 5.3, Fig. 5.4 and Fig. 5.5. It can be seen that exact values, represented by dots, are well fitted by respective approximate expressions, represented by solid

lines. Comparison of RHS of Eqs. (5.13) and (5.12) also reveals the reason for reversal of the curves' colors in Figs. 5.3 and 5.4. It is due to the opposite sign of the p-dependence of these approximations. The same reason is responsible for the color reversal also in the models including dephasing, see Sec. 5.5.

For the sake of comparison, the same list of values within $p \lesssim 0.1$ and $N \lesssim 10$ could be approximated for *odd* N with the following results

$$p_s^{(N)} \approx p^{\frac{N-1}{2}}, \tag{5.14}$$

$$\Delta E^{(N)} \approx \frac{N-1}{2}, \tag{5.15}$$

$$\Delta C^{(N)} \approx \frac{(N-1)(N-3)}{8}(1-\ln p)p, \tag{5.16}$$

where the approximation for energy gain $\Delta E^{(N)}$ is good enough only with a term p^0, whereas for an even N we included a linear term p^1 to improve fit substantially.

These results should be compared to the respective approximations of the global protocol, described in Chapter 4. We list the approximations of the corresponding values of the latter

$$p_s^{(N)} \approx Np, \tag{5.17}$$

$$\Delta E^{(N)} \approx 1 - \frac{N+1}{2}p, \tag{5.18}$$

$$\Delta C^{(N)} \approx \ln N - \frac{N+1}{2}(1-\ln p)p, \tag{5.19}$$

$$\Delta C_m^{(N)} \approx \ln N + \frac{N-1}{2}(1-\ln p)p - \frac{(N-1)^2}{N-2}\ln{(N-1)p}. \tag{5.20}$$

As we have checked numerically, the deviation $\lesssim 10\%$ of the global approximations holds in the range $p \lesssim 0.02$ for $p_s^{(N)}$, $p \lesssim 0.08$ for $\Delta E^{(N)}$, $p \lesssim 0.06$ for $\Delta C^{(N)}$, and $p \lesssim 0.11$ for $\Delta C_m^{(N)}$ (for all $N \lesssim 8$).

Additionally, we can also compare results of our pairwise protocol to

the results of *optimal* probabilistic distillation of pure states towards maximally coherent state in a given dimension, see e.g. [25]. Taking into account that our initial state is fixed, Eq. (4.31), and the final target state would be $|\Psi_m\rangle = 1/\sqrt{m}\sum_{i=1}^{m}|i\rangle$ with $m = 2^N$, such protocol optimized for global coherence gain Eq. (3.8) with use of strictly incoherent [25] operations, yields for $p \ll 1$

$$\Delta C_{\mathrm{opt}}^{(N)} = N\left[\ln 2 - p(1 - \ln p)\right], \tag{5.21}$$

being clearly superior (by construction $\propto N$) to our results Eq. (5.12) for even N ($\propto \ln N$). However, such protocol will certainly loose the universality feature, as the used strictly incoherent operation would necessarily be input state-dependent. On contrary, the success probability of reaching the maximally coherent state [25], again using the input state Eq. (4.31), reads

$$p_{s,\mathrm{opt}}^{(N)} = (2p)^N, \tag{5.22}$$

being always smaller (for $p \ll 1$) than the even N case of Eq. (5.10), showing an existing trade-off between attainable final state coherence and the success probability of achieving it. Simple discussion of mutual coherence increase of our protocol vs. the above mentioned global coherence-gain optimized one can not be performed. The class of maximally coherent states in Hilbert space with dimension $m = 2^N$ composed of tensor product of respective subsystems' Hilbert spaces includes separable, as well as maximally entangled states. Therefore, the mutual coherence values can span the whole interval $[0, N\ln 2]$. For this reason, such discussion exceeds the scope of this thesis.

5.3 Excitation probability dependence

For the sake of comparison with the results of global protocol presented in terms of dependence on p, see Sec. 4.4, in this section we present the behavior of $\Delta E^{(N)}$, $\Delta C^{(N)}$, $\Delta C_m^{(N)}$, and their corresponding approximations Eq. (5.11)- Eq. (5.13)(dashed lines in Figs. 5.7-5.9). Namely, we present here their p-dependence with the number of TLS N playing the role of the parameter. Figure 5.8 shows the main reason why we have restricted our attention to $p \ll 1$ region when dealing with $\Delta C^{(N)} > 0$, as the approximation Eq. (5.12) is accurate in this region only. In turn, we restrict our attention to this region for the rest of the quantities, as well.

On contrary, the approximations of the energy gain $\Delta E^{(N)} > 0$, Fig. 5.7, and mutual coherence gain $\Delta C_m^{(N)} > 0$, Fig. 5.9, reveal good match with the exact values in a wider region of p values.

5.4 Protocol optimisations

The aim of this section is to find a compromise between the following complementary figure of merits: energy gain (5.7), coherence gain (5.8) and probability of success (5.3). For instance, we won't invoke generalised measurements, or POVM (Sec. 2.2) for this purpose due to complicated strategy of measurement process, Eq. (5.2), as it would bring unnecessary numerical complexity, c.f. Sec. 4.3. Hence, we restrict optimisation process only to addition of the projector-based measurements on pairs of TLS.

Clearly, pairwise protocol has several significant drawbacks, namely, distinctively lower coherence gains for an odd number of TLS N in comparison to even N, Fig. 5.3, and small probability of success p_s, Fig. 5.5. Since a low probability of success is a direct consequence of the pairwise

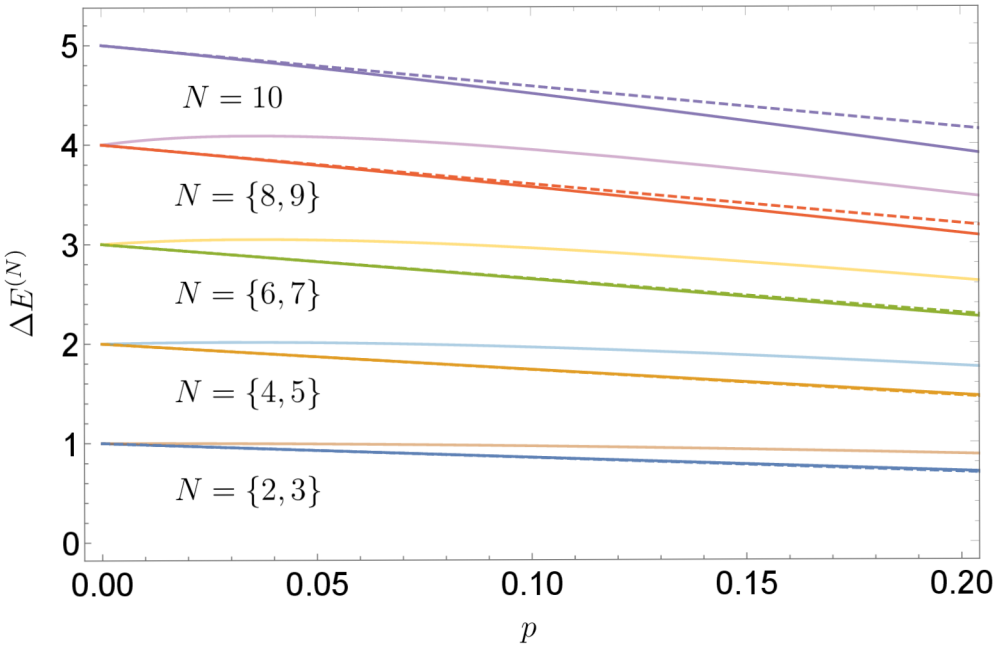

Figure 5.7: The plot of the normalized average energy gain $\Delta E^{(N)}$, Eq. (5.7). The values are plotted versus different excitation probabilities p, Eq. (4.1), and parameterised by the number of TLS N. For odd N the lines are made more transparent. Full lines correspond to exact results, the dashed lines show the corresponding approximations, Eq. (5.11). The energy gain $\Delta E^{(N)} > 0$ increases proportionally to the number N of TLS and decreases linearly with p for even N, which we focus at, see Fig. 5.8 for the reason.

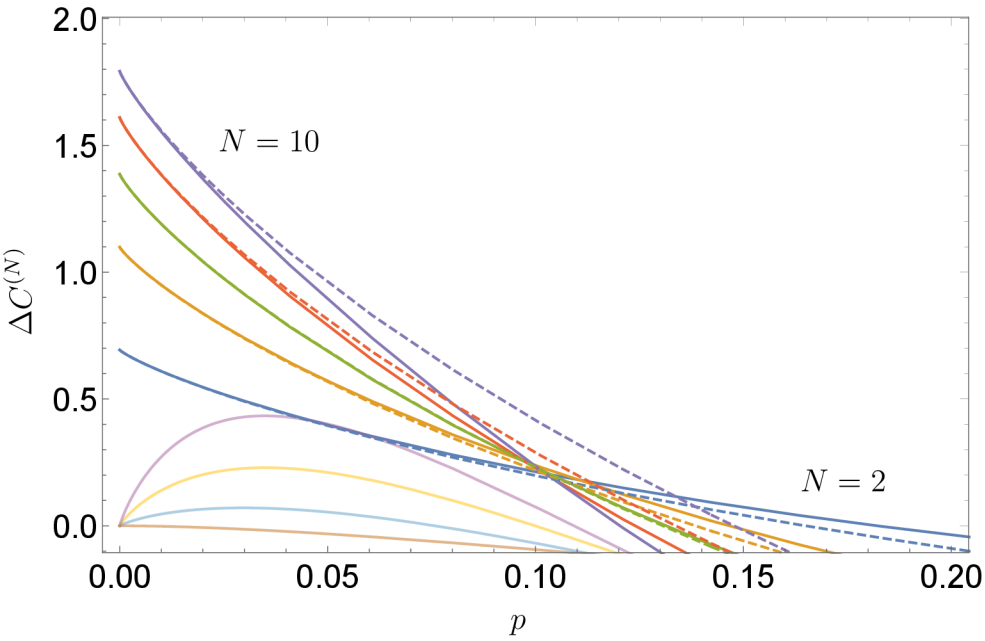

Figure 5.8: Plot of the coherence gain $\Delta C^{(N)}$, Eq. (5.8), dependence on the single TLS excitation probability p, Eq. (4.1). The different curves are parameterised by different values of N, the more transparent ones are for odd N, revealing quantitatively lower values of $\Delta C^{(N)}$. The color code of the lines remains the same as in Fig. 5.7. As seen from the plot, only low-excited TLS can be used to synthesize larger coherent system, as $\Delta C^{(N)} > 0$ noticeably only in the $p \ll 1$ region. The dashed lines represent the corresponding approximations (5.12). We stress again that the coherence gain $\Delta C^{(N)}$ differs for odd and even N with a significant advantage for even numbers of TLS used as an input for the protocol. Furthermore, we point out that the approximate results (dashed lines) are losing their accuracy with increasing N (even), being well valid in a shrinking interval of p.

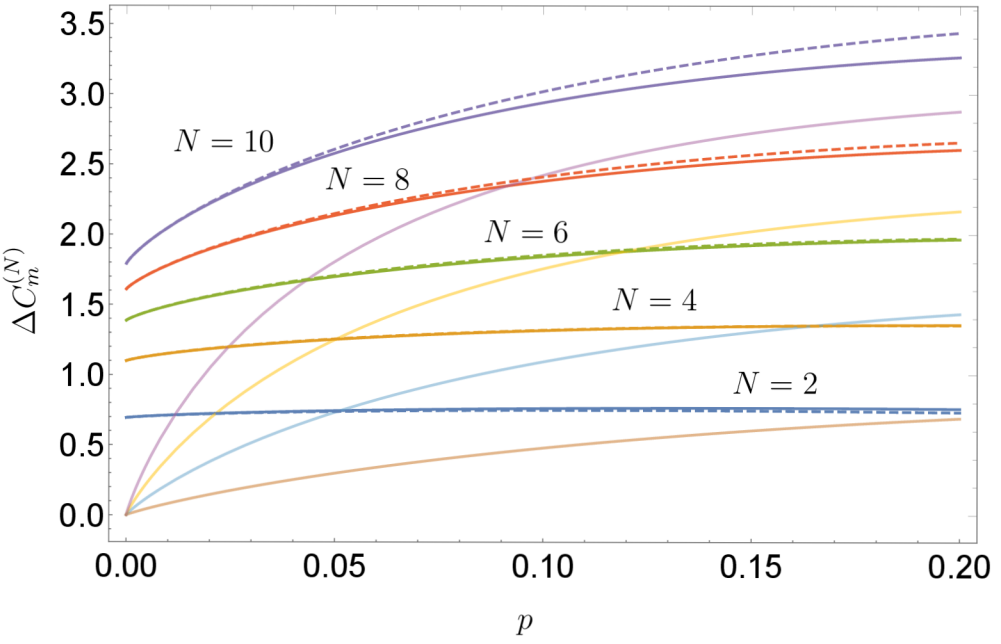

Figure 5.9: Plot of the p-dependence of mutual coherence gain $\Delta C_m^{(N)} > 0$, Eq. (2.23), of N TLS in pure initial states. The plot shows curves in region of $p \ll 1$, again parameterised by N, as in Fig. 5.7 and Fig. 5.8 (the color code being the same). The corresponding approximations are shown as the dashed lines for even N only. These results suggest, that the good match of the approximations holds in a comparable or larger interval of p, compared to the case of $\Delta C^{(N)}$ shown in Fig. 5.8. Qualitative comparison with Fig. 5.8 reveals, that the mutual coherence $\Delta C_m^{(N)}$ is a *non-decreasing* function of N and p as well, on contrary to $\Delta C^{(N)}$.

approach, i.e. with larger number of measurements, the probability of successful outcome in each step contributes into a rapid decrease of a total probability of success (5.3), asymptotically approaching $p_s^{(N)} \to 0$ with $N \to \infty$. Therefore, we won't concentrate on optimising this issue as it would require reduction of measurements leading to changing a core idea of the protocol. However, it would be interesting to consider for future investigations. Nevertheless, if the probability of success is an important aspect then global protocol, described in a Chapter 4, is a more suitable approach in this case.

In following, we show several optimisations of the pairwise protocol regarding the energy (5.7) and coherence (5.8) gains, i.e. addition of a single measurement over a pair of the first and last TLS, that would close a cycle of measurements, and measuring all possible combinations of pairs of TLS, both plotted in Fig 5.10.

1. *Closing a cycle.* This optimisation is aimed to improve the coherence gain for *odd* numbers N of Tls, that is drastically low for the current protocol. Fortunately, it can be realized by making just one more measurement of the pair of the first and last TLS. Namely, we measure TLS system in order of their appearance in sequence, and for an odd number of TLS it is necessary to measure one more pair, i.e. the first and the last TLS. The measurement process consists of measurements applied to TLS forming a cycle, therefore, such a strategy can be called as closing the cycle.

   Interestingly, this technique should be applied only for systems that consist of an odd number of TLS N. If applied to the system with an even N instead, it will result into the diminished coherence gain compared to one obtained by the original protocol. Hence, from this

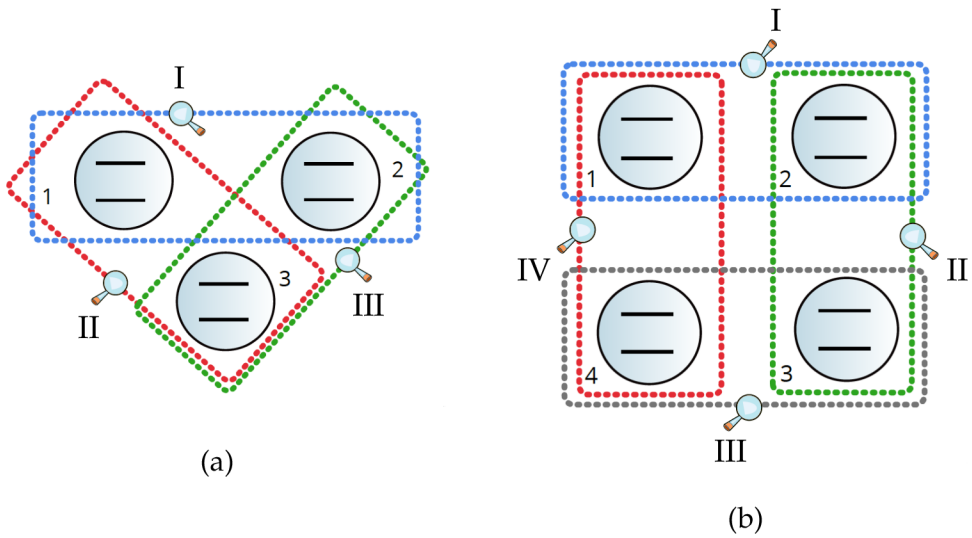

Figure 5.10: Figure representing the ”closing the cycle” and ”all possible measurements” (simultaneously) optimisations for $N = 3$ and the ”closing the cycle” optimisation for $N = 4$ TLS, respectively. The sequence of pairwise measurements is denoted by Roman numbers. The distinctive feature of the ”closing the cycle” approach (in comparison to pairwise protocol described in Sec. 5) relies in one more measurement between the first and last TLS associated with forming a cycle.

fact we can make a conclusion that there is some correlation between the number of TLS N and number of the measurements and it is more advantageous to use an odd number of measurements $N-1$ for both odd $N-1$ and even N numbers of TLS.

2. *All possible measurements.* Additionally, there is one more strategy that helps to improve coherence gain for an *odd* number N of TLS and, at the same time, to reach the *maximum possible energy gain* with a pairwise approach. It relies on measuring all possible combinations of pairs of TLS. In other words, N TLS can be paired in different ways. All the possible combinations of TLS pairs have to be measured. For example, in addition to measuring TLS in the sequence, Fig. 5.1, they have to be measured with non-neighboring TLS as well.

   This approach gives the largest possible energy per one cycle with a simultaneous increase in coherence. However, experimentally it can be quite challenging to realize such a protocol. Moreover, the probability of success of such approach is even less than of the original protocol.

For the purpose of convenience, we present the results of both optimisations in terms of energy, Fig. 5.11, and coherence, Fig. 5.12, for $N=3$ TLS as in this particular case both optimisations coincide. The corresponding values for global and pairwise protocol are plotted for comparison. To conclude this section, we would like to outline the following:

- Global protocol, Chap. 4, gives the largest possible coherence gain (3.8) and probability of success (4.8) achievable by the projective measurement filtering out the ground state of TLS, Sec. 3.2.

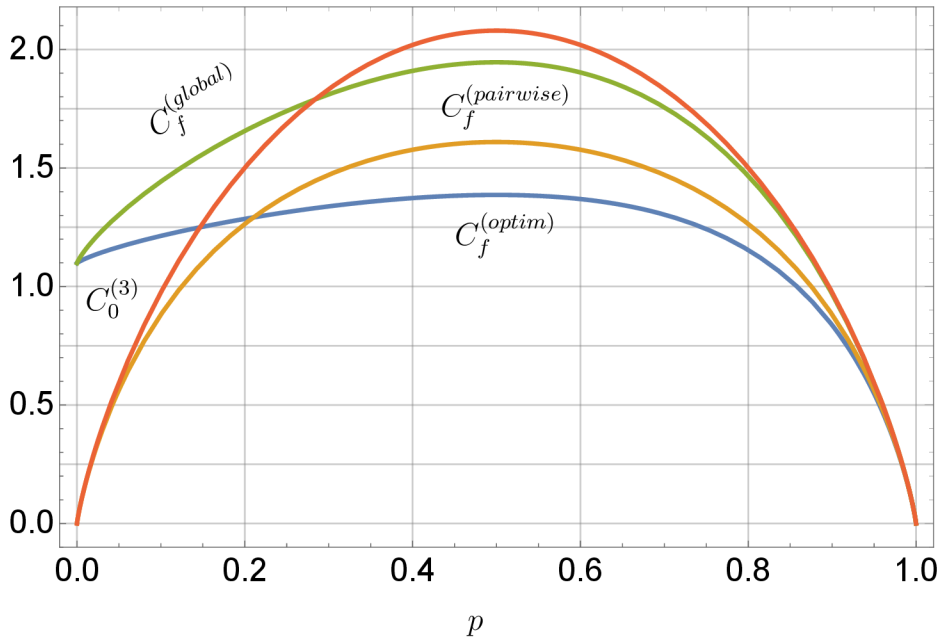

Figure 5.11: Comparison of the initial coherence $C_0^{(3)}$ (red line) and final coherence after applications of pairwise protocol (see Sec. 5) $C_f^{(3,pairwise)}$ (yellow line), global protocol (see Sec. 4) $C_f^{(3,global)}$ and optimized protocol (see Sec. 5.4) $C_f^{(3,optim)}$ (blue line) for $N = 3$ TLS, respectively. The dependence is plotted versus the excitation probability p, Eq. (4.1). The largest final coherence corresponds to the global protocol. The optimisation helps to improve the final coherence of a pairwise protocol in the range of small p.

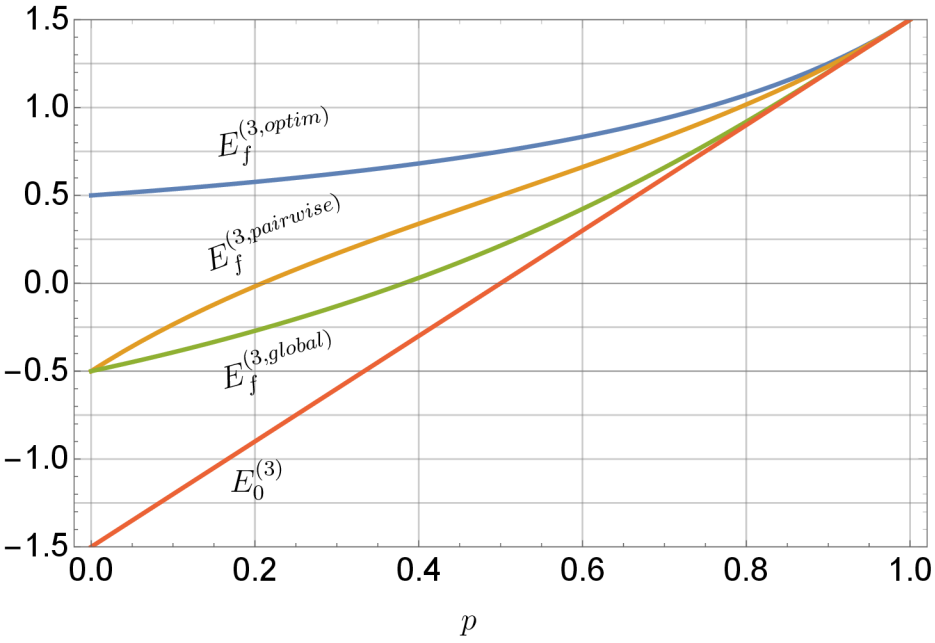

Figure 5.12: Comparison of the initial energy $E_0^{(3)}$ (red line) and final energy after applications of pairwise protocol (see Sec. 5) $E_f^{(3,pairwise)}$ (yellow line), global protocol (see Sec. 4) $E_f^{(3,global)}$ and optimized protocol (see Sec. 5.4) $E_f^{(3,optim)}$ (blue line) for $N = 3$ TLS, respectively. The dependence is plotted versus the excitation probability p, Eq. (4.1). The largest final energy corresponds to the optimized protocol.

- Optimisation of a pairwise protocol with *all possible measurements* gives the largest possible energy gain, see Fig. 5.12, achievable by the means of pairwise measurements filtering out the ground state. It has to be mentioned that coherence gain is also improved for all types N (odd and even) for small values of p, however, at the cost of the probability of success in such an approach.

- The *closing a cycle* strategy in a case of an odd number N of TLS constituting a battery is the simplest improvement of the original pairwise protocol as it fixes the disadvantage of small coherence gain, see Fig. 5.11, and leaving the other values almost unchanged.

5.5 Dephasing

In reality, partially coherent TLS have a decreased purity dominantly because of the dephasing [9, 73] reducing the off-diagonal elements in the energy representation. As the result of such irreversible process, the initial pure state of each TLS, rapidly degrade into partially coherent states. Of practical importance is to explore the suitability of using the mixed states resulting from the process of dephasing of TLS for robustness of the previous results. We do not consider spontaneous emission as in the previous approach as, firstly, it is less probabilistic process compared to dephasing and, secondly, due to its computational complexity in terms of considered protocol.

Hence, we consider dephasing of the initial and final states of the battery before and after measurement. As the dephasing commutes with the projective measurement (5.2) applied to the system, we can effectively collect the dephasing before and after the measurement and accumulate it

into the dephasing of initial state only. This fact will be explained in detail in Sec. 5.5.2. We are interested in whether the resulting coherence gains are going to change substantially. As the energy is defined only by the diagonal terms of the density matrix, it is clearly not affected by the dephasing process. Hence the results for the pure states for $\Delta E^{(N)}$, Eq. 5.7, hold. On the contrary, coherence comprises [14] the von Neumann entropy term, which takes into account non-diagonal terms of the density matrix and, hence, has a non-zero contribution in the case of partially coherent states. Therefore, it affects the initial $\overline{C}_0^{(N)}$ and final coherence $\overline{C}_f^{(N)}$ of the system before and after the measurement process, resulting in the change of coherence difference, $\Delta\overline{C}^{(N)}$, where a single bar labels quantities calculated with the effect of dephasing acting only on the initial TLS state. In analogy, we label the final coherence $\overline{\overline{C}}_f^{(N)}$ of the system with the dephasing of initial and final states before and after the measurement process, resulting in the change of coherence difference, $\Delta\overline{\overline{C}}^{(N)} = \overline{\overline{C}}_f^{(N)} - \overline{C}_f^{(0)}$, with the help of double bar .

For simplicity, we assume that all TLS undergo the dephasing process with the same rate ϵ. It is not the case in a reality, however it gives us a qualitative picture of the behaviour of our protocol under decoherence effects.

5.5.1 Dephasing of the initial state of TLS

At first, we are going to explore the effect of dephasing of the initial states of TLS only, Eq. (4.31). Let us assume that the initial pure state (4.1) of each

TLS after dephasing is characterized by the density matrix [9, 67]

$$\hat{\rho}_j = p\,|e_j\rangle\langle e_j| + \epsilon\sqrt{p(1-p)}(|e_j\rangle\langle g_j| + |g_j\rangle\langle e_j|) \\ +(1-p)\,|g_j\rangle\langle g_j|\,, \quad j = 1,\ldots,N, \tag{5.23}$$

where $0 \leq \epsilon \leq 1$ quantifies the effect of the dephasing. The initial state of the total system of N TLS reads

$$\hat{\rho}_i^{(N)} = \bigotimes_{j=1}^{N} \hat{\rho}_j. \tag{5.24}$$

Subjecting the initial state to the same projector-based charging procedure as in Sec. 5.1, $\{\hat{P}_1^{(N)},\ \hat{P}_0^{(N)}\}$, yields the final state

$$\hat{\rho}_f^{(N)} = \frac{\hat{P}_1^{(N)}\hat{\rho}_i^{(N)}\hat{P}_1^{(N)}}{\overline{p}_s}. \tag{5.25}$$

The complexity of the coherence (3.6) and mutual coherence (2.22) prevents us from determining $\Delta\overline{C}^{(N)}$ and $\Delta\overline{C}_m^{(N)}$ analytically for the initial state (5.24) and the final state (5.25). Thus, we focus our attention to the fully numerical results, presenting them only graphically.

The results for coherence and mutual coherence of the dephased initial state of the system are shown in Fig. 5.13 and Fig. 5.14, respectively, with the value $\epsilon = 0.9$. It can be seen that dephasing of the initial state diminishes both coherence and mutual coherence gains, especially for even numbers N of TLS. However, dephasing does not destroy the positive effect of the protocol completely. Quite generally, small dephasing, substantially below the "critical" value $\epsilon \approx 0.5$, may affect the system, while the coherence gain can still remain positive and non-negligible. The term "critical" is meant in the sense that such values of ϵ cause loss of the coherence gains, $\Delta\overline{C}^{(N)} \approx 0$ and $\Delta\overline{C}_m^{(N)} \approx 0$ for any N. For larger values of ϵ, dephasing generally causes appearance of a local maximum for certain

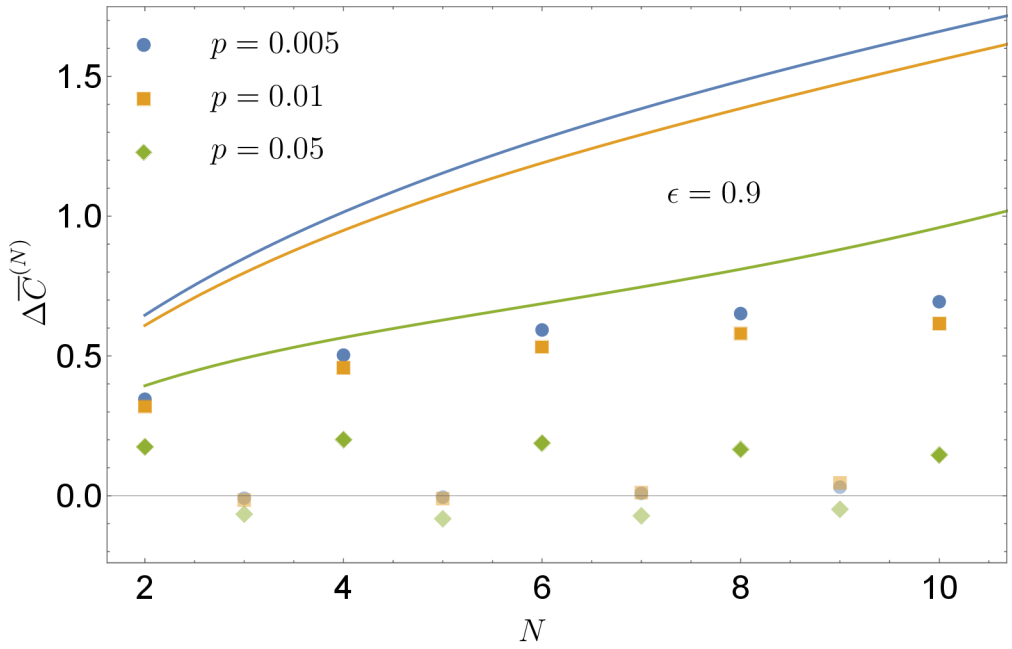

Figure 5.13: Conditional synthesis of coherence of N partially dephased TLS. The coherence gain $\Delta\overline{C}^{(N)}$, Eq. (5.8), for N TLS in the final state (5.25) and dephased initial state (5.24). The dephasing rate is set to $\epsilon = 0.9$. The values are plotted versus the number of TLS N, for different excitation probabilities p, Eq. (5.23). The marked discrete values are results of exact numerical calculation. The full lines recall the approximate results for pure initial states, see Fig. 5.3. The effect of the coherence gain decrease is significantly stronger for larger numbers of TLS constituting the system, causing the emergence of the local maximum at $N \approx 4$. Generally, the gain $\Delta\overline{C}^{(N)} > 0$ is preserved until the "critical" value $\epsilon \approx 0.5$, where it is lost even for small values of p and low N.

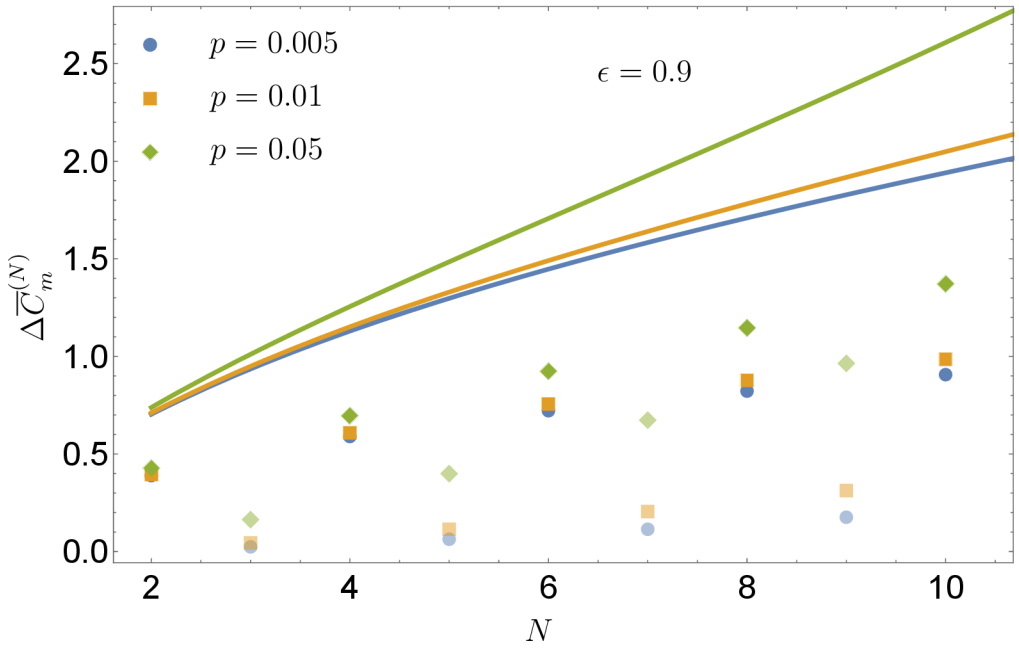

Figure 5.14: Conditional synthesis of mutual coherence of N partially dephased TLS. The mutual coherence gain $\Delta\overline{C}_m^{(N)}$ for N TLS in the final state (5.25) and dephased initial state (5.24) of TLS. The dephasing rate is set to $\epsilon = 0.9$. The values are plotted versus the number of TLS N, for different excitation probabilities p, Eq. (5.23). The marked discrete values are results of exact numerical calculation. The full lines recall the approximate results for pure initial states, see Fig. 5.4. Generally, the gain $\Delta\overline{C}_m^{(N)} > 0$ is preserved until the "critical" value $\epsilon \approx 0.5$, where it is lost even for small values of p and low N. Note as well the same curves' color reversal as pointed out in Fig. 5.4 and explained in Sec. 5.2.

N, as with N the negative effect of dephasing increases. We also point out that $\Delta\overline{C}^{(N)}$ and $\Delta\overline{C}_m^{(N)}$ keep irrespective of dephasing their decreasing and increasing dependence on p, respectively. This is manifested by the curves' opposite ordering with respect to values of p, as discussed in Sec. 5.2, and the same reason holds for dephasing affecting the final (post-protocol) state discussed in the next subsection.

Few things have to be taken into account, namely, that we considered only individually dephased TLS [9]. It, in turn, means that the dephasing of each TLS was independent and had no effect on the others or, in other words, it was not correlated to dephasing of other TLSs. We have also assumed they dephased with the same rate ϵ that may not be a case in reality. Indeed, each TLS's initial state may dephase in time with different values $\epsilon_1, \epsilon_2, \ldots, \epsilon_N$ as they are independent of each other, resulting in different total initial state of TLS before the measurement. We have explored such a situation and checked the protocol outcome numerically. For the sake of brevity, we present the results only in a few words: the local dephasing with different values of ϵ for each TLS, has no truly detrimental effect. As long as the dephasing parameters are bigger than critical value $\epsilon \gtrsim 0.5$ and the respective values are close to each other $\epsilon_i \approx \epsilon_j$, the coherence and mutual coherence gains decrease, but qualitatively, the main effect survives.

5.5.2 Dephasing after the synthesization

In this section, we are going to explore in addition to the dephasing of the initial also the dephasing of the final total state of the system, Eq. (5.25). We again assume that each TLS dephases locally with some rate $\bar{\epsilon}$, for simplicity same for all the TLS, and that these individual dephasing processes are not correlated with each other. Namely, dephasing of one TLS does not

affect dephasing processes of the others. As the final state of the system after measurement, Eq. (5.25) is non-separable, therefore, mathematically we could describe such a collective dephasing by the application of Kraus operators [15].

The rate $\overline{\epsilon}$ can be generally different from dephasing parameter ϵ of the initial state $\hat{\rho}_i^{(N)}$, Eq. (5.24). However, for the sake of not overcomplicating results, in the following we will assume $\epsilon = \overline{\epsilon}$ being equal.

For better understanding, let us at first show an effect of the application of Kraus operators $\hat{K}_0$, $\hat{K}_1$, on the state of a single TLS $\rho_f^{(1)}$

$$\hat{\overline{\rho}}_f^{(1)} = \hat{K}_0 \hat{\rho}_f^{(1)} \hat{K}_0 + \hat{K}_1 \hat{\rho}_f^{(1)} \hat{K}_1, \tag{5.26}$$

with the definitions

$$\hat{K}_0 = \sqrt{\frac{1+\epsilon}{2}} \hat{I}, \quad \hat{K}_1 = \sqrt{\frac{1-\epsilon}{2}} \hat{\sigma}_z, \tag{5.27}$$

resulting into the form of Eq. (5.23). In essence, the main impact is in the addition of ϵ to all the off-diagonal terms of the density matrix.

However, we want to apply the same procedure to each TLS constituting the system. Notably, we have to take into account the fact that they undergo the dephasing independently (locally). Therefore, we can write the total Kraus operator acting on the final state of system after measurement, Eq. (5.25), as the direct products of the individual Kraus operators on each TLS.

Such a double dephasing process will give the final state of the system after the measurement

$$\overline{\hat{\rho}}_f^{(N)} = \sum_{i=0}^{2^N-1} \hat{\mathcal{K}}_i \hat{\rho}_f^{(N)} \hat{\mathcal{K}}_i, \tag{5.28}$$

with the final coherence $\overline{\overline{C}}_f^{(N)} \equiv C(\overline{\hat{\rho}}_f^{(N)})$. The $\hat{\mathcal{K}}_i$ being the global Kraus

operators [15], having the form

$$\hat{\mathcal{K}}_i \equiv \hat{K}_{j_{N-1}^{(i)}} \bigotimes \cdots \bigotimes \hat{K}_{j_1^{(i)}} \bigotimes \hat{K}_{j_0^{(i)}}, \quad j_k^{(i)} = \{0, 1\}, \tag{5.29}$$

with $(j_{N-1}^{(i)} \cdots j_1^{(i)} j_0^{(i)})_2 = (i)_{10}$ being the binary representation of the index value $(i)_{10}$, e.g., $(7)_{10} = (0111)_2$ for $N = 4$.

Here, we want to stress out one important fact stemming from the diagonal form of the Kraus operators in Eq. (5.29). These diagonal operators commute with the, as well diagonal, projectors, Eq. (5.1), used in our protocol. This allows for possibility of formally interchanging the order of the second (post-protocol) dephasing and the measurements, in principle simplifying modelling of such environmental interaction. In other words, the dephasing before and after the measurement process with respective rates ϵ and $\bar{\epsilon}$ amounts effectively to only single dephasing with the total rate $\epsilon\bar{\epsilon} \equiv \epsilon^2$ due to the commutativity of measurement and dephasing represented by incoherent operators. Although being aware of this fact, we retain the description of the second (post-protocol) dephasing in the form of Eq. (5.28), for conceptual and pedagogical reasons.

It can be seen from Fig. 5.15 and Fig. 5.16 for $\epsilon = 0.9$ the dephasing of the final state of the battery affects the coherence gain by further decreasing it, $\Delta\overline{\overline{C}}^{(N)} < \Delta\overline{C}^{(N)}$. But with the dephasing parameter ϵ bigger than "critical" value 0.75, there still exists gain of the coherence, $\Delta\overline{\overline{C}}^{(N)} > 0$ in the range of small values of p. In the same way, the dephasing of initial and final states of the system affects the mutual coherence gain $\Delta\overline{\overline{C}}^{(N)}$, however the effect is weaker for larger N.

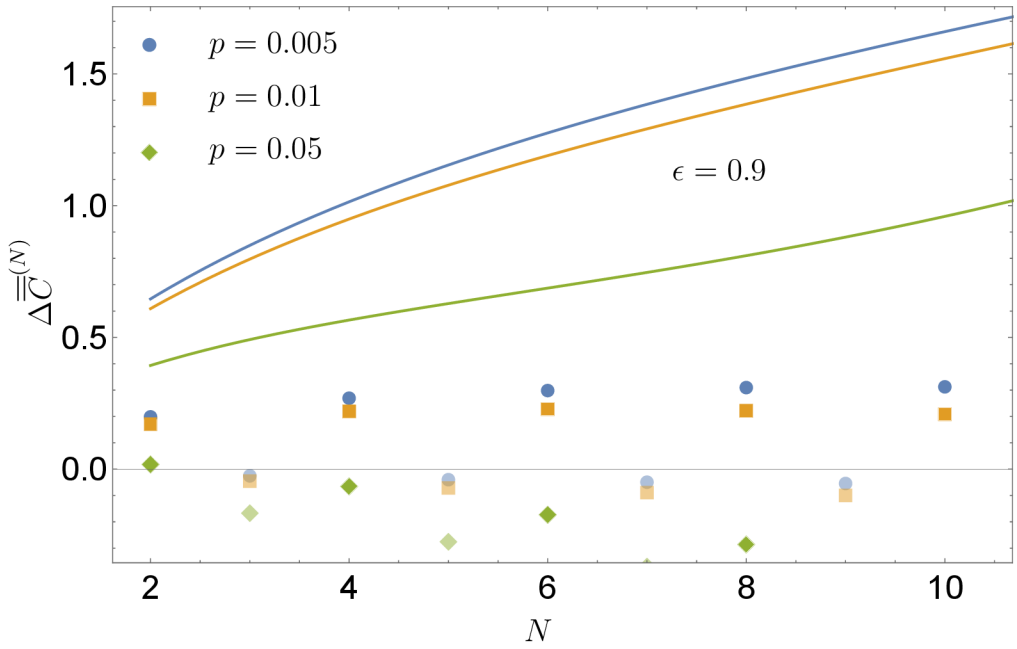

Figure 5.15: Effect of dephasing on the final state (5.25). The coherence gain $\Delta\overline{\overline{C}}^{(N)}$ of the system in the final state, Eq. (5.28), with $\epsilon = 0.9$. The values are plotted versus the number of TLS N, for different excitation probabilities p, Eq. (5.23). Solid lines represent the corresponding values for pure states, cf. Fig. 5.3, marked discrete points are exact numerical results. It can be seen by comparison with Fig. 5.13 that dephasing of initial state has much larger effect of diminishing the coherence gain, than dephasing process of final state of the system, suggesting that the final state is quite robust with respect to dephasing. However, even in this case dephasing decreases the gain in $\Delta\overline{\overline{C}}^{(N)}$, for larger N and low p, and causes the appearance of local maximum for $N \approx 6$ (orange squares).

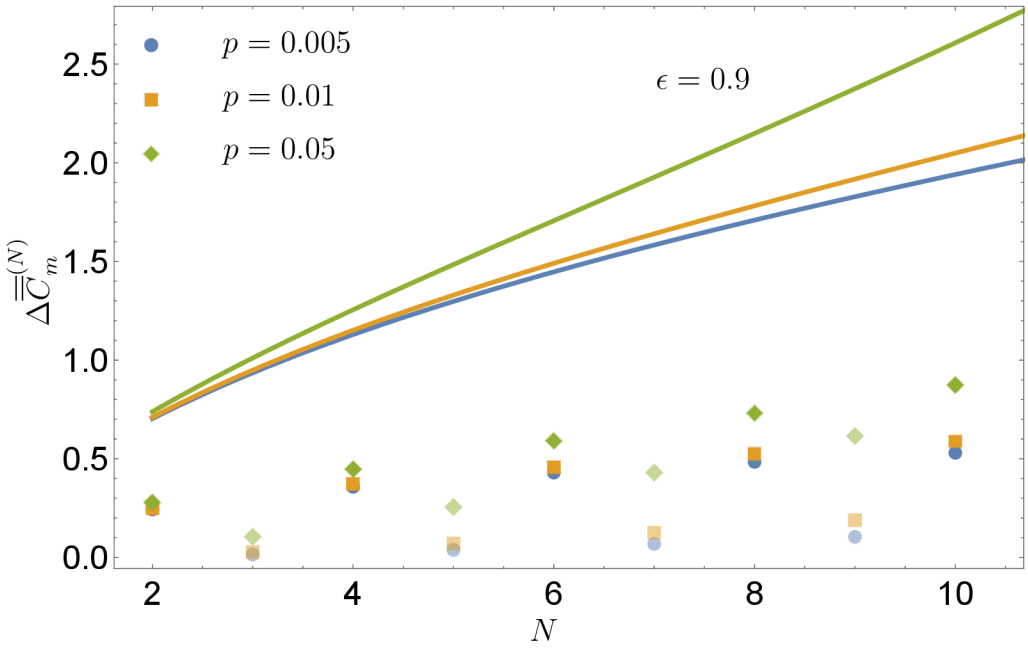

Figure 5.16: Effect of dephasing on the final state (5.25). The mutual coherence gain $\Delta\overline{\overline{C}}_m^{(N)}$ of the system in the final states, Eq. (5.28), with $\epsilon = 0.9$. The values are plotted versus the number of TLS N, for different excitation probabilities p, Eq. (5.23). Solid lines represent the corresponding values for pure states, Fig. 5.4, marked discrete points are exact numerical results. By comparison to Fig. 5.14 we see the same effect as for coherence gain, cf. 5.15: dephasing of initial state has much larger effect of diminishing the mutual coherence gain, than dephasing process of final state of the system.

5.6 Conclusions

In this chapter, we have introduced a quantum coherence synthesizing charging protocol that acts on pairs of TLS. Its feasibility stems from the fact it is experimentally less challenging to make projective measurements on smaller systems consisting of a few TLS rather then large ones described in the Chapter 4. It consists of projective measurements applied in a sequential manner to the pairs of non-interacting or independent TLS with low initial energy and coherence values. The projectors are diagonal in the energy basis, hence, they do not contribute to increase of the coherence of the system. The essence of their application lies in removing the cases of both measured TLS being in their ground states. As a result, they translate a system from a set of independent TLS with local coherences to a correlated larger system with global coherence (the difference quantified by mutual coherence, see Chapter 2, Sec. 2.5), scaling logarithmically with their number N. Moreover, the same procedure as well increases the energy of system, that scales linearly with N, rendering the protocol universal from this perspective.

The robustness of the pairwise protocol was tested for the means of dephasing of the initial and final states before and after the measurement, respectively. According to the outcome, Sec. 5.5, we can conclude that the effect of the latter on the system is not detrimental. Namely, it is still a practically useful strategy for synthesizing coherence with a simultaneous increase of energy, See Fig. 5.2 and Fig. 5.3. This approach gives the largest possible energy per one cycle with a simultaneous increase in coherence. However, experimentally it can be quite challenging to realize such a protocol.

The maximally coherent state is described by the coherence propor-

tional to $\propto N$. If we compare it to our protocol's coherence that is $\propto \ln N$, it is clear that we have enough space for improvements. However, we still are going to limit our optimisations, see Sec. 5.4 to the projective measurements case only, as with the introduction of generalised measurements, POVM, the problem becomes overly complicated and requires sufficient sources to solve it numerically. Therefore, our optimisations constitute in addition of more measurements over pairs of TLS and, therefore, further diminishing the probability of success at cost of improving coherence and energy gains.

We believe that the universality of pairwise protocol may be used as a springboard for others in the research directed toward quantum coherence manipulation [94, 95, 96, 26], or exploited in the field of quantum thermodynamics, e.g., as a quantum battery charging protocol [89, 35, 50]. In case of pairwise protocol, the proof-of-principle test will require many TLS that can be coupled in a pairwise manner, projected, and their overall state evaluated by a quantum-state tomography. Therefore, long-standing trapped ions [17, 18], progressing superconducting qubits [97] and recent optical experiments [98] can be used to test the predicted rules of quantum coherence synthesis.

Chapter 6

Discussions and Outlook

The manipulations of the quantum system with the help of projector-based protocols have two distinctive targets, namely, the concentration of energy and relative entropy of coherence. Consequently, the logical question arises on how would we exploit energy and coherence further? The first quantity, energy, as a basic quantity of thermodynamics constitutes an important resource. It can be converted into useful work that is the foundation of the working principle of heat engines and batteries (in a sense that the stored energy is further exploited for performing work and then the battery is recharged again). The transformations of energy to work and backward should, logically, hold in the quantum regime [99, 100, 63, 101, 102]. However, the latter can profit by the presence of coherence, which, in turn, also constitutes a useful resource itself in applications of quantum technology. The research on quantum coherence is of the main interest recently [19] and found a wide application in the fields of quantum information [103], quantum thermodynamics [104, 105] and quantum metrology [106], and even relatively new and speculative field of quantum biology [107]. It has a promising grounds and is still into the intensive investiga-

tion mode [108, 69, 71, 109] together with its connection to diverse forms of quantum correlations [53, 90, 91, 92, 93, 110].

Another interesting question related to the protocols described in the thesis would be what systems could we apply them to? Since the analysis has a fully theoretical character, in principle, any kind of practically feasible two-level systems [7] exhibiting quantum properties could be used, i.e. nuclear magnetic resonance systems (qubits would correspond to spin states) [10], trapped ions [11], quantum dots etc. Also, TLS states could be realized by atoms and solid-state objects induced by strong coherent force, electric and magnetic fields, or laser/maser radiation. However, the simplest proof-of-principle experimental realization of quantum coherence processing from the point of view of quantum optics would constitute a photonic setup [30] with several possibilities to encode ground and excited states of two-level systems: either in a so-called ”dual-rail” qubits fashion, where states are encoded into two different paths of a photon - it may be either two physically different fibres or two arms of Mach-Zender interferometer [55], and frequently used polarization encoding, i.e. vertical and horizontal polarizations correspond to ground and excited states, respectively. The example of an experimental realization of our idea with the help of a photonic setup where the projective measurements were realized with the help of quantum filters was presented in [74] with the possibility of the enhancement of coherence of such a system.

Bibliography

[1] Yuying Guo. "Introduction to quantum entanglement". In: *AIP Conference Proceedings* 2066.1 (2019), p. 020009. DOI: 10.1063/1.5089051. eprint: https://aip.scitation.org/doi/pdf/10.1063/1.5089051. URL: https://aip.scitation.org/doi/abs/10.1063/1.5089051.

[2] Ryszard Horodecki et al. "Quantum entanglement". In: *Reviews of Modern Physics* 81.2 (June 2009), pp. 865–942. DOI: 10.1103/revmodphys.81.865. URL: https://doi.org/10.1103%2Frevmodphys.81.865.

[3] Martin B. Plenio and S. Virmani. "An introduction to entanglement measures". In: (2005). DOI: 10.48550/ARXIV.QUANT-PH/0504163. URL: https://arxiv.org/abs/quant-ph/0504163.

[4] B. Hensen et al. "Loophole-free Bell inequality violation using electron spins separated by 1.3 kilometres". In: *Nature* 526.7575 (Oct. 2015), pp. 682–686. URL: https://doi.org/10.1038/nature15759.

[5] M. O. Gumberidze et al. "Bell nonlocality in the turbulent atmosphere". In: *Phys. Rev. A* 94 (5 Nov. 2016), p. 053801. DOI: 10.1103/

PhysRevA.94.053801. URL: https://link.aps.org/doi/10.1103/PhysRevA.94.053801.

[6] Nanxi Zou. "Quantum Entanglement and Its Application in Quantum Communication". In: *Journal of Physics: Conference Series* 1827 (Mar. 2021), p. 012120. DOI: 10.1088/1742-6596/1827/1/012120.

[7] M. Fox. *Quantum Optics: An Introduction*. Oxford Master Series in Physics. OUP Oxford, 2006. ISBN: 9780198566731. URL: https://books.google.cz/books?id=2%5C_ZP-LDF9jkC.

[8] Christopher Gerry and Peter Knight. "Applications of entanglement: Heisenberg-limited interferometry and quantum information processing". In: *Introductory Quantum Optics*. Cambridge University Press, 2004, pp. 263–293. DOI: 10.1017/CBO9780511791239.011.

[9] M.A. Nielsen and I.L. Chuang. *Quantum Computation and Quantum Information: 10th Anniversary Edition*. Cambridge University Press, 2010. ISBN: 9781139495486. URL: https://books.google.cz/books?id=-s4DEy7o-a0C.

[10] Tao Xin et al. "Nuclear magnetic resonance for quantum computing: Techniques and recent achievements". In: *Chinese Physics B* 27 (Feb. 2018), p. 020308. DOI: 10.1088/1674-1056/27/2/020308.

[11] Colin D. Bruzewicz et al. "Trapped-ion quantum computing: Progress and challenges". In: *Applied Physics Reviews* 6.2 (2019), p. 021314. DOI: 10.1063/1.5088164. URL: https://doi.org/10.1063/1.5088164.

[12] Thomas Maier et al. “Quantum cluster theories”. In: *Rev. Mod. Phys.* 77 (3 Oct. 2005), pp. 1027–1080. DOI: 10.1103/RevModPhys.77.1027. URL: https://link.aps.org/doi/10.1103/RevModPhys.77.1027.

[13] Zhangjie Qin et al. “Quantifying entanglement in cluster states built with error-prone interactions”. In: *Physical Review Research* 3.4 (Nov. 2021). DOI: 10.1103/physrevresearch.3.043118. URL: https://doi.org/10.1103%2Fphysrevresearch.3.043118.

[14] T. Baumgratz, Marcus Cramer, and M. Plenio. “Quantifying Coherence”. In: *Physical review letters* 113 (Nov. 2013). DOI: 10.1103/PhysRevLett.113.140401.

[15] K. Kraus. *Effects and Operations: Fundamental Notions of Quantum Theory*. Springer, 1983.

[16] Alexander Streltsov, Gerardo Adesso, and Martin B. Plenio. “Colloquium: Quantum coherence as a resource”. In: *Rev. Mod. Phys.* 89 (4 Oct. 2017), p. 041003. DOI: 10.1103/RevModPhys.89.041003. URL: https://link.aps.org/doi/10.1103/RevModPhys.89.041003.

[17] Thomas Monz et al. “14-Qubit Entanglement: Creation and Coherence”. In: *Phys. Rev. Lett.* 106 (13 Mar. 2011), p. 130506. DOI: 10.1103/PhysRevLett.106.130506. URL: https://link.aps.org/doi/10.1103/PhysRevLett.106.130506.

[18] Nicolai Friis et al. “Observation of Entangled States of a Fully Controlled 20-Qubit System”. In: *Phys. Rev. X* 8 (2 Apr. 2018), p. 021012. DOI: 10.1103/PhysRevX.8.021012. URL: https://link.aps.org/doi/10.1103/PhysRevX.8.021012.

[19] Alexander Streltsov et al. “Measuring Quantum Coherence with Entanglement”. In: *Phys. Rev. Lett.* 115 (2 July 2015), p. 020403. DOI: 10.1103/PhysRevLett.115.020403. URL: https://link.aps.org/doi/10.1103/PhysRevLett.115.020403.

[20] Andreas Winter and Dong Yang. “Operational Resource Theory of Coherence”. In: *Phys. Rev. Lett.* 116 (12 Mar. 2016), p. 120404. DOI: 10.1103/PhysRevLett.116.120404. URL: https://link.aps.org/doi/10.1103/PhysRevLett.116.120404.

[21] Shuanping Du, Zhaofang Bai, and Xiaofei Qi. “Coherence manipulation under incoherent operations”. In: *Phys. Rev. A* 100 (3 Sept. 2019), p. 032313. DOI: 10.1103/PhysRevA.100.032313. URL: https://link.aps.org/doi/10.1103/PhysRevA.100.032313.

[22] Bartosz Regula et al. “Coherence manipulation with dephasing-covariant operations”. In: *Phys. Rev. Research* 2 (1 Jan. 2020), p. 013109. DOI: 10.1103/PhysRevResearch.2.013109. URL: https://link.aps.org/doi/10.1103/PhysRevResearch.2.013109.

[23] C. L. Liu and D. L. Zhou. “Deterministic Coherence Distillation”. In: *Phys. Rev. Lett.* 123 (7 Aug. 2019), p. 070402. DOI: 10.1103/PhysRevLett.123.070402. URL: https://link.aps.org/doi/10.1103/PhysRevLett.123.070402.

[24] Zeng-Yu Pang and Ming-Jing Zhao. “Probabilistic coherence distillation with assisted setting”. In: *Quantum Information Processing* 19 (10 2020), p. 363. DOI: 10.1007/s11128-020-02857-5. URL: https://doi.org/10.1007/s11128-020-02857-5.

[25] Kun Fang et al. “Probabilistic Distillation of Quantum Coherence”. In: *Phys. Rev. Lett.* 121 (7 Aug. 2018), p. 070404. DOI: 10.1103/PhysRevLett.121.070404. URL: https://link.aps.org/doi/10.1103/PhysRevLett.121.070404.

[26] Kang-Da Wu et al. “Experimentally obtaining maximal coherence via assisted distillation process”. In: *Optica* 4.4 (Apr. 2017), pp. 454–459. DOI: 10.1364/OPTICA.4.000454. URL: http://www.osapublishing.org/optica/abstract.cfm?URI=optica-4-4-454.

[27] Qi Zhao et al. “One-Shot Coherence Dilution”. In: *Physical Review Letters* 120.7 (Feb. 2018). DOI: 10.1103/physrevlett.120.070403. URL: https://doi.org/10.1103%2Fphysrevlett.120.070403.

[28] Zhengjun Xi, Yu Luo, and Lian-He Shao. “Coherence manipulation under non-cohering operations”. In: *Journal of Physics A: Mathematical and Theoretical* 52.37 (Aug. 2019), p. 375301. DOI: 10.1088/1751-8121/ab35ad. URL: https://doi.org/10.1088/1751-8121/ab35ad.

[29] James Millen and André Xuereb. “The rise of the quantum machines”. In: *Physics World* 29.1 (Jan. 2016), pp. 23–26. DOI: https://doi.org/10.1088/2058-7058/29/1/30. URL: https://doi.org/10.1088%2F2058-7058%2F29%2F1%2F30.

[30] Sergei Slussarenko and Geoff J. Pryde. “Photonic quantum information processing: A concise review”. In: *Applied Physics Reviews* 6.4 (2019), p. 041303. DOI: 10.1063/1.5115814. URL: https://doi.org/10.1063/1.5115814.

[31] Francesco Campaioli, Felix A. Pollock, and Sai Vinjanampathy. "Quantum Batteries - Review Chapter". In: *arXiv: Quantum Physics* (2018).

[32] Giulia Gemme et al. *IBM quantum platforms: a quantum battery perspective*. 2022. DOI: 10.48550/ARXIV.2204.10786. URL: https://arxiv.org/abs/2204.10786.

[33] Gian Marcello Andolina et al. "Quantum versus classical many-body batteries". In: *Phys. Rev. B* 99 (20 May 2019), p. 205437. DOI: 10.1103/PhysRevB.99.205437. URL: https://link.aps.org/doi/10.1103/PhysRevB.99.205437.

[34] Gian Marcello Andolina et al. "Extractable Work, the Role of Correlations, and Asymptotic Freedom in Quantum Batteries". In: *Phys. Rev. Lett.* 122 (4 Feb. 2019), p. 047702. DOI: 10.1103/PhysRevLett.122.047702. URL: https://link.aps.org/doi/10.1103/PhysRevLett.122.047702.

[35] Felix C Binder et al. "Quantacell: powerful charging of quantum batteries". English. In: *New Journal of Physics* 17 (2015). ISSN: 1367-2630. DOI: https://doi.org/10.1088/1367-2630/17/7/075015.

[36] Nicolai Friis and Marcus Huber. "Precision and Work Fluctuations in Gaussian Battery Charging". In: *Quantum* 2 (Apr. 2018), p. 61. DOI: https://doi.org/10.22331/q-2018-04-23-61.

[37] Davide Rossini, Gian Marcello Andolina, and Marco Polini. "Many-body localized quantum batteries". In: *Phys. Rev. B* 100 (11 Sept. 2019), p. 115142. DOI: 10.1103/PhysRevB.100.115142. URL: https://link.aps.org/doi/10.1103/PhysRevB.100.115142.

[38] Donato Farina et al. “Charger-mediated energy transfer for quantum batteries: An open-system approach”. In: *Phys. Rev. B* 99 (3 Jan. 2019), p. 035421. DOI: 10.1103/PhysRevB.99.035421. URL: https://link.aps.org/doi/10.1103/PhysRevB.99.035421.

[39] Robert Alicki. “A quantum open system model of molecular battery charged by excitons”. In: *J. Chem. Phys. 150, 214110* 150 (214110 June 2019). DOI: https://doi.org/10.1063/1.5096772.

[40] Junjie Liu, Dvira Segal, and Gabriel Hanna. “Loss-Free Excitonic Quantum Battery”. In: *The Journal of Physical Chemistry C* 123.30 (2019), pp. 18303–18314. DOI: 10.1021/acs.jpcc.9b06373. eprint: https://doi.org/10.1021/acs.jpcc.9b06373. URL: https://doi.org/10.1021/acs.jpcc.9b06373.

[41] Felipe Barra. “Dissipative Charging of a Quantum Battery”. In: *Phys. Rev. Lett.* 122 (21 May 2019), p. 210601. DOI: 10.1103/PhysRevLett.122.210601. URL: https://link.aps.org/doi/10.1103/PhysRevLett.122.210601.

[42] Thao P. Le et al. “Spin-chain model of a many-body quantum battery”. In: *Phys. Rev. A* 97 (2 Feb. 2018), p. 022106. DOI: https://doi.org/10.1103/PhysRevA.97.022106. URL: https://link.aps.org/doi/10.1103/PhysRevA.97.022106.

[43] F. H. Kamin et al. “Entanglement, coherence, and charging process of quantum batteries”. In: *Phys. Rev. E* 102 (5 Nov. 2020), p. 052109. DOI: 10.1103/PhysRevE.102.052109. URL: https://link.aps.org/doi/10.1103/PhysRevE.102.052109.

[44] Srijon Ghosh, Titas Chanda, and Aditi Sen(De). "Enhancement in the performance of a quantum battery by ordered and disordered interactions". In: *Phys. Rev. A* 101 (3 Mar. 2020), p. 032115. DOI: 10.1103/PhysRevA.101.032115. URL: https://link.aps.org/doi/10.1103/PhysRevA.101.032115.

[45] Dario Ferraro et al. "High-Power Collective Charging of a Solid-State Quantum Battery". In: *Phys. Rev. Lett.* 120 (11 Mar. 2018), p. 117702. DOI: https://doi.org/10.1103/PhysRevLett.120.117702. URL: https://link.aps.org/doi/10.1103/PhysRevLett.120.117702.

[46] Yu-Yu Zhang et al. "Powerful harmonic charging in a quantum battery". In: *Phys. Rev. E* 99 (5 May 2019), p. 052106. DOI: 10.1103/PhysRevE.99.052106. URL: https://link.aps.org/doi/10.1103/PhysRevE.99.052106.

[47] Jingbiao Chen et al. "Charging Quantum Batteries with a General Harmonic Driving Field". In: *arXiv: Quantum Physics* (2019).

[48] Faezeh Pirmoradian and Klaus Mølmer. "Aging of a quantum battery". In: *Phys. Rev. A* 100 (4 Oct. 2019), p. 043833. DOI: 10.1103/PhysRevA.100.043833. URL: https://link.aps.org/doi/10.1103/PhysRevA.100.043833.

[49] Alan C. Santos et al. "Stable adiabatic quantum batteries". In: *Phys. Rev. E* 100 (3 Sept. 2019), p. 032107. DOI: 10.1103/PhysRevE.100.032107. URL: https://link.aps.org/doi/10.1103/PhysRevE.100.032107.

[50] Francesco Campaioli et al. "Enhancing the Charging Power of Quantum Batteries". In: *Phys. Rev. Lett.* 118 (15 Apr. 2017), p. 150601. DOI:

https://doi.org/10.1103/PhysRevLett.118.150601. URL: https://link.aps.org/doi/10.1103/PhysRevLett.118.150601.

[51] Stefano Gherardini et al. "Stabilizing open quantum batteries by sequential measurements". In: *Phys. Rev. Research* 2 (1 Jan. 2020), p. 013095. DOI: 10.1103/PhysRevResearch.2.013095. URL: https://link.aps.org/doi/10.1103/PhysRevResearch.2.013095.

[52] Mathieu Huot and Sam Staton. "Universal Properties in Quantum Theory". In: *Electronic Proceedings in Theoretical Computer Science* 287 (Jan. 2019). DOI: 10.4204/EPTCS.287.12.

[53] Zhengjun Xi, Yongming Li, and Heng Fan. "Quantum coherence and correlations in quantum system". In: *Scientific Reports* 5 (1 2015), p. 10922. DOI: 10.1038/srep10922. URL: https://doi.org/10.1038/srep10922.

[54] Ingemar Bengtsson and Karol Zyczkowski. "Geometry of Quantum States: An Introduction to Quantum Entanglement". In: (Aug. 2006). DOI: https://doi.org/10.1017/CBO9780511535048.

[55] Miloslav Dušek. *Koncepční otázky kvantové teorie /*. Jan. 2002.

[56] P. Kammerlander and J. Anders. "Coherence and measurement in quantum thermodynamics". In: *Scientific Reports* 6.1 (Feb. 2016), p. 22174. ISSN: 2045-2322. DOI: 10.1038/srep22174. URL: https://doi.org/10.1038/srep22174.

[57] Alain Deville and Yannick Deville. "Clarifying the link between von Neumann and thermodynamic entropies". In: *The European Physical Journal H* 38.1 (Jan. 2013), pp. 57–81. ISSN: 2102-6467. DOI:

10.1140/epjh/e2012-30032-0. URL: https://doi.org/10.1140/epjh/e2012-30032-0.

[58] Paul Skrzypczyk, Anthony J. Short, and Sandu Popescu. "Work extraction and thermodynamics for individual quantum systems". In: *Nature Communications* 5.1 (June 2014), p. 4185. ISSN: 2041-1723. DOI: 10.1038/ncomms5185. URL: https://doi.org/10.1038/ncomms5185.

[59] A. Ü. C. Hardal and O. E. Müstecaplıoğlu. "Superradiant Quantum Heat Engine". In: *Scientific Reports* 5.1 (Aug. 2015), p. 12953. DOI: https://doi.org/10.1038/srep12953. URL: https://doi.org/10.1038/srep12953.

[60] Gonzalo Manzano et al. "Entropy production and thermodynamic power of the squeezed thermal reservoir". In: *Phys. Rev. E* 93 (5 May 2016), p. 052120. DOI: 10.1103/PhysRevE.93.052120. URL: https://link.aps.org/doi/10.1103/PhysRevE.93.052120.

[61] Nicolas Brunner et al. "Entanglement enhances cooling in microscopic quantum refrigerators". In: *Phys. Rev. E* 89 (3 Mar. 2014), p. 032115. DOI: 10.1103/PhysRevE.89.032115. URL: https://link.aps.org/doi/10.1103/PhysRevE.89.032115.

[62] Raam Uzdin, Amikam Levy, and Ronnie Kosloff. "Equivalence of Quantum Heat Machines, and Quantum-Thermodynamic Signatures". In: *Phys. Rev. X* 5 (3 Sept. 2015), p. 031044. DOI: 10.1103/PhysRevX.5.031044. URL: https://link.aps.org/doi/10.1103/PhysRevX.5.031044.

[63] James Klatzow et al. “Experimental Demonstration of Quantum Effects in the Operation of Microscopic Heat Engines”. In: *Phys. Rev. Lett.* 122 (11 Mar. 2019), p. 110601. DOI: https://doi.org/10.1103/PhysRevLett.122.110601. URL: https://link.aps.org/doi/10.1103/PhysRevLett.122.110601.

[64] Serge Haroche. “Nobel Lecture: Controlling photons in a box and exploring the quantum to classical boundary”. In: *Rev. Mod. Phys.* 85 (3 July 2013), pp. 1083–1102. DOI: 10.1103/RevModPhys.85.1083. URL: https://link.aps.org/doi/10.1103/RevModPhys.85.1083.

[65] Dietrich Leibfried et al. “Quantum dynamics of single trapped ions”. In: *Reviews of Modern Physics* 75 (2003), pp. 281–324.

[66] Alexandre Blais et al. “Circuit quantum electrodynamics”. In: *Rev. Mod. Phys.* 93 (2 May 2021), p. 025005. DOI: 10.1103/RevModPhys.93.025005. URL: https://link.aps.org/doi/10.1103/RevModPhys.93.025005.

[67] Mariia Gumberidze, Michal Kolář, and Radim Filip. “Measurement Induced Synthesis of Coherent Quantum Batteries”. In: *Scientific Reports* 9 (1 Dec. 2019), p. 19628. DOI: 10.1038/s41598-019-56158-8. URL: https://doi.org/10.1038/s41598-019-56158-8.

[68] Giacomo Guarnieri, Michal Kolá ř, and Radim Filip. “Steady-State Coherences by Composite System-Bath Interactions”. In: *Phys. Rev. Lett.* 121 (7 Aug. 2018), p. 070401. DOI: https://doi.org/10.1103/PhysRevLett.121.070401. URL: https://link.aps.org/doi/10.1103/PhysRevLett.121.070401.

[69] Archak Purkayastha et al. “Tunable phonon-induced steady-state coherence in a double-quantum-dot charge qubit”. In: *npj Quantum Information* 6 (1 2020), p. 22. DOI: 10.1038/s41534-020-0256-6. URL: https://doi.org/10.1038/s41534-020-0256-6.

[70] Giacomo Guarnieri et al. “Non-equilibrium steady-states of memoryless quantum collision models”. In: *Physics Letters A* 384.24 (2020), p. 126576. ISSN: 0375-9601. DOI: https://doi.org/10.1016/j.physleta.2020.126576. URL: https://www.sciencedirect.com/science/article/pii/S0375960120304436.

[71] Ricardo Román-Ancheyta et al. “Enhanced steady-state coherence via repeated system-bath interactions”. In: *Phys. Rev. A* 104 (6 Dec. 2021), p. 062209. DOI: 10.1103/PhysRevA.104.062209. URL: https://link.aps.org/doi/10.1103/PhysRevA.104.062209.

[72] Artur Slobodeniuk, Tomáš Novotný, and Radim Filip. “Extraction of autonomous quantum coherences”. In: *Quantum* 6 (Apr. 2022), p. 689. DOI: 10.22331/q-2022-04-15-689. URL: https://doi.org/10.22331/q-2022-04-15-689.

[73] Christopher Gerry and Peter Knight. “Dissipative interactions and decoherence”. In: *Introductory Quantum Optics*. Cambridge University Press, 2004, pp. 195–212. DOI: 10.1017/CBO9780511791239.008.

[74] Robert Stárek et al. “Experimental demonstration of optimal probabilistic enhancement of quantum coherence”. In: *Quantum Science and Technology* 6.4 (July 2021), p. 045010. ISSN: 2058-9565. DOI: 10.

1088/2058-9565/ac10ef. URL: http://dx.doi.org/10.1088/2058-9565/ac10ef.

[75] Lucie Bartůšková et al. "Optical implementation of the encoding of two qubits to a single qutrit". In: *Phys. Rev. A* 74 (2 Aug. 2006), p. 022325. DOI: 10.1103/PhysRevA.74.022325. URL: https://link.aps.org/doi/10.1103/PhysRevA.74.022325.

[76] Martina Miková et al. "Carrying qubits with particles whose noninformational degrees of freedom are nonfactorable". In: *Phys. Rev. A* 87 (4 Apr. 2013), p. 042327. DOI: 10.1103/PhysRevA.87.042327. URL: https://link.aps.org/doi/10.1103/PhysRevA.87.042327.

[77] Mario A. Ciampini et al. "Experimental extractable work-based multipartite separability criteria". In: *npj Quantum Information* 3.1 (2017), p. 10. DOI: https://doi.org/10.1038/s41534-017-0011-9.

[78] Luca Mancino et al. "Experimental extractable work-based multipartite separability criteria". In: *npj Quantum Information* 4.1 (2018), p. 20. DOI: https://doi.org/10.1038/s41534-018-0069-z.

[79] D. L. Moehring et al. "Entanglement of single-atom quantum bits at a distance". In: *Nature* 449.1 (Sept. 2007), pp. 68–71. DOI: https://doi.org/10.1038/nature06118. URL: https://doi.org/10.1038/nature06118.

[80] L. Slodička et al. "Atom-Atom Entanglement by Single-Photon Detection". In: *Phys. Rev. Lett.* 110 (8 Feb. 2013), p. 083603. DOI: https:

//doi.org/10.1103/PhysRevLett.110.083603. URL: https://doi.org/10.1103/PhysRevLett.110.083603.

[81] Julian Hofmann et al. "Heralded Entanglement Between Widely Separated Atoms". In: *Science* 337.6090 (2012), pp. 72–75. ISSN: 0036-8075. DOI: 10.1126/science.1221856. eprint: https://science.sciencemag.org/content/337/6090/72.full.pdf. URL: https://science.sciencemag.org/content/337/6090/72.

[82] E. Togan et al. "Quantum entanglement between an optical photon and a solid-state spin qubit". In: *Nature* 466.1 (Aug. 2010), pp. 730–734. DOI: https://doi.org/10.1038/nature09256. URL: https://doi.org/10.1038/nature09256.

[83] B. Hensen et al. "Loophole-free Bell inequality violation using electron spins separated by 1.3 kilometres". In: *Nature* 526.1 (Aug. 2015), pp. 682–686. DOI: https://doi.org/10.1038/nature15759. URL: https://doi.org/10.1038/nature15759.

[84] J.J. Alonso, E. Lutz, and A. Romito. "Thermodynamics of Weakly Measured Quantum Systems". In: *Phys. Rev. Lett.* 116 (8 Feb. 2016), p. 080403. DOI: https://doi.org/10.1103/PhysRevLett.116.080403. URL: https://doi.org/10.1103/PhysRevLett.116.080403.

[85] Mihai D. Vidrighin et al. "Photonic Maxwell's Demon". In: *Phys. Rev. Lett.* 116 (5 Feb. 2016), p. 050401. DOI: https://doi.org/10.1103/PhysRevLett.116.050401. URL: https://link.aps.org/doi/10.1103/PhysRevLett.116.050401.

[86] Luca Mancino et al. “Quantum Simulation of Single-Qubit Thermometry Using Linear Optics”. In: *Phys. Rev. Lett.* 118 (13 Mar. 2017), p. 130502. DOI: https://doi.org/10.1103/PhysRevLett.118.130502. URL: https://doi.org/10.1103/PhysRevLett.118.130502.

[87] Luca Mancino et al. “Geometrical Bounds on Irreversibility in Open Quantum Systems”. In: *Phys. Rev. Lett.* 121 (16 Oct. 2018), p. 160602. DOI: https://doi.org/10.1103/PhysRevLett.121.160602. URL: https://doi.org/10.1103/PhysRevLett.121.160602.

[88] Mariia Gumberidze, Michal Kolář, and Radim Filip. “Pairwise-measurement-induced synthesis of quantum coherence”. In: *Phys. Rev. A* 105 (1 Jan. 2022), p. 012401. DOI: 10.1103/PhysRevA.105.012401. URL: https://link.aps.org/doi/10.1103/PhysRevA.105.012401.

[89] Robert Alicki and Mark Fannes. “Entanglement boost for extractable work from ensembles of quantum batteries”. In: *Phys. Rev. E* 87 (4 Apr. 2013), p. 042123. DOI: https://doi.org/10.1103/PhysRevE.87.042123. URL: https://link.aps.org/doi/10.1103/PhysRevE.87.042123.

[90] Yu Guo and Sumit Goswami. “Discordlike correlation of bipartite coherence”. In: *Phys. Rev. A* 95 (6 June 2017), p. 062340. DOI: 10.1103/PhysRevA.95.062340. URL: https://link.aps.org/doi/10.1103/PhysRevA.95.062340.

[91] Xiao-Li Wang et al. “Relating quantum coherence and correlations with entropy-based measures”. In: *Scientific Reports* 7 (1 2017), p. 12122.

DOI: 10.1038/s41598-017-09332-9. URL: https://doi.org/10.1038/s41598-017-09332-9.

[92] Kok Chuan Tan and Hyunseok Jeong. "Entanglement as the Symmetric Portion of Correlated Coherence". In: *Phys. Rev. Lett.* 121 (22 Nov. 2018), p. 220401. DOI: 10.1103/PhysRevLett.121.220401. URL: https://link.aps.org/doi/10.1103/PhysRevLett.121.220401.

[93] Tristan Kraft and Marco Piani. "Genuine correlated coherence". In: *Journal of Physics A: Mathematical and Theoretical* 51.41 (Sept. 2018), p. 414013. DOI: 10.1088/1751-8121/aab8ad. URL: https://doi.org/10.1088/1751-8121/aab8ad.

[94] Max Hofheinz et al. "Synthesizing arbitrary quantum states in a superconducting resonator". In: *Nature* 459 (7246 2009), p. 546. URL: https://doi.org/10.1038/nature08005.

[95] Zaki Leghtas et al. "Deterministic protocol for mapping a qubit to coherent state superpositions in a cavity". In: *Phys. Rev. A* 87 (4 Apr. 2013), p. 042315. DOI: 10.1103/PhysRevA.87.042315. URL: https://link.aps.org/doi/10.1103/PhysRevA.87.042315.

[96] Roshan Sharma and Frederick W. Strauch. "Quantum state synthesis of superconducting resonators". In: *Phys. Rev. A* 93 (1 Jan. 2016), p. 012342. DOI: 10.1103/PhysRevA.93.012342. URL: https://link.aps.org/doi/10.1103/PhysRevA.93.012342.

[97] Frank Arute et al. "Quantum supremacy using a programmable superconducting processor". In: *Nature* 574 (7779 2019). DOI: 10.

1038/s41586-019-1666-5. URL: https://doi.org/10.1038/s41586-019-1666-5.

[98] Hui Wang et al. "Boson Sampling with 20 Input Photons and a 60-Mode Interferometer in a 10^{14}-Dimensional Hilbert Space". In: *Phys. Rev. Lett.* 123 (25 Dec. 2019), p. 250503. DOI: 10.1103/PhysRevLett.123.250503. URL: https://link.aps.org/doi/10.1103/PhysRevLett.123.250503.

[99] Quentin Bouton et al. "A quantum heat engine driven by atomic collisions". In: *Nature Communications* 12.1 (Apr. 2021), p. 2063.

[100] Mohit Lal Bera et al. "Quantum heat engines with Carnot efficiency at maximum power". In: *Physical Review Research* 4.1 (Feb. 2022). DOI: 10.1103/physrevresearch.4.013157. URL: https://doi.org/10.1103%2Fphysrevresearch.4.013157.

[101] G. Francica et al. "Quantum Coherence and Ergotropy". In: *Phys. Rev. Lett.* 125 (18 Oct. 2020), p. 180603. DOI: 10.1103/PhysRevLett.125.180603. URL: https://link.aps.org/doi/10.1103/PhysRevLett.125.180603.

[102] Martí Perarnau-Llobet and Raam Uzdin. "Collective operations can extremely reduce work fluctuations". In: *New Journal of Physics* 21.8 (Aug. 2019), p. 083023. DOI: 10.1088/1367-2630/ab36a9. URL: https://doi.org/10.1088/1367-2630/ab36a9.

[103] G Wendin. "Quantum information processing with superconducting circuits: a review". In: *Reports on Progress in Physics* 80.10 (Sept. 2017), p. 106001. DOI: 10.1088/1361-6633/aa7e1a. URL: https://doi.org/10.1088/1361-6633/aa7e1a.

[104] Janet Anders and Massimiliano Esposito. “Focus on quantum thermodynamics”. In: *New Journal of Physics* 19.1 (Jan. 2017), p. 010201. DOI: 10.1088/1367-2630/19/1/010201. URL: https://doi.org/10.1088/1367-2630/19/1/010201.

[105] John Goold et al. “The role of quantum information in thermodynamics—a topical review”. In: *Journal of Physics A: Mathematical and Theoretical* 49.14 (Feb. 2016), p. 143001. DOI: 10.1088/1751-8113/49/14/143001. URL: https://doi.org/10.1088/1751-8113/49/14/143001.

[106] C. L. Degen, F. Reinhard, and P. Cappellaro. “Quantum sensing”. In: *Rev. Mod. Phys.* 89 (3 July 2017), p. 035002. DOI: 10.1103/RevModPhys.89.035002. URL: https://link.aps.org/doi/10.1103/RevModPhys.89.035002.

[107] Seth Lloyd. “Quantum coherence in biological systems”. In: *Journal of Physics: Conference Series* 302 (July 2011), p. 012037. DOI: 10.1088/1742-6596/302/1/012037. URL: https://doi.org/10.1088/1742-6596/302/1/012037.

[108] Kang-Da Wu et al. “Quantum coherence and state conversion: theory and experiment”. In: *npj Quantum Information* 6 (1 2020), p. 22. DOI: 10.1038/s41534-020-0250-z. URL: https://doi.org/10.1038/s41534-020-0250-z.

[109] Yao Yao et al. “Quantum coherence in multipartite systems”. In: *Phys. Rev. A* 92 (2 Aug. 2015), p. 022112. DOI: 10.1103/PhysRevA.92.022112. URL: https://link.aps.org/doi/10.1103/PhysRevA.92.022112.

[110] Jiajun Ma et al. “Converting Coherence to Quantum Correlations”. In: *Phys. Rev. Lett.* 116 (16 Apr. 2016), p. 160407. DOI: 10.1103/PhysRevLett.116.160407. URL: https://link.aps.org/doi/10.1103/PhysRevLett.116.160407.

Measurement Induced Synthesis of Energy and Quantum Coherence

a dissertation report

by Mariia Gumberidze

Faculty of science

Palacký University

Olomouc 2022

Title:	Measurement Induced Synthesis of Energy and Quantum Coherence
Author:	Mgr. Mariia Gumberidze
Supervisor:	Prof. Mgr. Radim Filip, Ph.D.
Co-supervisor:	Mgr. Michal Kolář, Ph.D.
Study progamme:	Optics and Optoelectronics
Institution:	Department of Optics, Faculty of Science, Palacký University Olomouc
Reviewers:	.....
	.....
	.....
	.....

The thesis is an original work of its author carried out under the guidance of a supervisor Prof. Mgr. Radim Filip, Ph.D. and a co-supervisor Mgr. Michal Kolář, Ph.D. It has not been submitted for a degree before. This thesis may be freely distributed in an unchanged form. Palacký University has the rights to archive, publish and distribute the thesis according to its internal regulations and Czech law.

The thesis is available for reading at the study department of the Faculty of Science, Palacký University, 17. listopadu 12, Olomouc. It is also available online at stag.upol.cz under Browse and Theses. The personal number is R16057.

Abstract

In the thesis, we study complementary values of energy and coherence of the system consisting of many copies of independent two-level systems (TLS) with initial non-zero but small energy and coherence values. Two methods of enhancement and simultaneous concentration of both quantities with the help of the measurement procedure were considered: global (acting on all TLS) and pairwise (acting on pairs of TLS) measurements protocols. The first one has a large probability of success whereas the second is presumably advantageous in more feasible experimental realization. Both approaches employ as a measurement a projector cancelling out the total ground state of all TLS at once or in a pairwise fashion, respectively. The procedure was optimized with the introduction of the projective operator valued measures and tested for decoherence-induced imperfections.

Keywords: quantum thermodynamics, energy, relative entropy of coherence, mutual coherence, two-level systems

Acknowledgements

I would like to thank my supervisor prof. Radim Filip and co-supervisor Michal Kolář for their unfailing guidance, brilliant ideas, support and endless useful scientific discussions throughout my PhD. My gratitude to the Department of Optics for a good working atmosphere. I appreciate the Fischer scholarship for the financing of my doctoral studies. Thanks to the group of prof. Lutz for welcoming me in Stuttgart and introducing the quantum thermodynamics field to me. I am grateful to all my friends and parents who were supporting me through this period. Eventually, I would like to dedicate this work to the light memory of my father.

Contents

1 Introduction

This report presents the main results of the thesis titled Measurement Induced Synthesis of Energy and Quantum Coherence. In the thesis, we want to study the simultaneous enhancement and synthesis of quantities and figures of merit, namely, energy and quantum coherence of the set of independent copies of two-level systems. We begin by introducing the concepts of projective and generalised measurements and the measures of coherence in Section 2. After a brief discussion of the above-mentioned tools, we then move to the basic notions of the thesis, Section 3. We introduce the system, afterwards, we define quantities of interest, namely, energy and coherence. In addition, we present some preliminary results discussed in the following Section. In the next Chpater 4, our goal is to study the enhancement of energy and coherence by the means of the protocol, that employs a global measurement over a system. After a brief characterisation of the latter, we probe the validity of our results un-

der decoherence process, namely, dephasing. Further, we illustrate our findings for the optimizations of the protocol with the help of projector-valued operator measures. To conclude the Section, we study generalisations of the global protocol to many copies of TLS. Then in the following Section 5, we move away from a single measurement over all TLS constituting the system and instead consider to the measurements over pairs of TLS. We begin by introducing the pairwise protocol assuming the system is in a pure state. Then we present approximations of the values of quantities of interest as their analytical full-form counterparts are cumbersome. Equipped with this knowledge we shift our focus to testing the robustness of the protocol. In particular, we study how two dephasing processes before and after measurement affect the results. Lastly, in Section 6, we conclude the thesis with a final discussion of our results.

2 Methods

Projective measurements

Projective measurements [1], shortly projections, in quantum mechanics are usually described by an observable

$$\hat{M} = \sum_m m\hat{P}_m \tag{1}$$

where m are the possible outcomes of the measurement corresponding to the projective operator $\hat{P}_m$. Projections satisfy the completeness relation $\sum_i \hat{P}_i = \hat{I}$. The property distinguishing them from other types of generalised measurements is their mutual orthogonality $\hat{P}_i\hat{P}_j = \hat{P}_i\delta_{ij}$ and, therefore, repeatability $\hat{P}_m\hat{P}_m = \hat{P}_m$.

The projective measurement is called selective [2] if the specific out-

come with a concrete eigenvalue is observed. Let's assume the system we measure is in a pure state $|\psi\rangle$. A selective measurement would give a concrete outcome with an eigenvalue m and a resulting post-measurement state

$$|\psi'\rangle = \frac{\hat{P}_m |\psi\rangle}{\sqrt{\langle\psi| \hat{P}_m |\psi\rangle}}. \tag{2}$$

POVM

Positive operator valued measures, or POVMs [1], are defined as a set of operators $\{E_m\}$ called POVM elements, that satisfy the completness relation

$$\sum_m \hat{E}_m = \hat{I}, \tag{3}$$

with the probability of m-th outcome

$$p_m = \langle\psi| \hat{E}_m |\psi\rangle . \tag{4}$$

In the thesis POVMs are considered as an alternative to projections for optimization purposes. We can define the measurement operators $\hat{M}_m = \sqrt{\hat{E}_m}$, that are non-orthogonal, therefore, unrepeatable $\hat{M}_m \hat{M}_m \neq \hat{M}_m$. In addition, the requirement of positivity is introduced $\hat{E}_m \geqslant 0$, namely, for every state $|\psi\rangle$ we can write $\langle\psi| \hat{E}_m |\psi\rangle \geqslant 0$.

Relative entropy of coherence

The choice of the relative entropy of coherence, Eq. (5), as our measure is motivated by the recognized connection of $C(\hat{\rho})$ with thermodynamic quantities [3] and the notion of von Neumann entropy, naturally connecting this measure and thermodynamics in much broader sense [4]. The latter is defined as

$$S(\hat{\rho}||\hat{\sigma}) = \mathrm{Tr}(\hat{\rho} \ln \hat{\rho}) - \mathrm{Tr}(\hat{\rho} \ln \hat{\sigma}), \tag{5}$$

where $\hat{\sigma}$ is the *diagonal* version of the state $\hat{\rho}$ in the *energy* basis.

Mutual coherence

For the sake of distinguishing between local and global coherence, we introduce a quantity called *mutual relative entropy of coherence* [5]. It represents

$$C_m(\hat{\rho}) = S(\hat{\rho}||\bigotimes_i \hat{\rho}_i) - S(\hat{\rho}^{diag}||\bigotimes_i \hat{\rho}_i^{diag}) \tag{6}$$

where $\hat{\rho}$, $\hat{\rho}_i = \mathrm{Tr}_{\forall j \neq i}(\hat{\rho})$ denote the total state of the system and the local states of its constituents, respectively, whereas $\hat{\rho}^{diag}$, $\hat{\rho}_i^{diag}$ are the diagonal (or fully dephased) versions of states. The mutual coherence specifies how much the distance (characterized by the relative entropy, however, not in a strict sense as it does not have properties of distance) of the state $\hat{\rho}$ with respect to the corresponding product of local states $\bigotimes_{i=1}^{N} \hat{\rho}_i$ increases compared to distance between diagonal (fully dephased) versions of that states. The RHS of Eq. (6) can be, after some algebra, simplified to

$$C_m(\hat{\rho}) = C(\hat{\rho}) - C^{loc}(\hat{\rho}), \tag{7}$$

where $C^{loc}(\hat{\rho}) \equiv \sum_i C(\hat{\rho}_i)$, with the local states $\hat{\rho}_i$ defined as in (6).

3 Basic notions

In this thesis we aim to coherently charge and synthesize a system comprised of many TLS by the means of projective measurements. The benefits of energy gain is clear from the point of view of thermodynamics as we get charging device or a battery. Latest research shows that quantum coherence is a useful resource: these could be extracting larger average amount of energy from a quantum system [6], increasing the potential

usefulness of the thermal reservoirs [7, 8] or increase in the power output of thermal machines [9], [10], even with experimental demonstration [11].

System of interest

As a simplified system, at first, we consider two independent copies of TLS, denoted 1 and 2, with a non-zero energy gap E between the states. The preferred basis of the pair of TLSs, which we will uniquely refer to throughout the thesis, will be given by the TLS energy eigenstates labeling the ground and excited state, respectively, $\{|g_j\rangle, |e_j\rangle\}$, for both subsystems $j = 1, 2$. The Hamiltonians defining these states read

$$\hat{H}_j = \frac{E}{2}\left(|e_j\rangle\langle e_j| - |g_j\rangle\langle g_j|\right), \quad j = 1, 2, \tag{8}$$

yielding the Hamiltonian of the total system

$$\hat{H} = \hat{H}_1 \otimes \hat{1}_2 + \hat{1}_1 \otimes \hat{H}_2. \tag{9}$$

In general, our system may consist of an arbitrary number N of TLS. The Hamiltonian of the total system would be then

$$\hat{H}^{(N)} = \sum_{j=1}^{N} \hat{H}_j \bigotimes_{\substack{k=1 \\ k\neq j}}^{N} \hat{\mathbb{1}}^{(k)}, \tag{10}$$

where the Hamiltonian of a single TLS is given by (8).

Energy and coherence

The average energy of any quantum state of our system is determined in a standard way as $\langle E\rangle = \mathrm{Tr}(\hat{\rho}\hat{H})$. To quantify coherence of the state, we use the relative entropy of coherence (denoted simply "coherence" from now on) defined as [12]

$$C(\hat{\rho}) = S(\hat{\rho}_{diag}) - S(\hat{\rho}), \tag{11}$$

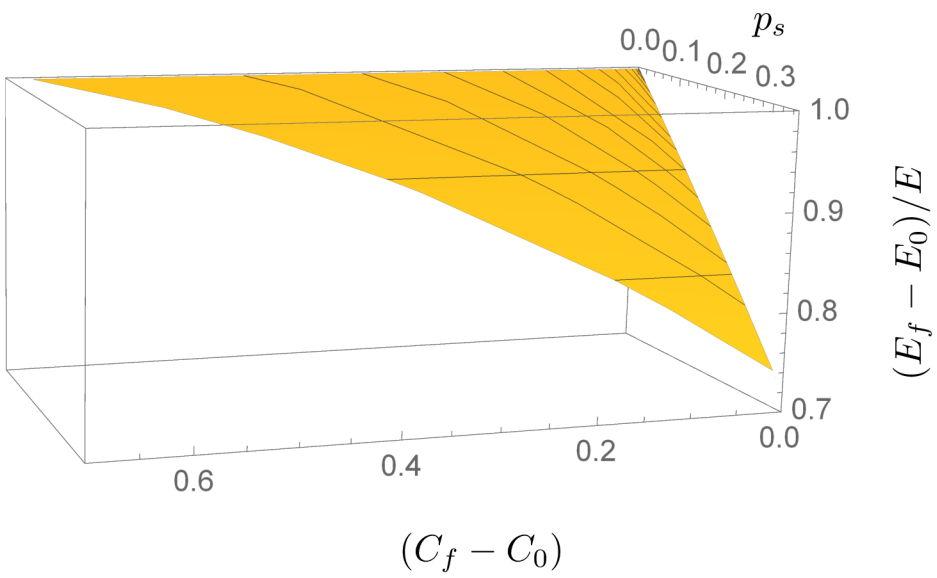

Figure 1: Parametric 3D plot of the relative entropy of coherence difference ΔC, Eq. (13), on x-axis, the normalized average energy difference $\Delta E/E$, Eq. (12), on z-axis and single run probability of success p_s on y-axis. It demonstrates the basic result of the global protocol, Sec. 4, for a pair of TLS: simultaneous increase in the energy and coherence of the battery (after the charging process) with sufficient probability of success.

where $S(\hat{\rho}) = -\mathrm{Tr}(\hat{\rho}\ln\hat{\rho})$ is von Neumann entropy and $S(\hat{\rho}_{diag})$ is the entropy of the *diagonal* version of the state with respect to the *energy* basis.

As we are interested in changes of the battery energy and coherence, we focus on the behavior of the energy difference

$$\Delta E = E_f - E_0, \quad E_f \equiv \mathrm{Tr}(\hat{\rho}_f \hat{H}), \quad E_0 \equiv \mathrm{Tr}(\hat{\rho}_0 \hat{H}), \tag{12}$$

between the final energy after the charging and the initial energy before the charging process, respectively. Similarly, we focus on the change of the coherence

$$\Delta C = C_f - C_0, \quad C_f \equiv C(\hat{\rho}_f), \quad C_0 \equiv C(\hat{\rho}_0), \tag{13}$$

of the battery state.

By advancing substantially presentation of the results, we can see the opening result for a global protocol plotted in Fig. 1. The plot shows the simultaneous increase in the energy $\Delta E > 0$ and coherence $\Delta C > 0$ of the battery after charging process with non-negligible probability of success p_s.

4 Energy and coherence synthesis by a global protocol

This Section is based on the publication by Gumberidze *et al.* [13].

Pure states

For instance, let us assume the charging of a battery consisting of a pair of TLS in pure states

$$|\psi_j\rangle = \sqrt{p}\ |e_j\rangle + \sqrt{1-p}\ |g_j\rangle\,, \quad j = 1, 2, \tag{14}$$

where the Hamiltonians defining the respective energy eigenstates are in Eq. (8). Hence the total state of the system will be the direct product of two single TLS states

$$|\Psi_i\rangle = |\psi_1\rangle \otimes |\psi_2\rangle\,.$$

Such a system has the following initial average energy and coherence equal to

$$E_0 = \langle\Psi_i|\,\hat{H}\,|\Psi_i\rangle = (2p-1)E, \tag{15}$$

$$C_0 = -2\left[p\ln p + (1-p)\ln(1-p)\right], \tag{16}$$

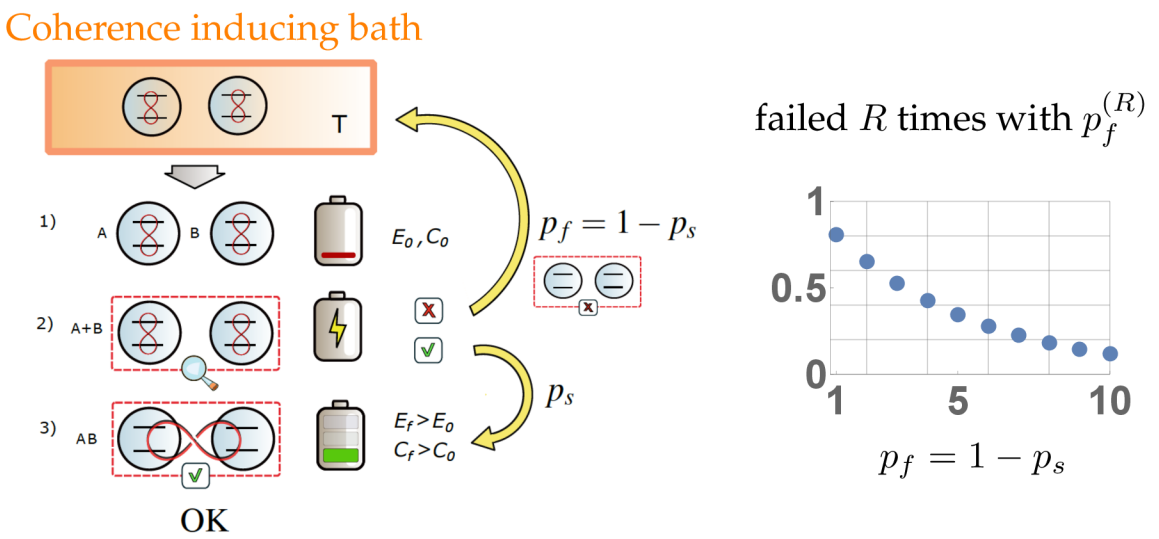

Figure 2: Schematics showing the idea of the 2-TLS battery charging process in three steps and (inset) the total probability of failure $p_f^{(R)}$ after R unsuccessful repetitions. In the initial step 1) the pair of TLS leaves the cold coherence inducing bath [14] and enters the process, assumed to be almost discharged with low initial energy E_0 and coherence C_0 (red loops connecting the levels). Step 2) represents the *conditional* stage of the charging operation. If the outcome of this step is successful (see step 3) with the single run probability of success p_s, the battery is made more coherent and simultaneously charged, i.e., has higher energy $E_f > E_0$ and increased coherence $C_f > C_0$ as well, both with respect to the eigenbasis of Hamiltonian (9). If the charging fails, with the single run probability $p_f = (1 - p_s)$ in step 2), the battery is completely discharged and incoherent. In principle it can be recycled by bringing it in contact with the bath again and the protocol is repeated until success (RUS). If the charging does not successfully occur in R recycling runs, the total probability of failure, $p_f^{(R)} = (1 - p_s)^R$, is exponentially converging to zero with the number of repetitions, see the inset for a typical behavior.

with respect to Hamiltonian (9). We choose the pair of two complementary projective operators $\{\hat{P}_0, \hat{P}_1 = \hat{1} - \hat{P}_0\}$, with

$$\hat{P}_0 = |g_1 g_2\rangle \langle g_1 g_2|, \quad \hat{P}_1 = \hat{1} - |g_1 g_2\rangle \langle g_1 g_2|. \tag{17}$$

The final state of the system after application of the pair (17) will be of the form

$$|\Psi_0\rangle = \frac{\hat{P}_0 |\Psi_i\rangle}{\sqrt{1-p_s}} = |g_1 g_2\rangle, \tag{18}$$

$$|\Psi_f\rangle = \frac{\hat{P}_1 |\Psi_i\rangle}{\sqrt{p_s}} = \frac{p |e_1 e_2\rangle + \sqrt{p(1-p)}\,(|e_1 g_2\rangle + |g_1 e_2\rangle)}{\sqrt{p(2-p)}}, \quad p \neq 0, \tag{19}$$

where we are more interested into the state $|\Psi_f\rangle$ as it represents the successful outcome of the measurement process with th. probability of success $p_s = p(2-p)$.

If we consider the pair of our TLS as a battery to be charged then the procedure described before would serve as a probabilistic protocol of charging, Fig. 2.

The final energy and coherence of the state are

$$E_f = \langle \Psi_f | \hat{H} | \Psi_f \rangle = \frac{pE}{2-p}, \tag{20}$$

$$C_f = \ln(2-p) - \frac{2(1-p)}{2-p} \ln(1-p) - \frac{p}{2-p} \ln p. \tag{21}$$

The formulas (20), (21) yield the increase in both quantities ΔE and ΔC.

Dephasing effect

We take into consideration the pure dephasing process [1, 15, 16] of TLSs constituting the system. The initial state, in this case, will be of the form

$$\begin{aligned} \hat{\rho}_j = p |e_j\rangle \langle e_j| + \epsilon \sqrt{p(1-p)} (|e_j\rangle \langle g_j| + |g_j\rangle \langle e_j|) + \\ + (1-p) |g_j\rangle \langle g_j|, \quad j = 1, 2, \end{aligned} \tag{22}$$

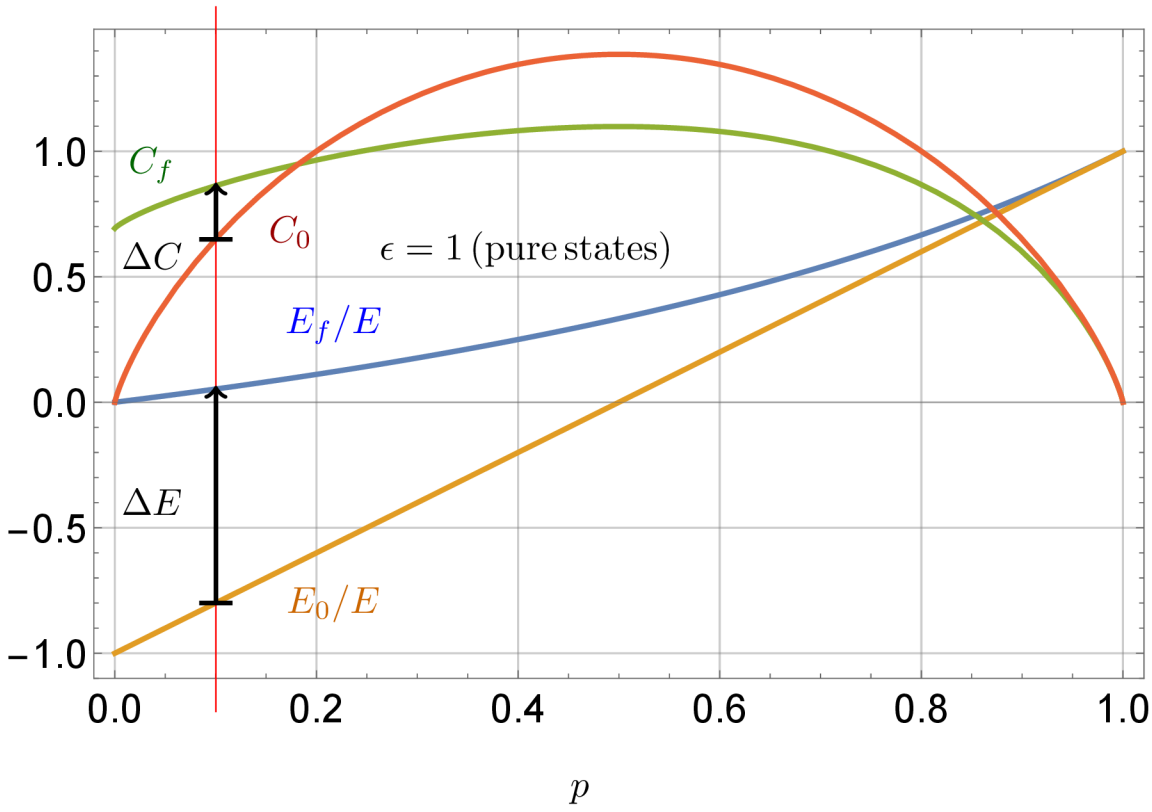

Figure 3: The plot of the normalized average energy E_f/E, E_0/E and the relative entropy of coherence C_f, C_0 for the final state $|\Psi_f\rangle$, Eq. (19), and the initial state $|\Psi_i\rangle$, Eq. (15), for a pair of TLS in pure states. The values are plotted vesrus the TLS excitation probability p, Eq. (14), with the red vertical line guiding the eye for the value $p = 0.1$ and black arrows expressing the coherence and energy increase. The conditional increase of the final energy over the initial one, $(E_f - E_0)/E > 0$, is achieved with maximum in the region of small p. The final entropy of coherence can be conditionally increased above the initial one in a region of small excitation probabilities p, up to the point $\tilde{C}_0 \approx 0.96$.

where $0 \leq \epsilon < 1$ is the dephasing rate of the state of the system. The total initial density matrix will be the direct product $\hat{\rho}_i = \hat{\rho}_1 \otimes \hat{\rho}_2$.

As dephasing affects only off-diagonal terms of the density matrix, the final energy of the resulting successful state is going to be similar to the case of pure state, Eq. (20). The resulting change of the coherence difference can be written as

$$\Delta C \approx \left(\frac{5-\epsilon}{10} \ln 2 - 1 \right) C_0 + \epsilon^2 \operatorname{arctanh} \epsilon^2 + \ln \sqrt{1-\epsilon^4}. \tag{23}$$

Protocol optimizations by POVM

We numerically generalize and optimize the charging protocol for the use of generalized measurement elements, c.f. Eq. (17), of the form $\{\hat{M}_0, \hat{M}_1 = \hat{1} - \hat{M}_0\}$ with

$$\hat{M}_0 = a \left|g_1 g_2\right\rangle \left\langle g_1 g_2\right| + b \left(\left|g_1 e_2\right\rangle \left\langle g_1 e_2\right| + \left|e_1 g_2\right\rangle \left\langle e_1 g_2\right| \right), \quad 0 \leq a, b \leq 1, \tag{24}$$

applied to the pure initial state, Eq. (15).

Figures 6 and 5 represent the results for two specific types of POVMs: the first one, determined by the arbitrary values of $0 \leq a, b \leq 1$ and, therefore, dubbed as a general; the second with $a = 1$, $0 \leq b \leq 1$, dubbed as a restricted one. The choice was dictated by the values to be optimized, whether it is a coherence only or a advantageous ratio between the coherence and energy gains. Both types of POVMs are compared to projector case $a = 1, b = 0$.

The optimization process for both types of protocol was made with respect to the final coherence value C_f, Eq. (11). Therefore, the general type of POVM, Eq. (24), was optimized over parameters a, b, resulting into the most advantageous option $C_f(\overline{a}, \overline{b})$, where the relation between parameters $\overline{a}$ and $\overline{b}$ is defined as $\overline{b} = 1 - \sqrt{1-\overline{a}}$. Substituting latter to the

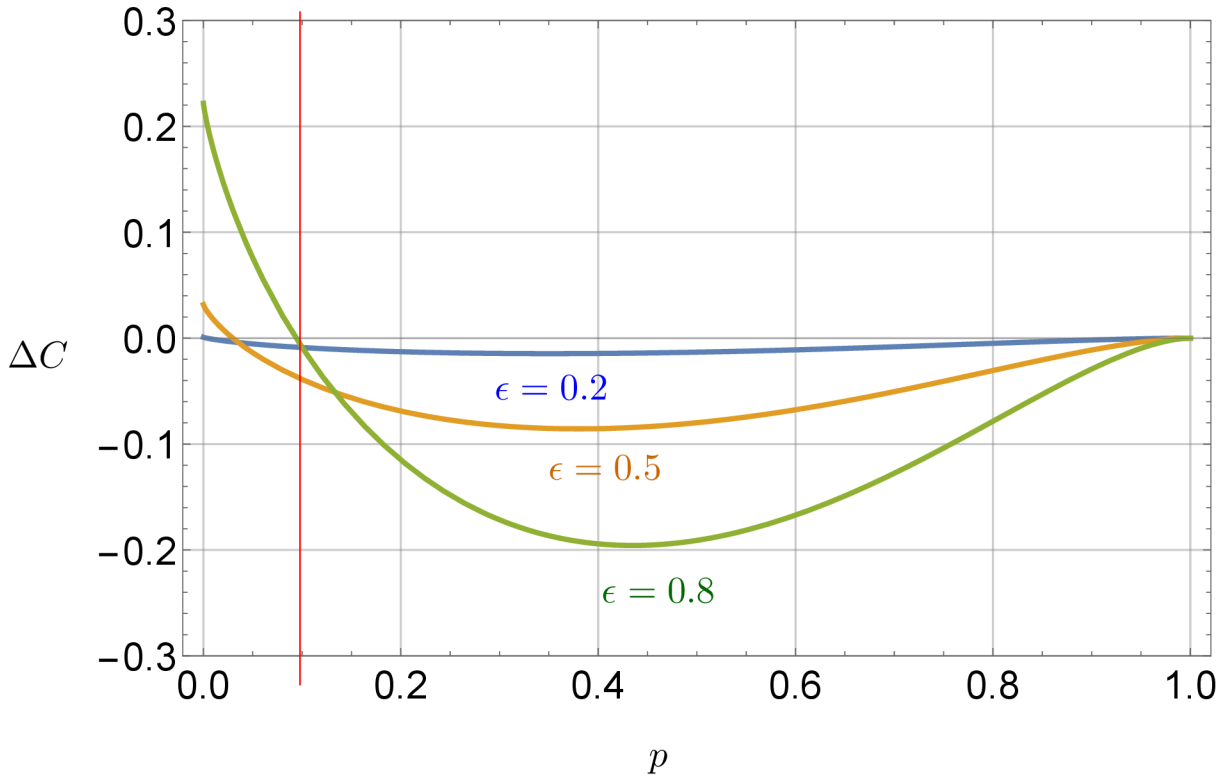

Figure 4: Plot of the difference between the final and initial relative entropy of coherence, $\Delta C = C_f - C_0$, Eq. (23), for a pair of TLS in partially-coherent states with different values of ϵ. The values are plotted versus the TLS excitation probability p, Eq. (22), again the red vertical line guides the eye for the value $p = 0.1$, as in Fig. 3. The final entropy of coherence can be conditionally increased above the initial one in a region of small excitation probabilities p. The final and initial energy, E_f/E and E_0/E of the system are identical to the case of pure states, cf. Fig. 3, as energy is determined by diagonal terms of density matrix $\hat{\rho}$ only and is independent of ϵ.

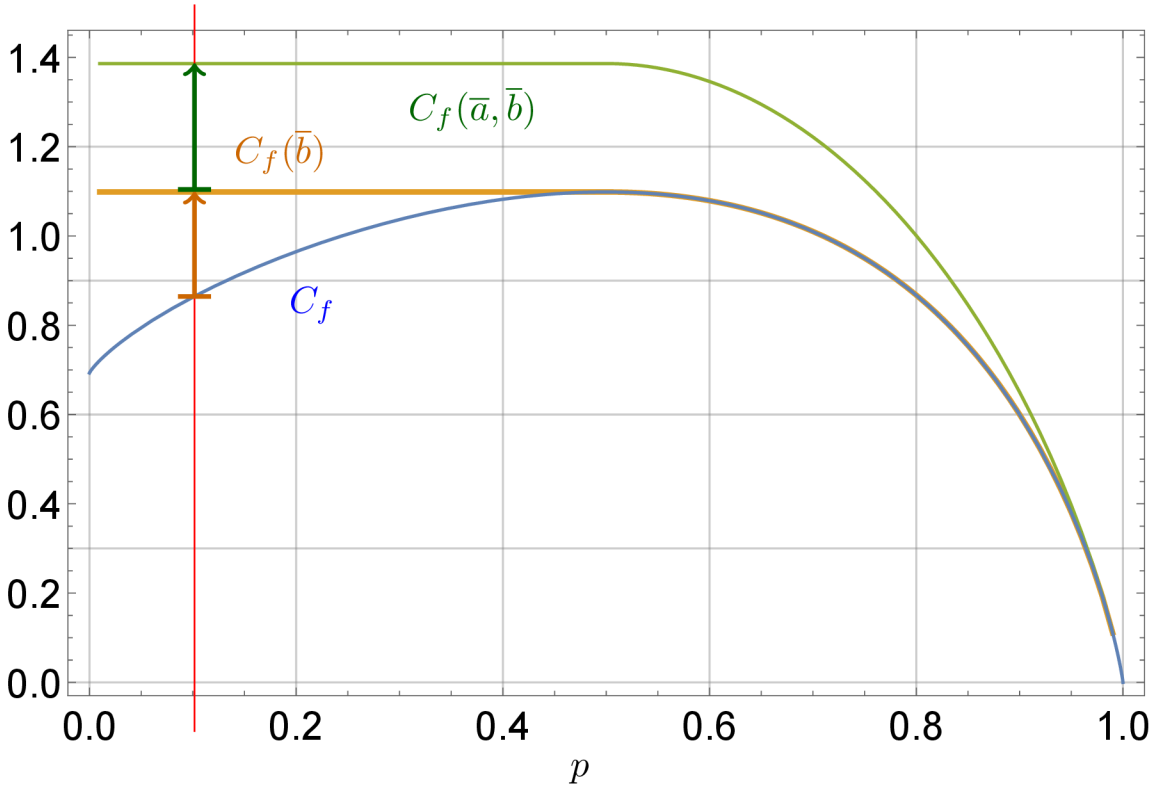

Figure 5: Plots of the optimal coherence after the charging for general POVM (green), cf. Eq. (24), and its restricted class with $a = 1$ (orange), applied to the initial state $|\Psi_i\rangle$, Eq. (15). These are compared to blue line C_f from Fig. 3, respectively. The relation of optimal values of parameters $\overline{a}$ and $\overline{b}$ for which the final coherences $C_f(\overline{b})$ and $C_f(\overline{a},\overline{b})$ are maximized is given as $\overline{b} = 1 - \sqrt{1-\overline{a}}$. The coherence $C_f(\overline{a},\overline{b})$ (green line), for the general type of POVM, shows substantial increase over the whole range of p (e.g., green arrow for $p = 0.2$ in Fig. 5). The result for restricted type of POVM (orange line) show increase of the coherence values (e.g., orange arrow for $p = 0.2$ in Fig. 5) over the interval of $p < 1/2$, with respect to the simple projector case, Eq. (17).

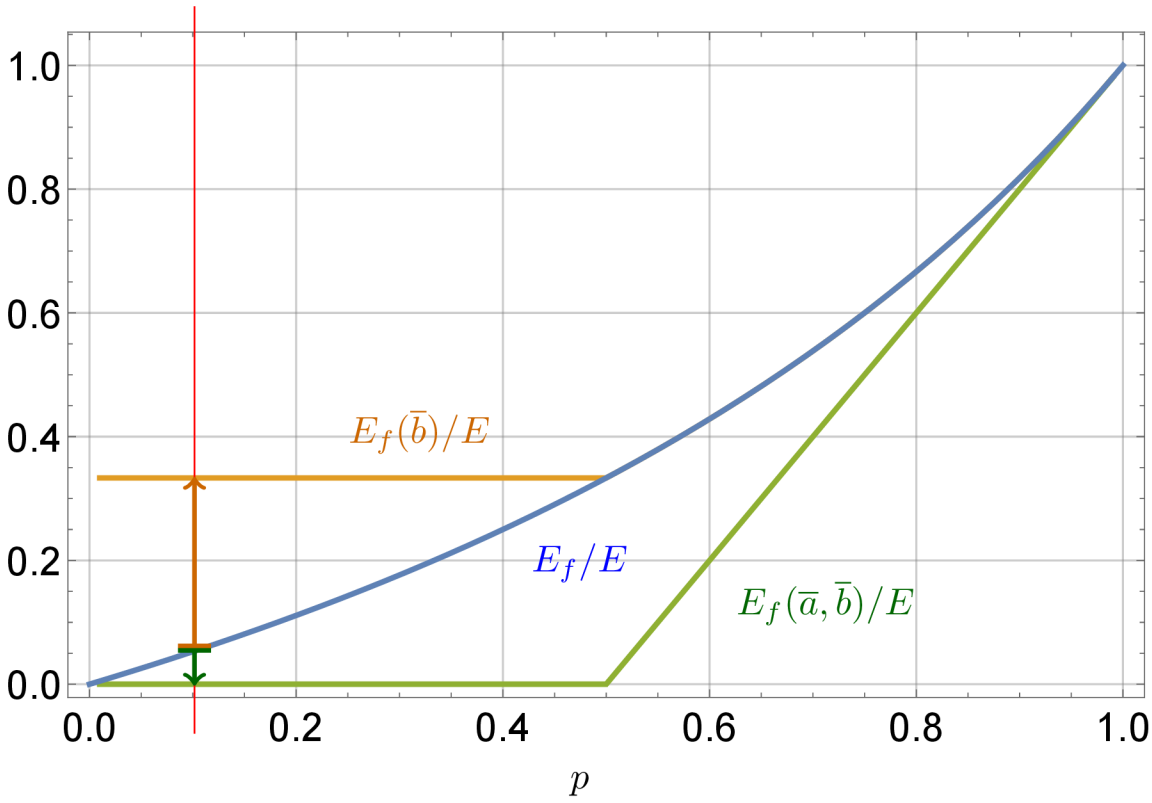

Figure 6: Plots of the optimal energy after the charging for general POVM (green), cf. Eq. (24), and its restricted class with $a = 1$ (orange), applied to the initial state $|\Psi_i\rangle$, Eq. (15). These are compared to blue lines showing E_f/E from Fig. 3, respectively. The energy values are given for optimal values of parameters $\overline{a}$ and $\overline{b}$ for which the final coherences $C_f(\overline{b})$ and $C_f(\overline{a},\overline{b})$ are maximized. The highest coherence $C_f(\overline{a},\overline{b})$ value (see green line in Fig. 5) is compensated by smaller increase in the energy compared to the simple projection, Eq. (17) (e.g., green arrow for $p = 0.2$ in Fig. 6). The result for restricted type of POVM (see orange line in Fig. 5) with the coherence $C_f(\overline{b})$ shows simultaneous improvement of the post measurement energy values (e.g., orange arrow for $p = 0.2$ in Fig. 6) on the same interval of p, with respect to the simple projector case, Eq. (17).

general form of POVM, Eq. (24), we get the coherence-maximising POVM

$$\hat{K}_0 = \overline{a}\,|g_1g_2\rangle\langle g_1g_2| + (1-\sqrt{1-\overline{a}})\,(|g_1e_2\rangle\langle g_1e_2| + \\ + |e_1g_2\rangle\langle e_1g_2|), \quad 0 \leq \overline{a} \leq 1, \tag{25}$$

whereas the relationship between the optimal value $\overline{a}$ and the excitation probability p can be well approximated by the polynomial dependence $\overline{a} \approx 1 - 3/2p^2 - 8p^4$ in the interval $0 \leq p \leq 2/5$. Similarly, the second type of POVM was optimized over a single parameter b to reach the corresponding maximal final coherence value $C_f(\overline{b})$ with the parameter $\overline{b}$.

Generalisation to N-TLS

In this section, we generalise the result to N TLS system. For simplicity, we consider them in pure states, Eq. (14), yielding the total initial state of the system

$$|\Psi_i^{(N)}\rangle = \bigotimes_{j=1}^{N} |\psi_j\rangle, \tag{26}$$

where $j = 1, \cdots, N$ labels the copies of TLS. The Hamiltonian of the system comprises the Hamiltonians of independent TLS, Eq. (8), and equals to Eq. (10). Subsequently, the initial energy of the system is given by a straightforward due to its additivity generalization of Eq. (15), yielding

$$E_0^{(N)} = \frac{NE_0}{2} = \frac{NE}{2}(2p-1). \tag{27}$$

The charging process in the same way as in the previous sections consists of application of a pair of global projectors
$\{\hat{P}_0^{(N)},\ \hat{P}_1^{(N)} = \hat{1} - \hat{P}_0^{(N)}\}$, where

$$\hat{P}_0^{(N)} = \bigotimes_{j=1}^{N} |g_j\rangle\langle g_j|, \quad \hat{P}_1^{(N)} = \hat{1} - \hat{P}_0^{(N)}, \tag{28}$$

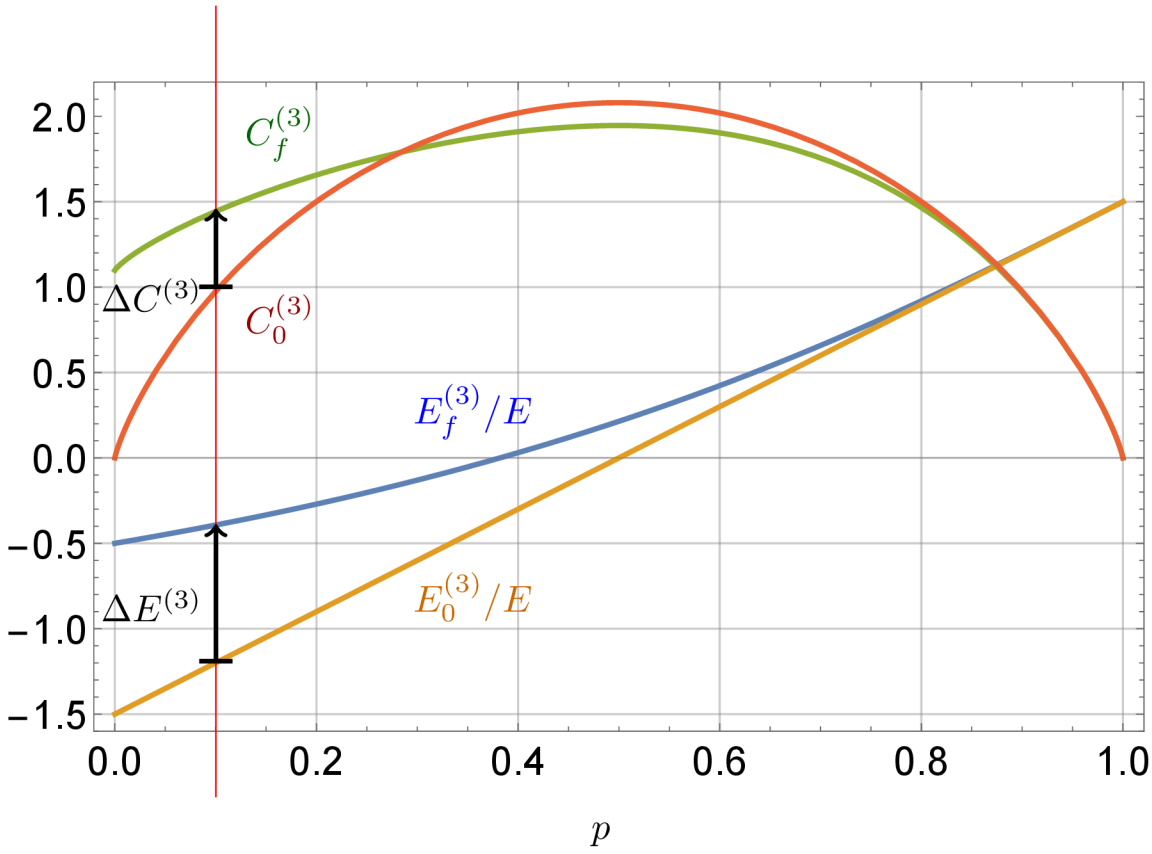

Figure 7: The plot of the normalized average energy $E_f^{(N)}/E$ (31), $E_0^{(N)}/E$ (27), and the relative entropy of coherence $C_f^{(N)}$ (32), $C_0^{(N)}$ (33), for the final state $|\Psi_f^{(N)}\rangle$, Eq. (29), and the initial state $|\Psi_i^{(N)}\rangle$, Eq. (26), for $N = 3$ TLS. The values are plotted versus the higher level excitation probability p, Eq. (14). The average energy gain, $0 \leq E_f^{(N)} - E_0^{(N)}$, is achieved with maximum for $p \to 0$. The final entropy of coherence $C_f^{(N)}$ can be conditionally increased above the initial one $C_0^{(N)}$ in a region of small excitation probabilities p. The red vertical line is a guide for the eye at $p = 0.1$ and the black arrows indicate the energy and coherence increase for each respective N.

is the projector on the global ground state of the system, cf. Eq. (17). Application of the projector $\hat{P}_1^{(N)}$ to the state (26) results in successfully charged state

$$|\Psi_f^{(N)}\rangle = \frac{\hat{P}_1^{(N)}\,|\Psi_i^{(N)}\rangle}{\sqrt{p_s^{(N)}}}, \tag{29}$$

with the probability of success $p_s^{(N)}$

$$p_s^{(N)} = 1 - (1-p)^N \neq 0, \tag{30}$$

converging to 1 with N, for any finite $p \neq 0$, and the corresponding energy of the final, successful state

$$E_f^{(N)} = \frac{NE}{2}\left[\frac{2p}{1-(1-p)^N} - 1\right]. \tag{31}$$

The expression for the final coherence $C_f^{(N)}$ for the successful measurement outcome in the case of pure initial state (26) reads

$$C_f^{(N)} = -\sum_{k=1}^{N} \binom{N}{k} \frac{p^k(1-p)^{N-k}}{1-(1-p)^N} \ln\left[\frac{p^k(1-p)^{N-k}}{1-(1-p)^N}\right], \tag{32}$$

and should be compared to the coherence of the initial pure state, Eq. (26),

$$C_0^{(N)} = -\sum_{k=0}^{N} \binom{N}{k} p^k(1-p)^{N-k} \ln\left[p^k(1-p)^{N-k}\right]. \tag{33}$$

5 Energy and coherence synthesis by a pairwise protocol

This Section is based on the publication by Gumberidze *et al.* [17].

Pure states

The main difference with global protocol constitutes the measurement process, namely, in pairwise protocol [17] we have repeated projective

measurements over pairs of TLS. Therefore, we denote the pair of complementary projectors $\{\hat{P}_0^{(j,k)},\ \hat{P}_1^{(j,k)}\}$

$$\hat{P}_0^{(j,k)} = |g_j g_k\rangle \langle g_j g_k|, \quad \hat{P}_1^{(j,k)} = \hat{1} - \hat{P}_0^{(j,k)}, \tag{34}$$

where subscripts "0" and "1" stand for failure and success, respectively. These projectors act on a pair of j-th and k-th TLS.

In any scenario, the total projector on N-TLS, $\hat{P}_1^{(N)}$, is invariant with respect to completely successful measurement sequence and constitutes the product of local projectors $\hat{P}_1^{(j,k)}$

$$\hat{P}_1^{(N)} = \prod_{\substack{j=1 \\ k=j+1}}^{N} \hat{P}_1^{(j,k)}, \quad \hat{P}_0^{(N)} = \hat{1} - \hat{P}_1^{(N)}. \tag{35}$$

Application of the projector $\hat{P}_1^{(N)}$ to the state (26) results in the successfully charged state

$$|\Psi_f^{(N)}\rangle = \frac{\hat{P}_1^{(N)} |\Psi_i^{(N)}\rangle}{\sqrt{p_s^{(N)}}}, \tag{36}$$

with the following probability of success $p_s^{(N)}$, corresponding final energy $E_f^{(N)}$, and final coherence $C_f^{(N)}$ of the state, respectively

$$\begin{aligned} p_s^{(N)} = &\sum_{k=0}^{1} \binom{N}{k} p^{N-k} (1-p)^k \\ &+ \sum_{k=2}^{t} \binom{N-k+1}{k} p^{N-k} (1-p)^k \neq 0, \end{aligned} \tag{37}$$

$$\begin{aligned} E_f^{(N)} = \frac{E}{2\, p_s^{(N)}} \Bigg[&\sum_{k=0}^{1} \binom{N}{k} (N-2k)\, p^{N-k} (1-p)^k \\ &+ \sum_{k=2}^{t} \binom{N-k+1}{k} (N-2k)\, p^{N-k} (1-p)^k \Bigg], \end{aligned} \tag{38}$$

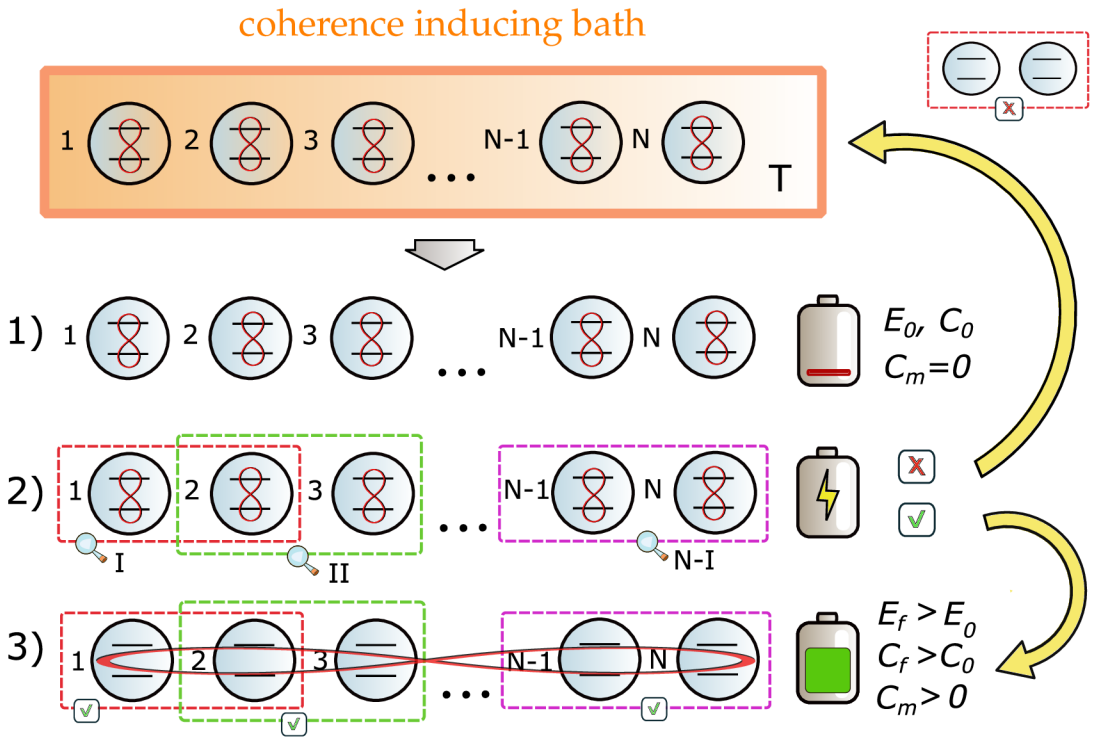

Figure 8: Schematics showing the idea of N-TLS coherence synthesis in three steps. **1)** TLS leave a low-coherence inducing bath [14] assumed to be almost discharged with low initial energy $E_0^{(N)}$ and coherence $C_0^{(N)}$ (marked by red loops connecting the levels). **2)** *Conditional* stage of the synthesis operation where measurements on pairs of TLS in a sequence marked by $\{\mathrm{I}, \mathrm{II}, ...\}$ are performed. If all of them are successful with the single run probability of success $p_s^{(N)}$, the coherence is synthesized $C_f^{(N)} > C_0^{(N)}$ and the system has higher energy $E_f^{(N)} > E_0^{(N)}$ as well, both with respect to the eigenbasis of Hamiltonian (10). **3)** TLS constituting the system become correlated (represented by a large red loop in step 3). Moreover, the mutual coherence, Eq. (7), increases, $\Delta C_m^{(N)} > 0$. If the outcome of step 2 is unsuccessful, with the single run probability $p_f^{(N)} = 1 - p_s^{(N)}$, the system is completely discharged and incoherent. To achieve a successful synthesis, TLS can be recycled by bringing them in contact with the bath again and the protocol is *repeated until success* (RUS).

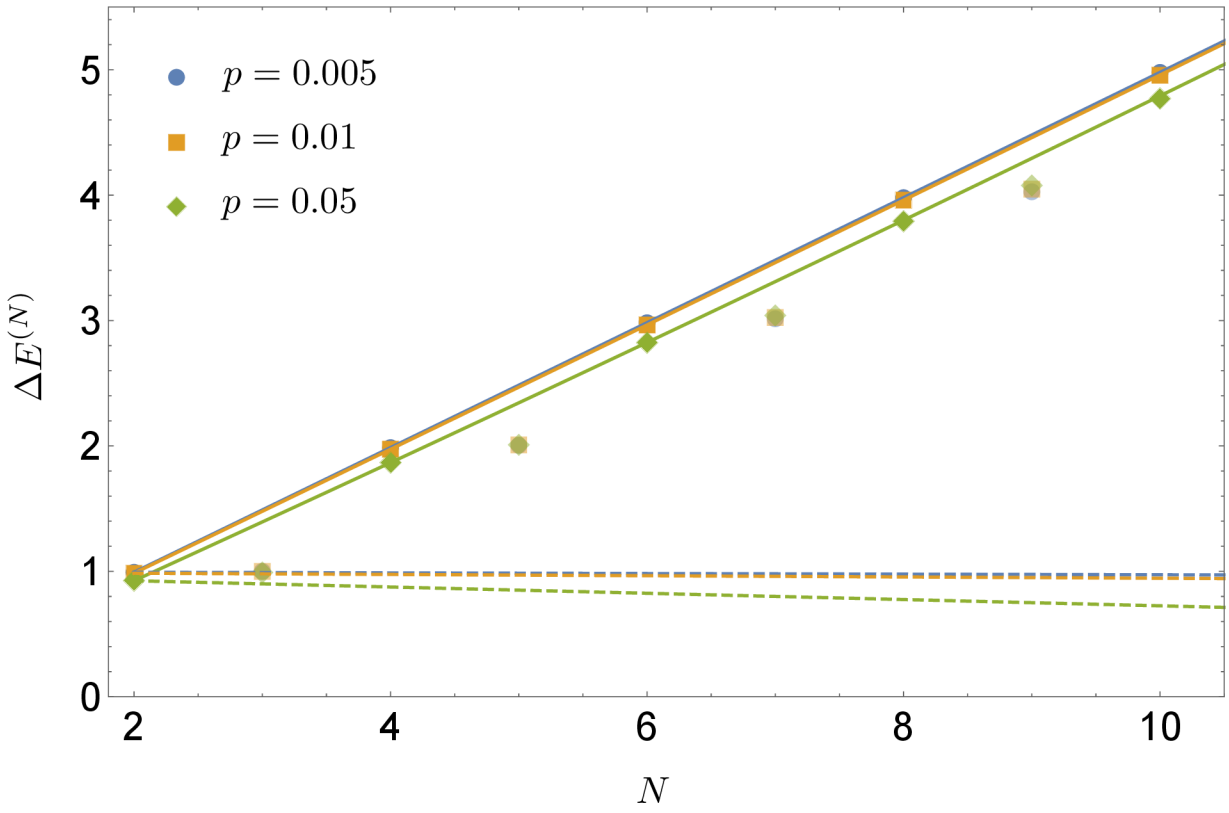

Figure 9: Conditional synthesis of energy of N TLS. The plot of the normalized average energy gain $\Delta E^{(N)}$, Eq. (12), of N TLS in pure initial state, Eq. (26). The values are plotted versus the number of TLS N for different excitation probabilities p, Eq. (14). The differently marked discrete points are exact numerical results, full lines are approximate results and dashed lines remind of the results of global protocol [13]. The energy gain $\Delta E^{(N)}$ increases proportionally to the number N of TLS, however, it is a decreasing function of $p \ll 1$. Note, the results for $p = 0.005$ and $p = 0.01$ almost coincide.

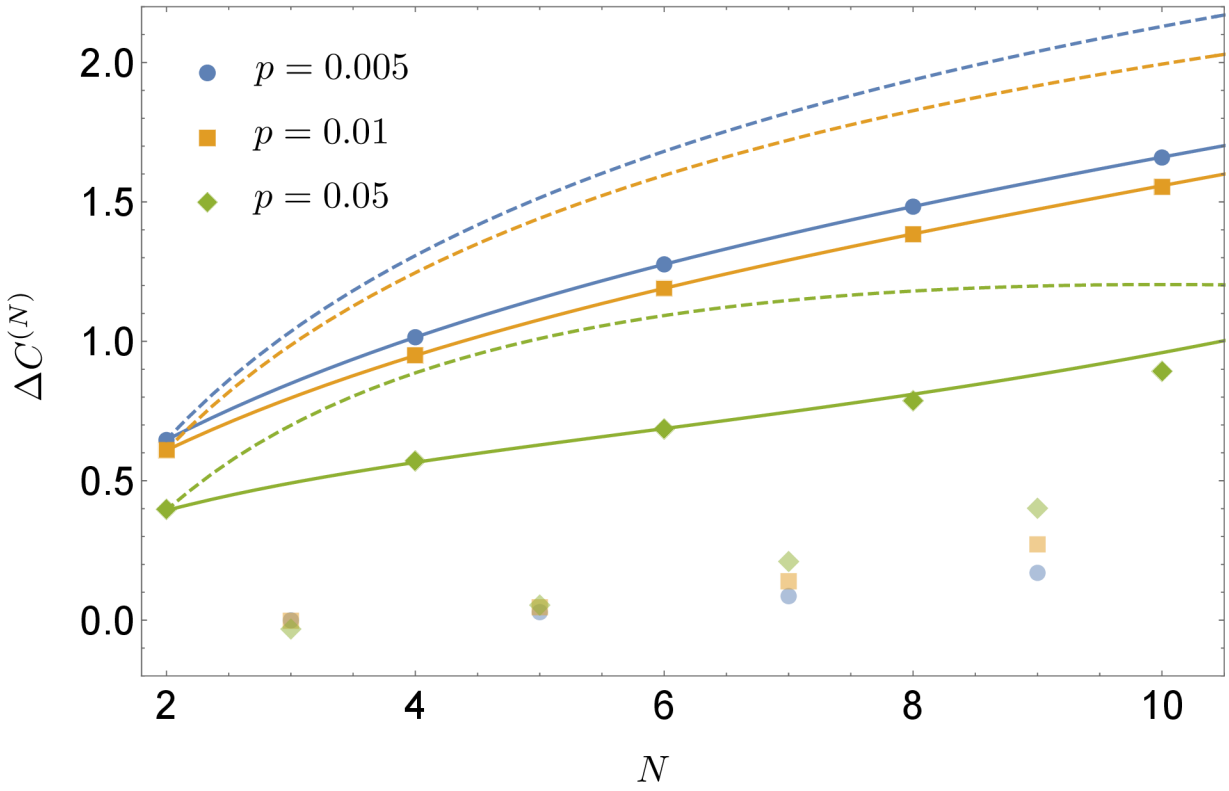

Figure 10: Conditional synthesis of coherence of N TLS. The plot of the relative entropy of coherence gain $\Delta C^{(N)}$, Eq. (13), of N TLS in pure initial state, Eq. (26). The values are plotted versus the number of TLS N for different excitation probabilities p, Eq. (14). The differently marked discrete points are exact numerical results, full lines are approximate results and dashed lines remind of the results of global protocol [13]. The coherence gain $\Delta C^{(N)}$, as energy gain $\Delta E^{(N)}$, c.f. Fig. (9), is a decreasing function of $p \ll 1$. Note, the coherence gain $\Delta C^{(N)}$ differs for odd and even N with a significant advantage for even N.

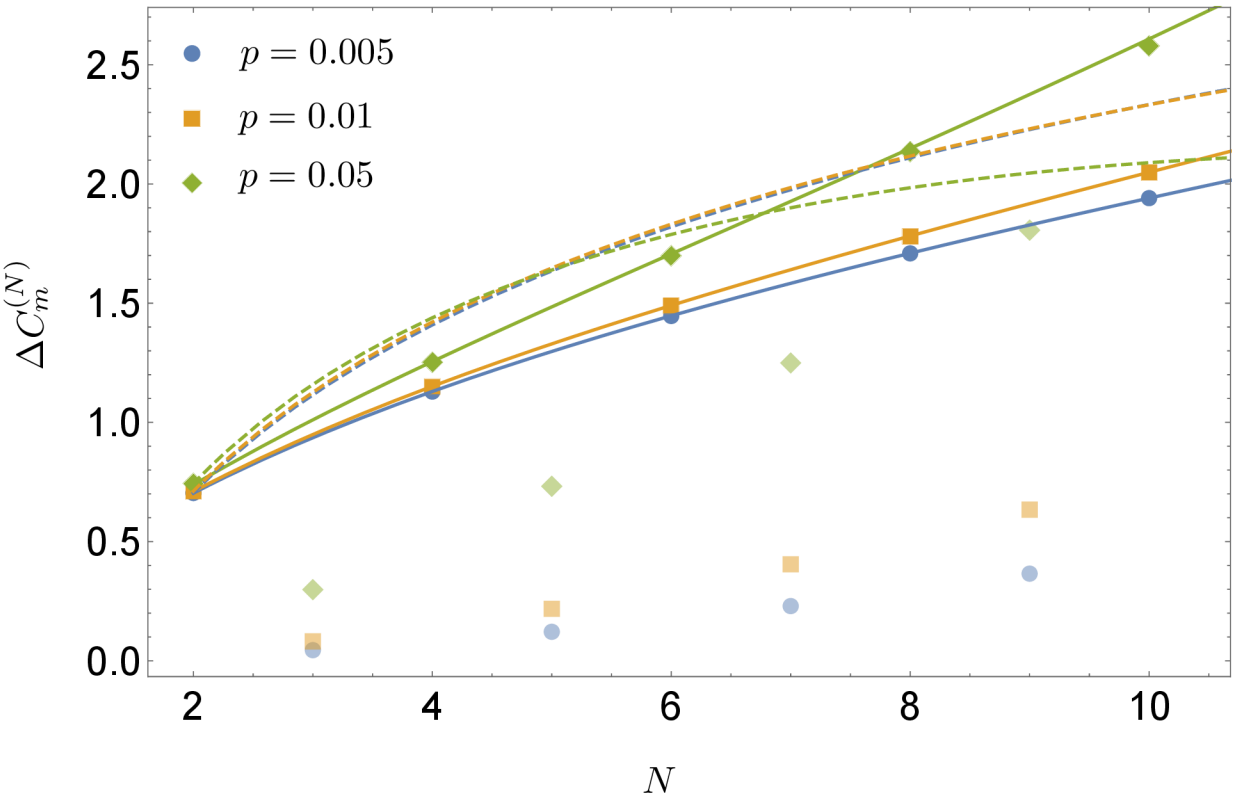

Figure 11: Conditional synthesis of mutual coherence of N TLS. The plot of the mutual coherence gain $\Delta C_m^{(N)}$, Eq. (7), of N TLS in pure initial state, Eq. (26). The values are plotted versus the number of TLS N for different excitation probabilities p, Eq. (14). The differently marked discrete points are exact numerical results, full lines are approximate results and dashed lines remind of the results of global protocol [13]. Note the reversed order of colors of full curves for $\Delta C_m^{(N)}$ and others, reflecting that $\Delta C_m^{(N)}$ is a non-decreasing function of $p \ll 1$, on contrary to $\Delta C^{(N)}$ and $\Delta E^{(N)}$. Note, the pairwise protocol overcomes the global one, for $N \gtrsim 6$ and $p \gtrsim 0.01$, corresponding to an untypical situation, cf. Fig. 9 and Fig. 10.

$$C_f^{(N)} = -\sum_{k=0}^{1} \binom{N}{k} \frac{p^{N-k}\,(1-p)^k}{p_s^{(N)}} \ln\left[\frac{p^{N-k}\,(1-p)^k}{p_s^{(N)}}\right] - \sum_{k=2}^{t} \binom{N-k+1}{k} \frac{p^{N-k}\,(1-p)^k}{p_s^{(N)}} \ln\left[\frac{p^{N-k}\,(1-p)^k}{p_s^{(N)}}\right], \tag{39}$$

where $t = (N+1)/2$ if the number of TLS N is odd and $t = N/2$ if N is even.

Approximations

The principal interest for us represents the results of pairwise protocol for even numbers of TLS. For this purpose, we limited the range of excitation probability to small values $p \lesssim 0.1$ and the number of TLS constituting the system to $N \lesssim 10$. It was done since the quantities of interest, $\Delta E^{(N)} > 0$, $\Delta C^{(N)} > 0$, mostly have an increase in the region specified before. We explore approximations of their dependence on the probability of excitation p and for *even* N the results are following

$$p_s^{(N)} \approx \left(\frac{N}{2}+1\right) p^{\frac{N}{2}}, \tag{40}$$

$$\Delta E^{(N)} \approx \frac{N}{2} - \frac{N(20-N)}{24} p, \tag{41}$$

$$\Delta C^{(N)} \approx \ln\left(\frac{N}{2}+1\right) - \frac{N(20-N)}{24}(1-\ln p)p, \tag{42}$$

$$\Delta C_m^{(N)} \equiv C_{m,f}^{(N)} = C_f^{(N)} - C_f^{(N)loc} \approx \ln\left(\frac{N}{2}+1\right) + \frac{N(N+4)}{24}(1-\ln p)p - \ln\left[\frac{3}{2}\left(\frac{N}{2}+1\right)!\right]p. \tag{43}$$

These results should be compared to the respective approximations of the global protocol, described in Section 4. We list the approximations of

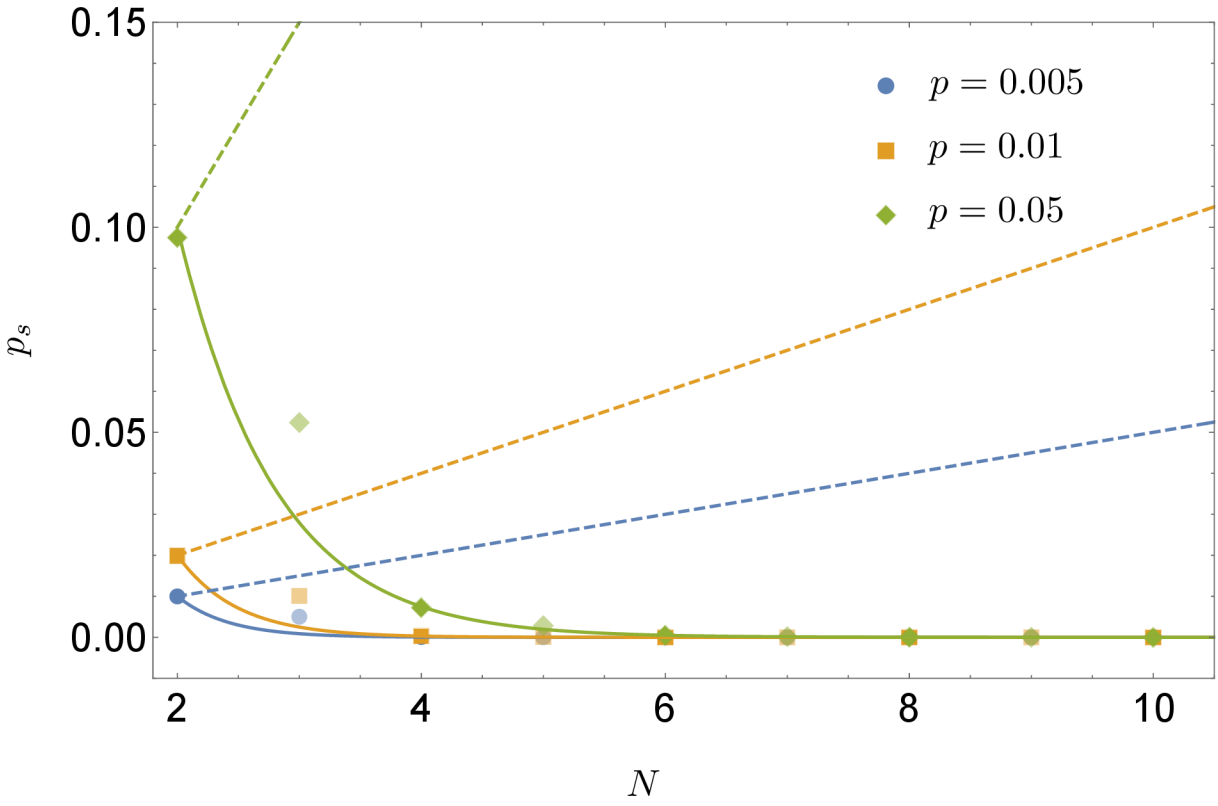

Figure 12: Repeat-until-success strategy for coherence synthesis. The plot of probability of success p_s, Eq. (37), of the projective measurement $\hat{P}_1^{(N)}$, Eq. (35), defined by the successful outcome with the final state $|\Psi_f^{(N)}\rangle$, Eq. (36). The values are plotted versus the number of TLS N for different excitation probabilities p, Eq. (14). The probability of success $p_s \to 0$ with increasing N. Solid and dashed lines represent approximate expressions for even numbers N of TLS for the pairwise and global [13] protocol, respectively. The discrete marked points represent exact numerical results for the pairwise protocol.

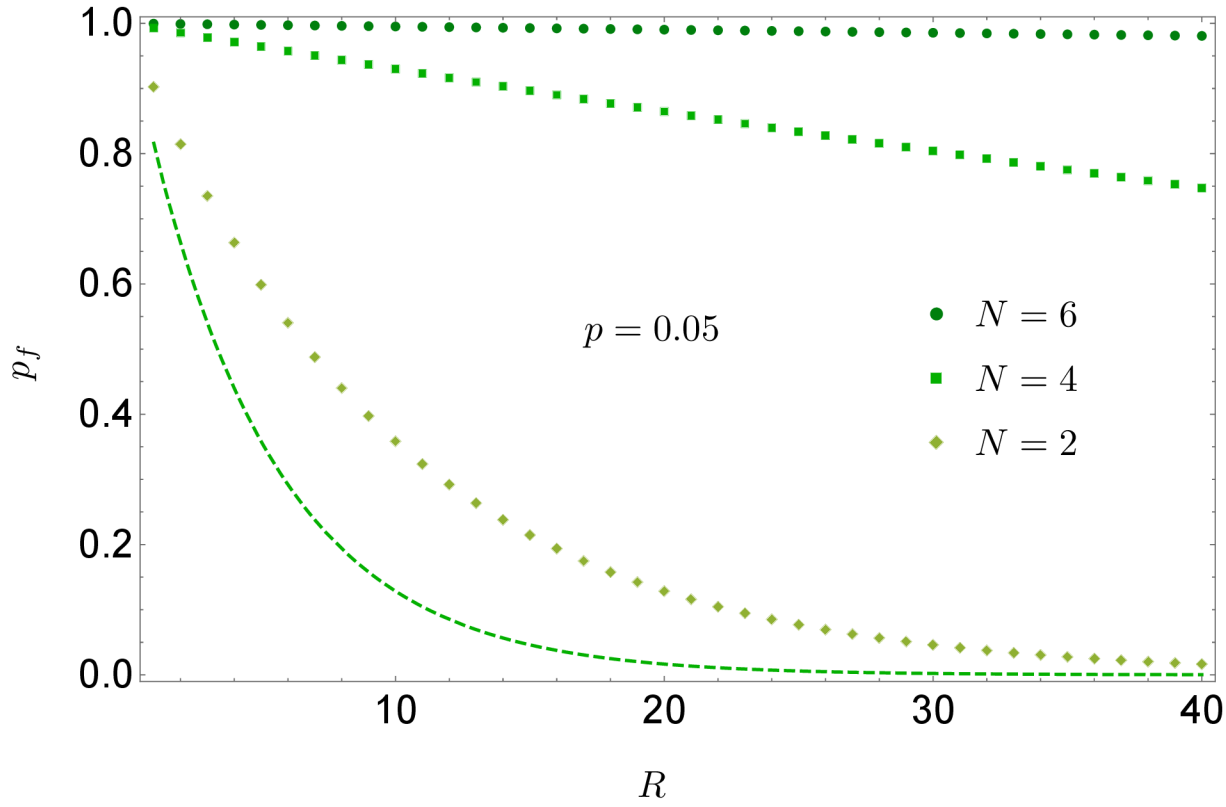

Figure 13: Repeat-until-success strategy for coherence synthesis. The dependence of probability of failure p_f in the repeat until success (RUS) strategy on the number of repetitions R for $N = \{2, 4, 6\}$ TLS. The values are plotted for an example of the fixed probability of excited state $p = 0.05$. On contrary to the probability of success p_s, probability of failure $p_f \to 1$ with larger number N and smaller excitation probability p. The dashed line represents respective probability of failure of global protocol [13] for $N = 4$ TLS.

the corresponding values of the latter

$$p_s^{(N)} \approx Np, \tag{44}$$

$$\Delta E^{(N)} \approx 1 - \frac{N+1}{2}p, \tag{45}$$

$$\Delta C^{(N)} \approx \ln N - \frac{N+1}{2}(1-\ln p)p, \tag{46}$$

$$\Delta C_m^{(N)} \approx \ln N + \frac{N-1}{2}(1-\ln p)p - \frac{(N-1)^2}{N-2}\ln{(N-1)p}. \tag{47}$$

Dephasing

At first, we are going to explore the effect of dephasing of the initial states of TLS only, Eq. (26). Let us assume that the initial pure state (14) of each TLS after dephasing is characterized by the density matrix [1, 13]

$$\begin{aligned}\hat{\rho}_j = p\left|e_j\right\rangle\left\langle e_j\right| + \epsilon\sqrt{p(1-p)}(\left|e_j\right\rangle\left\langle g_j\right| + \left|g_j\right\rangle\left\langle e_j\right|) \\ +(1-p)\left|g_j\right\rangle\left\langle g_j\right|, \quad j=1,\ldots,N,\end{aligned} \tag{48}$$

where $0 \leq \epsilon \leq 1$ quantifies the effect of the dephasing. The initial state of the total system of N TLS reads

$$\hat{\rho}_i^{(N)} = \bigotimes_{j=1}^{N}\hat{\rho}_j. \tag{49}$$

Subjecting the initial state to the same projector-based charging procedure $\{\hat{P}_1^{(N)},\ \hat{P}_0^{(N)}\}$, yields the final state

$$\hat{\rho}_f^{(N)} = \frac{\hat{P}_1^{(N)}\hat{\rho}_i^{(N)}\hat{P}_1^{(N)}}{\overline{p}_s}. \tag{50}$$

The complexity of the coherence (11) and mutual coherence (6) prevents us from determining $\Delta\overline{C}^{(N)}$ and $\Delta\overline{C}_m^{(N)}$ analytically for the initial state (49) and the final state (50). Thus, we focus our attention to the fully numerical results, presenting them only graphically.

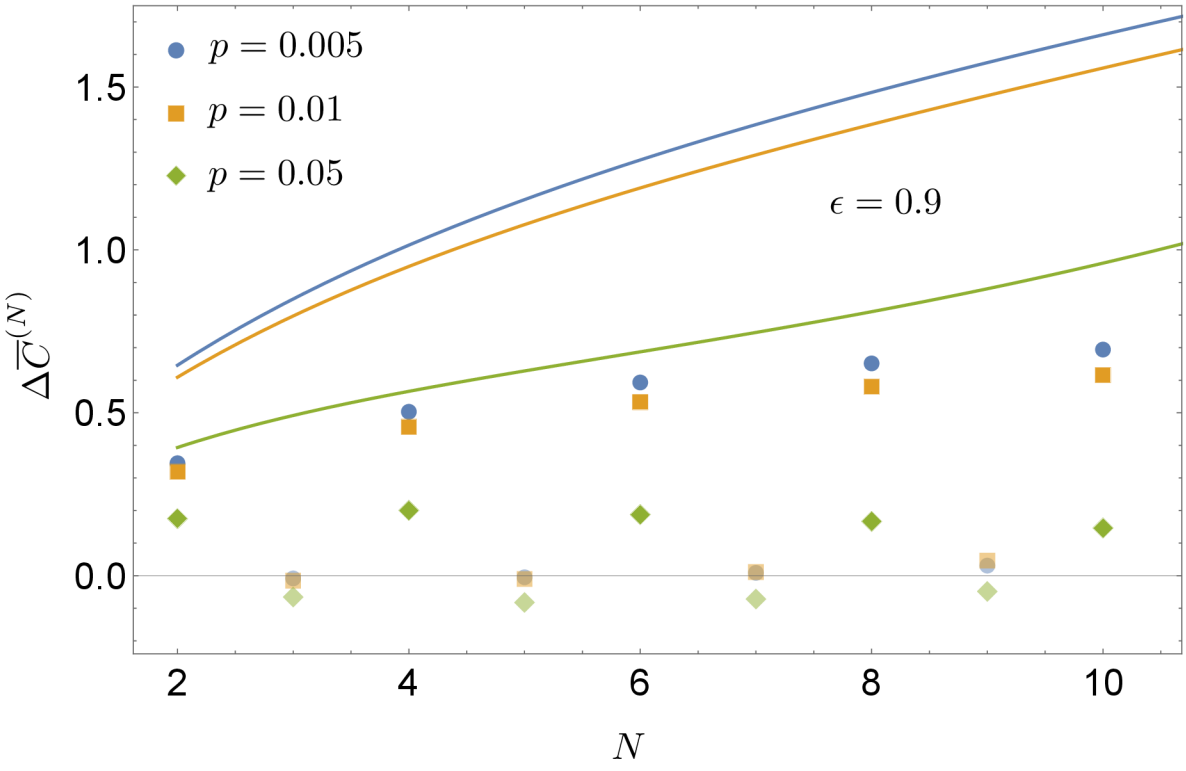

Figure 14: Conditional synthesis of coherence of N partially dephased TLS. The coherence gain $\Delta\overline{C}^{(N)}$, Eq. (13), for N TLS in the final state (50) and dephased initial state (49). The dephasing rate is set to $\epsilon = 0.9$. The values are plotted versus the number of TLS N, for different excitation probabilities p, Eq. (48). The marked discrete values are results of exact numerical calculation. The full lines recall the approximate results for pure initial states, see Fig. 10. The effect of the coherence gain decrease is significantly stronger for larger numbers of TLS constituting the system, causing the emergence of the local maximum at $N \approx 4$. Generally, the gain $\Delta\overline{C}^{(N)} > 0$ is preserved until the "critical" value $\epsilon \approx 0.5$, where it is lost even for small values of p and low N.

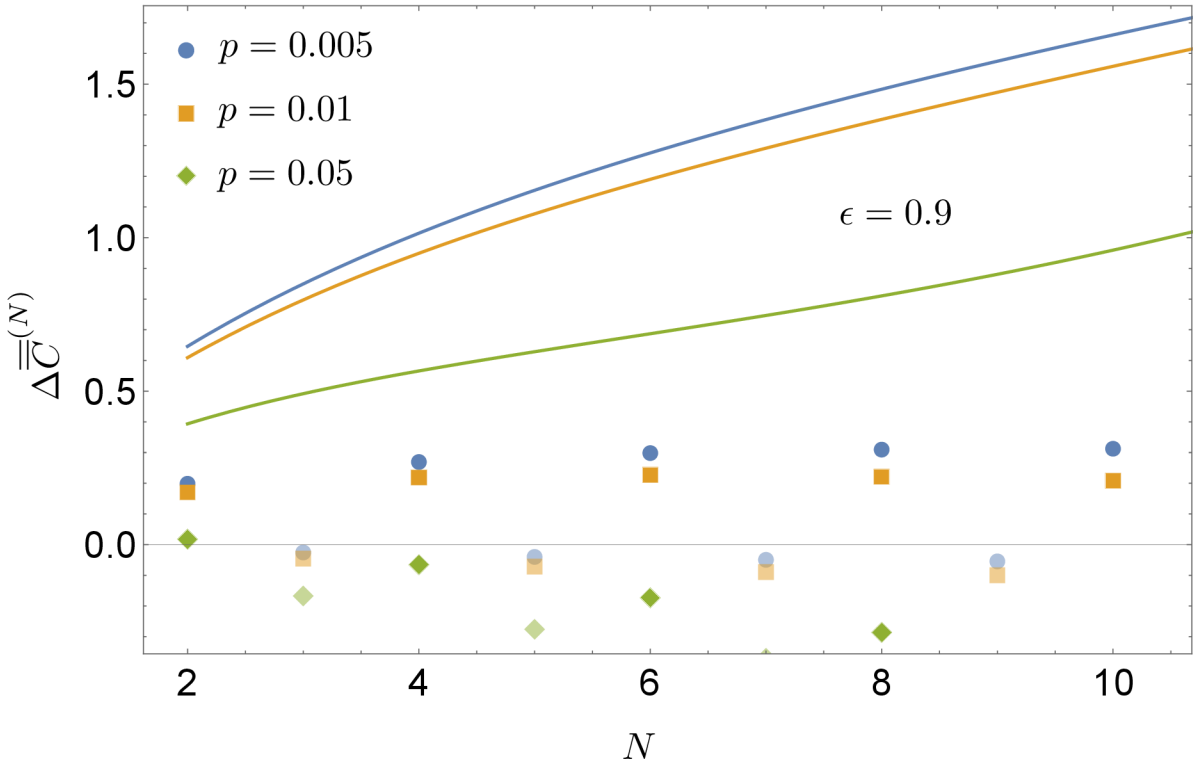

Figure 15: Effect of dephasing on the final state (50). The coherence gain $\Delta\overline{\overline{C}}^{(N)}$ of the system in the final state, Eq. (51), with $\epsilon = 0.9$. The values are plotted versus the number of TLS N, for different excitation probabilities p, Eq. (48). Solid lines represent the corresponding values for pure states, cf. Fig. 10, marked discrete points are exact numerical results. It can be seen by comparison with Fig. 14 that dephasing of initial state has much larger effect of diminishing the coherence gain, than dephasing process of final state of the system, suggesting that the final state is quite robust with respect to dephasing. However, even in this case dephasing decreases the gain in $\Delta\overline{\overline{C}}^{(N)}$, for larger N and low p, and causes the appearance of local maximum for $N \approx 6$ (orange squares).

Moreover, we are going to explore in addition to the dephasing of the initial also the dephasing of the final total state of the system, Eq. (50). For the sake of not overcomplicating results, in the following we will assume $\epsilon = \bar{\epsilon}$ being equal. Such a double dephasing process will give the final state of the system after the measurement

$$\bar{\hat{\rho}}_f^{(N)} = \sum_{i=0}^{2^N-1} \hat{\mathcal{K}}_i \hat{\rho}_f^{(N)} \hat{\mathcal{K}}_i, \tag{51}$$

with the final coherence $\bar{\bar{C}}_f^{(N)} \equiv C(\bar{\hat{\rho}}_f^{(N)})$. The $\hat{\mathcal{K}}_i$ being the global Kraus operators [16], having the form

$$\hat{\mathcal{K}}_i \equiv \hat{K}_{j_{N-1}^{(i)}} \bigotimes \cdots \bigotimes \hat{K}_{j_1^{(i)}} \bigotimes \hat{K}_{j_0^{(i)}}, \quad j_k^{(i)} = \{0, 1\}, \tag{52}$$

with $(j_{N-1}^{(i)} \cdots j_1^{(i)} j_0^{(i)})_2 = (i)_{10}$ being the binary representation of the index value $(i)_{10}$, e.g., $(7)_{10} = (0111)_2$ for $N = 4$.

6 Conclusions

We presented two protocols for the repeat-until-success charging and synthesizing of the quantum battery by means of quantum measurements diagonal in the energy basis. The building blocks of our battery are factorized copies of identical two-level systems (TLS) with nonzero, although possibly very small, population of the excited state, and some small residual coherence that can be achieved by a suitable interaction with a sufficiently cold thermal bath [14, 18, 19, 20, 21]. In a global protocol a pair of TLS subsequently undergoes a single, unity-resolving measurement with two possible outcomes, each represented by an operator diagonal in the TLS energy basis. Pairwise protocol consists of projective measurements applied in a sequential manner to the pairs of non-interacting or independent TLS. The essence of their application lies in removing the cases

of both measured TLS being in their ground states. The projectors are diagonal in the energy basis, hence, they do not contribute to increase of the coherence of the system. As a result, they translate a system from a set of independent TLS with local coherences to a correlated larger system with global coherence (the difference quantified by mutual coherence), rendering the protocol universal from this perspective. Pairwise protocol is experimentally less challenging as it requires projective measurements on smaller systems consisting of a few TLS rather then large ones described global protocol.

In both cases if the protocol succeeds, we synthesize the initially independent pair of TLS into a system with non-factorized state and higher coherent energy. The failure of the protocol results in reducing the initial energy and coherence to zero. These two possibilities represent the outcomes of the inherently conditional protocol, however with the possibility of increasing the success probability arbitrarily close to one (using repeat-until-success strategy), making the protocol effectively approach to a deterministic one. Our results show that the dephasing of the energy of the initial state decreases the positive effect of the charging, but does not prevent the charging in principle.

The results of the projector-based charging protocol were generalized to the case of using N-TLS, either in a global or pairwise measurement approach. The final value of the coherent energy can be increased even more, due to optimization, if the measurement consists of POVM elements. Such protocol is superior in the value of coherence and energy with respect to the results of the projective measurement. The results stimulated proof-of-principle experimental verification of such energy synthesizing using controlled quantum systems [22] in Olomouc Quantum Laboratory.

Bibliography

[1] M.A. Nielsen and I.L. Chuang. *Quantum Computation and Quantum Information: 10th Anniversary Edition*. Cambridge University Press, 2010. ISBN: 9781139495486. URL: https://books.google.cz/books?id=-s4DEy7o-a0C.

[2] Ingemar Bengtsson and Karol Zyczkowski. "Geometry of Quantum States: An Introduction to Quantum Entanglement". In: (Aug. 2006). DOI: https://doi.org/10.1017/CBO9780511535048.

[3] P. Kammerlander and J. Anders. "Coherence and measurement in quantum thermodynamics". In: *Scientific Reports* 6.1 (Feb. 2016), p. 22174. ISSN: 2045-2322. DOI: 10.1038/srep22174. URL: https://doi.org/10.1038/srep22174.

[4] Alain Deville and Yannick Deville. "Clarifying the link between von Neumann and thermodynamic entropies". In: *The European Physical Journal H* 38.1 (Jan. 2013), pp. 57–81. ISSN: 2102-6467. DOI: 10.1140/epjh/e2012-30032-0. URL: https://doi.org/10.1140/epjh/e2012-30032-0.

[5] Zhengjun Xi, Yongming Li, and Heng Fan. "Quantum coherence and correlations in quantum system". In: *Scientific Reports* 5 (1 2015),

p. 10922. DOI: 10.1038/srep10922. URL: https://doi.org/10.1038/srep10922.

[6] Paul Skrzypczyk, Anthony J. Short, and Sandu Popescu. "Work extraction and thermodynamics for individual quantum systems". In: *Nature Communications* 5.1 (June 2014), p. 4185. ISSN: 2041-1723. DOI: 10.1038/ncomms5185. URL: https://doi.org/10.1038/ncomms5185.

[7] A. Ü. C. Hardal and O. E. Müstecaplıoğlu. "Superradiant Quantum Heat Engine". In: *Scientific Reports* 5.1 (Aug. 2015), p. 12953. DOI: https://doi.org/10.1038/srep12953. URL: https://doi.org/10.1038/srep12953.

[8] Gonzalo Manzano et al. "Entropy production and thermodynamic power of the squeezed thermal reservoir". In: *Phys. Rev. E* 93 (5 May 2016), p. 052120. DOI: 10.1103/PhysRevE.93.052120. URL: https://link.aps.org/doi/10.1103/PhysRevE.93.052120.

[9] Nicolas Brunner et al. "Entanglement enhances cooling in microscopic quantum refrigerators". In: *Phys. Rev. E* 89 (3 Mar. 2014), p. 032115. DOI: 10.1103/PhysRevE.89.032115. URL: https://link.aps.org/doi/10.1103/PhysRevE.89.032115.

[10] Raam Uzdin, Amikam Levy, and Ronnie Kosloff. "Equivalence of Quantum Heat Machines, and Quantum-Thermodynamic Signatures". In: *Phys. Rev. X* 5 (3 Sept. 2015), p. 031044. DOI: 10.1103/PhysRevX.5.031044. URL: https://link.aps.org/doi/10.1103/PhysRevX.5.031044.

[11] James Klatzow et al. “Experimental Demonstration of Quantum Effects in the Operation of Microscopic Heat Engines”. In: *Phys. Rev. Lett.* 122 (11 Mar. 2019), p. 110601. DOI: https://doi.org/10.1103/PhysRevLett.122.110601. URL: https://link.aps.org/doi/10.1103/PhysRevLett.122.110601.

[12] T. Baumgratz, Marcus Cramer, and M. Plenio. “Quantifying Coherence”. In: *Physical review letters* 113 (Nov. 2013). DOI: 10.1103/PhysRevLett.113.140401.

[13] Mariia Gumberidze, Michal Kolář, and Radim Filip. “Measurement Induced Synthesis of Coherent Quantum Batteries”. In: *Scientific Reports* 9 (1 Dec. 2019), p. 19628. DOI: 10.1038/s41598-019-56158-8. URL: https://doi.org/10.1038/s41598-019-56158-8.

[14] Giacomo Guarnieri, Michal Kolá ř, and Radim Filip. “Steady-State Coherences by Composite System-Bath Interactions”. In: *Phys. Rev. Lett.* 121 (7 Aug. 2018), p. 070401. DOI: https://doi.org/10.1103/PhysRevLett.121.070401. URL: https://link.aps.org/doi/10.1103/PhysRevLett.121.070401.

[15] Christopher Gerry and Peter Knight. “Dissipative interactions and decoherence”. In: *Introductory Quantum Optics*. Cambridge University Press, 2004, pp. 195–212. DOI: 10.1017/CBO9780511791239.008.

[16] K. Kraus. *Effects and Operations: Fundamental Notions of Quantum Theory*. Springer, 1983.

[17] Mariia Gumberidze, Michal Kolář, and Radim Filip. “Pairwise-measurement-induced synthesis of quantum coherence”. In: *Phys. Rev. A* 105 (1 Jan. 2022), p. 012401. DOI: 10.1103/PhysRevA.

105.012401. URL: https://link.aps.org/doi/10.1103/PhysRevA.105.012401.

[18] Archak Purkayastha et al. "Tunable phonon-induced steady-state coherence in a double-quantum-dot charge qubit". In: *npj Quantum Information* 6 (1 2020), p. 22. DOI: 10.1038/s41534-020-0256-6. URL: https://doi.org/10.1038/s41534-020-0256-6.

[19] Giacomo Guarnieri et al. "Non-equilibrium steady-states of memoryless quantum collision models". In: *Physics Letters A* 384.24 (2020), p. 126576. ISSN: 0375-9601. DOI: https://doi.org/10.1016/j.physleta.2020.126576. URL: https://www.sciencedirect.com/science/article/pii/S0375960120304436.

[20] Ricardo Román-Ancheyta et al. "Enhanced steady-state coherence via repeated system-bath interactions". In: *Phys. Rev. A* 104 (6 Dec. 2021), p. 062209. DOI: 10.1103/PhysRevA.104.062209. URL: https://link.aps.org/doi/10.1103/PhysRevA.104.062209.

[21] Artur Slobodeniuk, Tomáš Novotný, and Radim Filip. "Extraction of autonomous quantum coherences". In: *Quantum* 6 (Apr. 2022), p. 689. DOI: 10.22331/q-2022-04-15-689. URL: https://doi.org/10.22331/q-2022-04-15-689.

[22] Robert Stárek et al. "Experimental demonstration of optimal probabilistic enhancement of quantum coherence". In: *Quantum Science and Technology* 6.4 (July 2021), p. 045010. ISSN: 2058-9565. DOI: 10.1088/2058-9565/ac10ef. URL: http://dx.doi.org/10.1088/2058-9565/ac10ef.

Publications covering thesis

[13] Mariia Gumberidze, Michal Kolář, and Radim Filip. "Measurement Induced Synthesis of Coherent Quantum Batteries". In: *Scientific Reports* 9 (1 Dec. 2019), p. 19628. DOI: 10.1038/s41598-019-56158-8. URL: https://doi.org/10.1038/s41598-019-56158-8.

[17] Mariia Gumberidze, Michal Kolář, and Radim Filip. "Pairwise-measurement-induced synthesis of quantum coherence". In: *Phys. Rev. A* 105 (1 Jan. 2022), p. 012401. DOI: 10.1103/PhysRevA.105.012401. URL: https://link.aps.org/doi/10.1103/PhysRevA.105.012401.